

SYNTHESIS, CHARACTERIZATION, AND RISK  
ASSESSMENT PLANNING FOR NOVEL DEGRADABLE AND IMAGEABLE  
EMBOLIC AGENTS

by

Jensen S Doucet

Submitted in partial fulfillment of the requirements  
for the degree of Master of Applied Science

at

Dalhousie University  
Halifax, Nova Scotia  
June 2018

© Copyright by Jensen Doucet, 2018

# Table of Contents

<b>LIST OF TABLES .....</b>	<b>vi</b>
<b>LIST OF FIGURES .....</b>	<b>vii</b>
<b>ABSTRACT .....</b>	<b>ix</b>
<b>LIST OF ABBREVIATIONS AND SYMBOLS USED .....</b>	<b>x</b>
<b>ACKNOWLEDGEMENTS .....</b>	<b>xiii</b>
<b>CHAPTER 1: INTRODUCTION .....</b>	<b>1</b>
<b>1.1. Uterine Leiomyoma .....</b>	<b>1</b>
1.1.1. Pathophysiology of Uterine Leiomyomas .....	1
1.1.2. Current Treatments .....	3
1.1.2.1. Surgical Options .....	3
1.1.2.2. Commercially Available UAE Microspheres .....	6
<b>1.2. Advances in Degradable Embolic Microspheres: A State of the     Art Review .....</b>	<b>8</b>
1.2.1. Abstract .....	9
1.2.2. Introduction .....	9
1.2.3. Methodology .....	12
1.2.4. Current State of the Art .....	14
1.2.4.1. PLGA .....	14
1.2.4.1.1. PLGA: Basic Chemistry and Mechanisms of Degradation ....	14
1.2.4.1.2. PLGA: Safety, Efficacy, and Performance .....	15
1.2.4.1.3. Key Advantages of PLGA Microspheres .....	19
1.2.4.1.4. Key Limitations of PLGA Microspheres .....	19
1.2.4.2. PLGA-PEG-PLGA .....	20
1.2.4.2.1. PLGA-PEG-PLGA: Basic Chemistry and Mechanisms of Degradation .....	20
1.2.4.2.2. PLGA-PEG-PLGA: Safety, Efficacy, and Performance .....	20

1.2.4.2.3. Key Advantages of PLGA-PEG-PLGA Microspheres .....	24
1.2.4.2.4. Key Limitations of PLGA-PEG-PLGA Microspheres .....	24
1.2.4.3. CMC-CNN .....	25
1.2.4.3.1. CMC-CNN: Basic Chemistry and Mechanisms of Degradation .....	25
1.2.4.3.2. CMC-CNN: Safety, Efficacy, and Performance .....	26
1.2.4.3.3. Key Advantages of CMC-CNN Microspheres .....	29
1.2.4.3.4. Key Limitations of CMC-CNN Microspheres .....	29
1.2.4.4. Chitosan .....	29
1.2.4.4.1. Chitosan: Basic Chemistry and Mechanisms of Degradation .....	29
1.2.4.4.2. Chitosan: Safety, Efficacy, and Performance .....	30
1.2.4.4.3. Key Advantages of Chitosan Microspheres .....	34
1.2.4.4.4. Key Limitations of Chitosan Microspheres .....	34
1.2.4.5 HEA .....	34
1.2.4.5.1. HEA: Basic Chemistry and Mechanisms of Degradation .....	34
1.2.4.5.2. HEA: Safety, Efficacy, and Performance .....	35
1.2.4.5.3. Key Advantages of HEA Microspheres .....	38
1.2.4.5.4. Key Limitations of HEA Microspheres .....	38
1.2.5. Preclinical Models .....	38
1.2.6. Conclusion .....	40
<b>1.3. Consolidated Design Inputs .....</b>	<b>41</b>
<b>1.4. Glasses as Candidate Embolic Agents .....</b>	<b>42</b>
1.4.1. Borate Glasses .....	43
1.4.2. Modifier Ions .....	45
1.4.2.1. Rubidium .....	46
1.4.2.2. Strontium .....	47
1.4.2.3. Gallium .....	48
<b>1.5. The Problem Statement .....</b>	<b>50</b>
 <b>CHAPTER 2: OVERARCHING THESIS OBJECTIVES .....</b>	 <b>51</b>

<b>CHAPTER 3: EXPERIMENT 1&amp;2: MULTI-MODAL IMAGEABILITY &amp; DEGRADATION CHARACTERISTICS OF BORATE NETWORKS .....</b>	<b>53</b>
<b>3.1. Abstract .....</b>	<b>56</b>
<b>3.2. Introduction .....</b>	<b>56</b>
<b>3.3. Methods .....</b>	<b>59</b>
3.3.1. Glass Synthesis .....	59
3.3.2. X-Ray Diffraction Analysis .....	60
3.3.3. Solid State NMR Spectroscopy .....	60
3.3.4. Glass Density .....	61
3.3.5. Thermal Analysis .....	61
3.3.6. Computed Tomography Imaging .....	61
3.3.7. Magnetic Resonance Imaging .....	62
3.3.8. Glass Cylinder Synthesis for Mass Loss Evaluation .....	62
3.3.9. Mass Loss Evaluation .....	63
3.3.10. Statistical Analysis .....	63
<b>3.4. Results .....</b>	<b>64</b>
<b>3.5. Discussion .....</b>	<b>73</b>
<b>3.6. Limitations .....</b>	<b>77</b>
<b>3.7. Conclusion .....</b>	<b>78</b>
<b>CHAPTER 4: EXPERIMENT 3: PILOT BENCHTOP MIGRATION AND PRE-CLINICAL PREPARATION .....</b>	<b>80</b>
<b>4.1. Part 1: Benchtop Migration Method Development .....</b>	<b>80</b>
4.1.1. Objective .....	80
4.1.2. Rationale .....	80
4.1.3. Materials & Methods .....	82
4.1.4.1. Model Set-Up .....	82
4.1.4.2. Experimental Design .....	82
4.1.4. Results and Discussion .....	83
4.1.5. Limitations and Future Considerations .....	86
<b>4.2. Part 2: Microsphere Synthesis and Embolization Effectiveness.....</b>	<b>87</b>
4.2.1. Objective .....	87

4.2.2. Hypothesis .....	87
4.2.3. Rationale .....	87
4.2.4. Materials & Methods .....	91
4.2.4.1. Glass Synthesis and Recharacterization .....	91
4.2.4.2. Spherical Processing and Recharacterization .....	91
4.2.4.3. Packaging and Sterilization .....	92
4.2.4.4. Statistical Analysis of Glass Properties .....	93
4.2.4.5. Pre-Clinical Protocol .....	93
4.2.5. Results .....	96
4.2.6. Discussion .....	100
4.2.6. Conclusion .....	104
<b>CHAPTER 5: CONCLUSIONS .....</b>	<b>106</b>
<b>REFERENCES .....</b>	<b>116</b>
<b>APPENDIX A .....</b>	<b>132</b>
<b>APPENDIX B .....</b>	<b>135</b>
<b>APPENDIX C: PRECLINICAL RESEARCH PROTOCOL .....</b>	<b>138</b>

## List of Tables

<b>Table 1.1:</b> Comparison of quality of life after UAE and hysterectomy .....	<b>5</b>
<b>Table 1.2:</b> Materials reviewed and generalized search parameters for PubMed and Web of Science .....	<b>12</b>
<b>Table 1.3:</b> Initial Returned Searches based on Table 1, with Articles Meeting Inclusion Criteria .....	<b>13</b>
<b>Table 1.4:</b> Pre-clinical safety summary for hydrolysis mediated degradable PLGA microspheres .....	<b>16</b>
<b>Table 1.5:</b> Pre-clinical safety summary for hydrolysis mediated degradable PEG-PLGA-PEG microspheres.....	<b>21</b>
<b>Table 1.6:</b> Pre-clinical safety summary for hydrolysis mediated degradable CMC microspheres .....	<b>27</b>
<b>Table 1.7:</b> Pre-clinical safety summary for hydrolysis mediated degradable Chitin microspheres.....	<b>31</b>
<b>Table 1.8:</b> Pre-clinical safety summary for hydrolysis mediated degradable HEA microspheres .....	<b>36</b>
<b>Table 1.9:</b> Mass attenuation and toxicity information for B, Rb, Sr and Ga .....	<b>46</b>
<b>Table 3.1:</b> Glass compositions by molar fraction (pre-fired material) .....	<b>60</b>
<b>Table 3.2:</b> 100% volume fraction values of R1, R2, and R2* extrapolated from given data .....	<b>71</b>
<b>Table 4.1:</b> Test and Control Article Allocation .....	<b>93</b>
<b>Table 4.2:</b> Characterization data of BRS2 glass frit .....	<b>97</b>
<b>Table 4.3:</b> Thermal Analysis Data for Frit versus Spheres .....	<b>99</b>
<b>Table 4.4:</b> Spherical Data and Particle Sizes of BRS2 Microspheres .....	<b>100</b>

# List of Figures

<b>Figure 1.1:</b> Vascular anatomy of uterine leiomyoma .....	2
<b>Figure 1.2:</b> Distribution, $x_i$ , of the borate basic structural unit species, $B^{(n)}$ , in monovalent substituted glasses. The solid lines correspond to the model distribution of (super)structural units .....	44
<b>Figure 3.1:</b> XRD analysis of A) 5 gallium series glass compositions and B) 5 strontium series glass compositions showing two amorphous peaks, at $2\theta$ values of approximately 25 and 45, corresponding to 3 and 4 coordinated boron centers in the glass.....	64
<b>Figure 3.2:</b> Particle size analysis of A) BRG series and B) BRS series where D90, D50 and D10 stand for particle diameters at 90%, 50% and 10% cumulative size, respectively. Error bars are plotted for all points, but are contained within the size of the symbol.....	64
<b>Figure 3.3:</b> $^{11}B$ MAS NMR line spectra of A) the BRS series, and B) the BRG series. The X value indicated the percentage of Sr or Ga substituted .....	65
<b>Figure 3.4:</b> Fraction of four coordinated boron content by mol% of substituted ion .....	66
<b>Figure 3.5:</b> Plot of B4 concentrations versus oxygen to boron ratios of the BRS series (overlapping blue squares) and the BRG series (red). The blue line marks the theoretical values predicted in alkali modified glasses (see text), and the orange points mark the estimated values when the B4 percentage is compared to both Ga and B as network formers (circle) and when all tetrahedral (B and presumably Ga) are compared to both Ga and B as network formers (dash) .....	66
<b>Figure 3.6:</b> A) Density and B) molar density analysis of all 11 glass compositions displayed by percentage of ion substitution. Error bars are plotted for all points, but are contained within the size of the symbol .....	67
<b>Figure 3.7:</b> Glass transition temperatures, both onset and inflection, of the BRS glass compositions .....	68
<b>Figure 3.8:</b> Glass stability ( $\Delta T = T_{p1} - T_g$ ) of the BRS glass compositions, calculated with both $T_g$ onset and $T_g$ inflection .....	68

<b>Figure 3.9:</b> CT radiopacity values of all 11 glass compositions at (A) 120 kVp and 80 kVp, and (B) 120kVp with comparisons. The dashed line at 7733 HU represents 40-150 $\mu\text{m}$ ORP5 radiopacity, and the dashed line at 2455 HU represents the radiopacity of half strength contrast media .....	<b>69</b>
<b>Figure 3.10:</b> MRI results for A) R1 values of i) BRG and ii) BRS, B) R2 values of i) BRG and ii) BRS, and C) R2* values of i) BRG and ii) BRS .....	<b>70</b>
<b>Figure 3.11:</b> MRI delta chi ( $\Delta\chi$ ) values for A) BRG compositions, and B) BRS compositions .....	<b>70</b>
<b>Figure 3.12:</b> Percentage dissolved by mass of A) the BRG series and B) the BRS series over 6, 12, 24, 36, and 48 hours .....	<b>72</b>
<b>Figure 3.13:</b> Slope of dissolution data vs composition for the BRS series .....	<b>72</b>
<b>Figure 4.1:</b> Benchtop renal artery model. (A) represents the fluid reservoir and the pump which approximates the heart. (B) indicates the area that has been modified to incorporate the capillary bed (C) denotes the percutaneous introducer used to insert the catheter (<20Fr) into the model for embolization .....	<b>82</b>
<b>Figure 4.2:</b> A) Complete setup of the benchtop model, B) stepwise reduction from the ‘renal artery’ to the ‘arteriole’ to the capillary bed .....	<b>83</b>
<b>Figure 4.3:</b> Reduction adaptor and micro-tubing filled with EmboSphere® suspended in DMEM following completion of one trial .....	<b>85</b>
<b>Figure 4.4:</b> Division System Method: D1 refers to the immediate and largest branches of the caudal artery, subsequent branches of this artery are labelled D2, further branches labelled D3, etc .....	<b>96</b>
<b>Figure 4.5:</b> A) XRD data for the BRS2 glass frit and the microspheres. Two amorphous peaks can be seen at $2\theta$ values of approximately 25 and 45, corresponding to 3 and 4 coordinated boron centers in the glass. B) Density and molar density data for the original BRS2 glass frit and the microspheres. C) Glass transition temperatures and glass stabilities (both onset and inflection) for the BRS2 glass frit and the microspheres. D) CT radiopacity for the BRS2 glass frit and the microspheres at 80 kVp and 120 kVp .....	<b>98</b>
<b>Figure 4.6:</b> SEM images of microspherical particles (100x) .....	<b>99</b>
<b>Figure 4.7:</b> The volume-temperature diagram for a glass-forming liquid, superimposed with the accompanying atomic structure. “L” signifies liquid phase, “G” signifies glass, and “X” signifies .....	<b>101</b>



## Abstract

Transarterial embolization (TAE) is a minimally invasive procedure proven to reduce health care costs and recovery times while maximizing quality of life for patients. Next generation microspheres for TAE are required to be degradable and exhibit multi-modal imageability. Accordingly, two series of borate networks were investigated as candidate degradable radiopaque embolic agents for use in uterine artery embolization (UAE). The effect of substitutions of SrO or Ga<sub>2</sub>O<sub>3</sub> for Rb<sub>2</sub>O on the structure and properties of borate networks was evaluated using density, differential scanning calorimetry, <sup>11</sup>B MAS-NMR, mass loss, CT and MRI experiments. The glasses exhibited high radiopacities (over 3200 HU) and various degradation timeframes (from under 6 hours to over 48 hours). To assess the safety and efficacy of novel degradable, imageable microsphere for use in UAE an *in vivo* animal study protocol was developed. Additionally, an *in vitro* methodology was developed to objectively assess the risk of migration.

## List of Abbreviations and Symbols Used

%	Percent
°	Degree
°C	Degree Celsius
$\Delta T$	Melt/Glass Stability
$\Delta\chi$	Delta Chi
$\lambda$	Wavelength
Å	Angstrom
A	Atomic Mass
ANOVA	Standard Analysis of Variance
ATP	Adenosine Tri-Phosphate
ATSDR	Agency for Toxic Substances and Disease Registry
B	Boron
B3	Three-fold Coordinate Boron
B4	Four-fold Coordinate Boron
BIC	Best In Class
BRMS	Bio-Resorbable Microspheres
C <sub>6</sub> NCL	N,N'-(dimethacryloyloxy)adipamide Crosslinker
CBCT	Cone Beam Computed Tomography
CCAC	Canadian Council on Animal Care
CHUM	Centre Hospitalier de l'Université de Montréal
cm	Centimeter
CMC	Carboxymethylcellulose
CMC-CNN	Carboxymethylcellulose-chitosan
CT	Computed Tomography
DEB TACE	Drug Eluting Bead Transarterial Chemoembolization
dFMEA	Design Failure Mode and Effect Analysis
DMEM	Dulbecco's Modified Eagle's Medium
DSC	Differential Scanning Calorimetry
FBS	Fetal Bovine Serum
FDA	Food and Drug Administration
g	gram
Ga	Gallium
Gy	Gray
HCl	Hydrochloric Acid
HEA	Hydroxyethyl acrylate
HU	Hounsfield Units
ICP-OES	Inductively Coupled Plasma Optical Emission Spectroscopy
ID	Inner Diameter
IEL	Internal Elastic Lamina
K	Potassium
kGy	Kilogray
kHz	Kilohertz
kVp	Peak kilo Voltage
La	Lanthanum

LOAEL	Lowest Observed Adverse Effect Level
LRA	Left Renal Artery
mg	Milligram
min	minute
mL	Milliliter
mm	Millimeter
mol	Mole
mol%	Mole Percent
MAS-NMR	Magic Angle Spinning Nuclear Magnetic Resonance
MRI	Magnetic Resonance Imaging
Na	Sodium
NaBH <sub>4</sub>	Sodium Borohydride
NBO	Non-Bridging Oxygen
NHS	National Health Service
NIST	National Institute of Standards and Technology
NMR	Nuclear Magnetic Resonance
NOAEL	No Observable Adverse Effects Level
NSAID	Nonsteroidal Anti-Inflammatory Drugs
NTE	Non-Target Embolization
O	Oxygen
PBS	Phosphate Buffered Saline
PEG	Polyethylene Glycol
PES	Post-Embolization Syndrome
PET	Positron Emission Tomography
PLA	Polylactic Acid
PLG	Polyglycolic Acid
PLGA	Polylactic-co-glycolic Acid
PSA	Particle Size Analysis
PVA	Polyvinyl Alcohol
Rb	Rubidium
RbF	Rubidium Fluoride
ROI	Region of Interest
rpm	Revolutions per Minute
RRA	Right Renal Artery
s	second
SD	Standard Deviation
SEM	Scanning Electron Microscopy
Sr	Strontium
TA	Test Article
TAE	Transarterial Embolization
TAG	Tris-Acryl Gelatin
TAGM	Tris-Acryl Gelatin Microspheres
TGMS	Tris-Acryl Gelatin Microspheres
T <sub>g</sub>	Glass Transition Temperature
T <sub>m</sub>	Melting Temperature
T <sub>p1</sub>	First Crystalline Peak

UAE	Uterine Artery Embolization
UFE	Uterine Fibroid Embolization
$V_f$	Volume Fraction
V-T Diagram	Volume-Temperature Diagram
wt%	Weight Percent
XRD	X-Ray Diffraction
$\mu\text{m}$	Micron
$\mu\text{s}$	microsecond
Z	Atomic Number

## Acknowledgments

First and foremost, I would like to thank my supervisor, Dr. Daniel Boyd for all the work you put into turning me into the student I am now (and I know that wasn't easy). You made it clear right from the beginning that you were going to do everything in your power to help get me to where I want to be, and I wouldn't have been able to do it without your enthusiasm and expertise. Even though you are officially old now, and ditched me for most of the year to go on sabbatical, I still think you're pretty cool.

I would also like to thank my committee members, Dr. Robert Abraham, Dr. Steven Beyea, and Dr. Mark Filiaggi for their time and energy. Your insightful comments and questions helped me to develop my research further, and answer questions more completely. Thank you very much for putting up with the early morning meetings, and for being so helpful and kind.

I would like to thank Dr. Kimberly Brewer, Dr. Elena Tonkopi, and Dr. Ulriki Werner-Zwanzinger for their expertise – both technical and intellectual – in their respective fields. Their willingness to share their immense knowledge with me helped to bring my project to new heights. It has been a privilege working with you all.

I would not have been able to complete this project without my labmates and group members, Dr. Kathleen MacDonald-Parsons Dr. Kathleen O'Connell, Dr. Alicia Oickle, and soon to be (different kind of) Dr. Lauren Kiri. You guys have put up with my stupid questions and annoying tendency to be around when everything breaks, and for that I want to thank you. Even though most of you ditched me at the end for bigger and better things, I'm so glad to have met you. I also want to thank my office pals, Brendan, Camryn, Hayden, Kat (again), Taylor, and Tyler for always being available for a chat and a laugh.

I would like to acknowledge the financial assistance of NSERC that made this project possible.

Last but certainly not least, I would like to thank my family for their continuing love and support. To my parents, Cyndy and Gerry: Thank you for helping me get through the hard parts and taking time to celebrate the good parts. You are the strongest people I know and I love you to MB and back. To my siblings/pseudo-children, Breton, Camryn, and Aidan: I would like to say that even though you are a pain in my neck and take up energy & time I should be spending on my research, I wouldn't want it any other way. I love you all so much and am grateful for you each and every day. Camryn, I want to thank you specially for putting up with my crazy school schedule and helping me complete this project; you're the best room/labmate a girl could ask for.

Halifax, June 2018  
Jensen Doucet

# CHAPTER 1

## Introduction

The fundamental objective of this thesis is to examine the composition-structure-property relationship of ternary, high borate glass networks, and to assess their potential as novel degradable, imageable embolic agents. The specific clinical context for this work involves the management of hypervascular tumors, specifically uterine leiomyomas. To fully understand the results of this study, this chapter provides an overview on uterine leiomyomas, existing treatment approaches, and limitations with current embolic materials.

### 1.1. Uterine Leiomyoma

Uterine leiomyomas are the most common benign tumors of the female reproductive tract for premenopausal women [1]. The exact prevalence of the disease is difficult to ascertain due to their low symptomatic nature in many patients; however, it is accepted that uterine leiomyomas are present in up to 70% of women of reproductive age [2,3]. Although technically benign, leiomyomas may cause a variety of debilitating symptoms such as heavy bleeding, pain, subfertility, pelvic pressure, dyspareunia, urinary frequency and urgency, and other pelvic symptoms. Treatment of leiomyomas is provided when patients experience severely uncomfortable symptoms, particularly those that inhibit day-to-day tasks and compromise quality of life [1,2]. Generally, their overall incidence is reported to be 29.7 per 1000 patient/year, with peak incidence occurring among women who are in their early to mid-40s [1].

#### 1.1.1. Pathophysiology of Uterine Leiomyomas

Uterine leiomyomas are benign monoclonal tumors of the uterus composed of smooth muscle cells and an extracellular matrix of collagen, fibronectin, and proteoglycans [1]. Their etiology remains unclear; however it is believed that the growth of leiomyomas is affected by the presence of growth factors such as estrogen and progesterone, as leiomyomas are not seen in children and regress after menopause [1]. As they develop, leiomyomas cause enlargement of the uterus. Leiomyomas located in a submucosal

position, as well as intramural leiomyomas that abut the endometrial lining (Fig 1.1) are associated with heavy menstrual bleeding. Additionally, the presence of large leiomyoma, with overall enlargement of the uterus, is associated with local pressure, pain, or compressive effects [1].

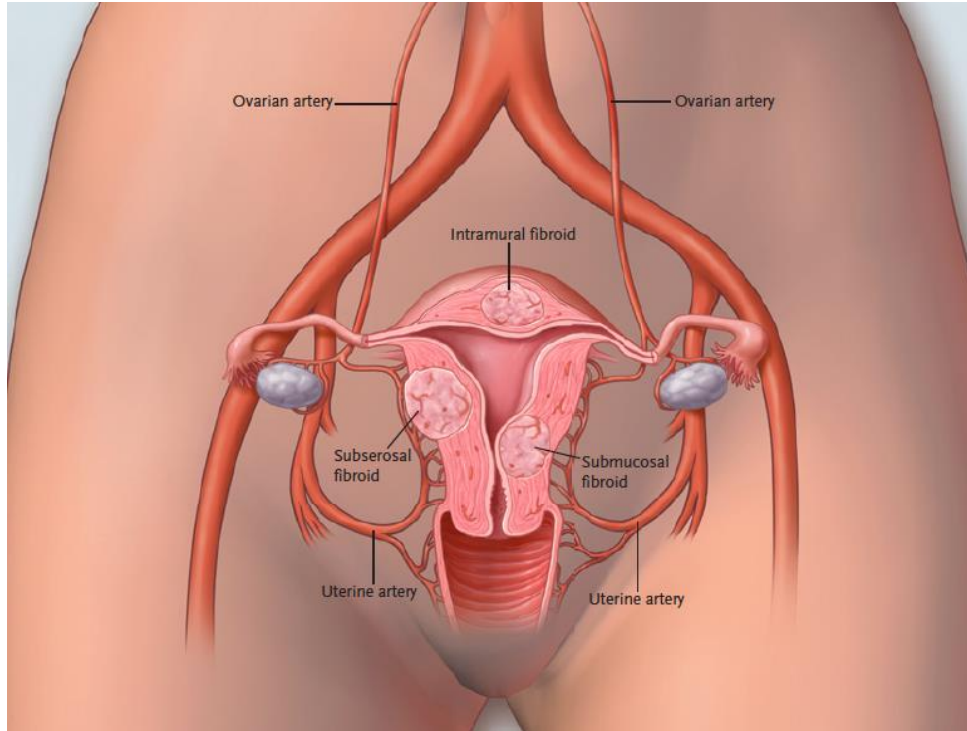


**Figure 1.1:** Vascular anatomy of uterine leiomyoma [1]

From a vascular anatomy standpoint, 90-95% of leiomyomas receive their blood supply from the uterine artery, with perfusion from the ovarian artery being present in *ca.* 5 - 10% of cases [1,4]. Anastomoses between the left and right uterine arteries occur in *ca.* 10% of patients, and between the uterine and ovarian arteries in *ca.* 10 - 30% of patients. Furthermore, it is important to note that a dense arterial plexus typically surrounds these tumors, whereas the center of the leiomyoma itself is relatively hypovascular [1].

### **1.1.2. Current Treatments**

In some cases, medicinal intervention is sufficient for the treatment of symptomatic uterine leiomyomas. Acetaminophen and nonsteroidal anti-inflammatory drugs (NSAIDs)

are often effective for the relief of pain, although these drugs do not reduce bleeding [1]. Gonadotrophin releasing hormone-analogues can effectively reduce bleeding and decrease leiomyoma size; however, they can only be used for a limited time because of their adverse effect on bone mass [2]. Other hormone therapies are considered in the literature, including: (i) a combination of oral contraceptive pills, which are effective at decreasing heavy menstrual bleeding, but are generally not recommended as they have no effect on decreasing leiomyoma size, or (ii) Danazol, an antiestrogenic therapy, which decreases leiomyoma size and increases hemoglobin concentrations but commonly causes unwanted side effects (e.g. painful muscle cramps, edema, depression, etc.) [3]. In addition to these limitations it is important to understand that many patients wish to avoid hormonal therapy and/or do not tolerate it well [1].

#### 1.1.2.1. Surgical Options

Many women with symptomatic leiomyomas seek surgical options for treatment. To clarify, it is estimated that 30-70% of the ~ 600,000 hysterectomies performed each year in the USA are uterine leiomyoma related [2]. In fact, leiomyomas are the most common indication for hysterectomy in the USA. The total direct cost for treating leiomyomas was estimated to range from US\$4.1 to \$9.4 billion in 2010 [5], and more than 70% of those costs were directly related to hysterectomies [1]. In addition to hysterectomy, patients may also be eligible for other surgical treatments of leiomyomas including, for example, hysteroscopic endometrial ablation, trans-cervical resection of the submucous myoma, laparoscopic myomectomy, laparoscopic bipolar coagulation and/or dissection of uterine vessels, or myomectomy [2].

Uterine-artery embolization (UAE), frequently referred to as uterine fibroid embolization (UFE), was introduced in 1995 as an alternative technique for the treatment of leiomyomas. Since then, UAE has become increasingly accepted as a minimally invasive, uterine-sparing procedure [6]. UAE involves occlusion of the uterine arteries with particulate emboli. The intention is to cause ischaemic necrosis of the uterine leiomyomas, without permanent adverse effects on otherwise healthy tissues (supported by a healthy myometrium which can rapidly establish new blood supply through collateral vessels from the ovarian and vaginal circulations) [2]. Myomas appear to be fed by end arteries, and are



therefore preferentially affected by the temporary reduction in flow; accordingly, UAE leads to an average decrease in myoma volume of 30-50% [2]. The treated leiomyomas shrink over the course of several months to years and, in general, a successfully treated leiomyoma will be permanently devascularized [1].

Surgical intervention for the treatment of uterine leiomyomas, like all surgeries, comes with potential risks. Hysterectomies have *ca.* 3% incidence of major complications [2]. Myomectomies have a less well-defined incidence of major complications, but are associated with long-term problems such as leiomyoma reoccurrence, adhesion formation, and an increased probability of uterine rupture during pregnancy and vaginal delivery [2].

Similar to myomectomy, UAE is a uterine-sparing procedure, and the American College of Obstetricians and Gynecologists agree that “uterine artery embolization is a safe and effective option for appropriately selected women who wish to retain their uteri” [2,6]. However, UAE does come with its own set of complications. According to a review by Gupta *et al.*, while there are no significant differences in major complication rates between UAE and hysterectomies, UAE does present more minor complications within 42 days of discharge including, for example, vaginal discharge, post puncture hematoma, and post embolization syndrome. [2]

Clinical data (Level 1) examining UAE versus surgical treatment for leiomyomas exists [6]; for example, in a multicenter study of 157 patients, randomly assigned to either surgery (hysterectomy or myomectomy) or embolization, the investigators found no differences in quality of life measures between both groups after treatment. However, a higher incidence of major adverse events occurred in the surgical group during the initial hospital stay. It is worth noting that the reverse was true after discharge. In particular, ten re-interventions occurred for patients in the embolization group in the following 12 months due to treatment failure, with an additional eleven re-interventions during the subsequent follow-up period of 32 months [1,6]. The REST investigators showed that embolization leads to a shorter hospital stays than hysterectomies (Table 1.1), and allowed patients to return to regular day-to-day activities more quickly. It can also be seen that the embolization group showed a lower mean score on the pain index [6]. These data indicate the objective benefits and risks associated with UAE and indicate it as an effective treatment measure in the management of uterine leiomyoma.

**Table 1.1:** Comparison of quality of life after UAE and hysterectomy. Adapted from [6]

Effect	Embolization Group (N=106)	Surgical Group (N=51)	Percent Difference (95% CI)	P Value
<b>At 1 month</b>				
No. of patients	95	47		
<b>Score</b>				
Physical function	85 ± 16	57 ± 25	-26 (-32 to -20)	<0.001
Physical role	37 ± 44	11 ± 24	-25 (-38 to -12)	<0.001
General health	70 ± 19	74 ± 17	4 (-1 to 10)	0.13
Vitality	47 ± 22	42 ± 24	-6 (-13 to 1)	0.11
Social function	64 ± 27	44 ± 29	-19 (-28 to -9)	<0.001
Emotional role	72 ± 41	64 ± 44	-7 (-22 to 7)	0.32
Mental Health	72 ± 17	74 ± 18	2 (-3 to 8)	0.39
<b>24-hour pain score</b>				
No. of patients	99	49		
Score	3.0 ± 2.1	4.6 ± 2.3	1.6 (0.8 to 2.3)	<0.001
<b>Hospital stay &amp; time to resumption of usual activities (days)</b>			<b>95% CI</b>	
Hospital Stay			3 to 4	<0.001
Median	1	5		
Interquartile range	1-2	3-6		
<b>Drove car</b>				
Median	8	34		<0.001
Interquartile Range	5-10	27-43		
<b>Returned to work</b>				
Median	20	62		<0.001
Interquartile Range	14-30	39-90		
<b>Had sexual intercourse</b>				
Median	21	53		<0.001
Interquartile Range	13-31	29-91		

In addition to being beneficial to patient health, UAE is also cost effective, a feature which encourages further adoption. In the USA, it is estimated that leiomyomas now have an annual direct cost of up to US\$9.4 billion, which includes surgery, hospital admissions,

outpatient visits, and medications [5]. Accordingly, any progress towards cost reduction, without additional risk to patients, is beneficial from a cost containment perspective. The National Health Service (NHS) of Great Britain and Northern Ireland has established that embolization is more cost-effective than surgery for patients with symptomatic uterine leiomyomas. In particular it has been determined that UAE had a mean decrease in cost of £951 (\$1,712 at an exchange rate of £1 = \$1.80) over hysterectomies, and remained a cost-effective option even when the assumed cost of follow up imaging was increased [6]. A similar study conducted in the USA supports the UK data, showing the average total cost of UAE (including follow up and morbidity costs) until menopause to be \$6,915, vs. \$7,847 for hysterectomies [7].

#### 1.1.2.2. Commercially Available UAE Microspheres

While there are many types of products available for uterine artery embolization – ranging from coils, to balloons, to liquids [8] – embolic agents consisting of micro-particles are the focus of this thesis. Tris-acryl gelatine (TAG) in the form of EmboSphere® and PVA microspheres are amongst the most commonly used for UAE [8]. Both particles are spherical in shape, minimizing the risk of particle aggregation and catheter occlusion. PVA and TAG microspheres operate via similar mechanisms of occlusion: permanent occlusion leading to an inflammatory reaction and focal angionecrosis, with vessel fibrosis developing over time [8]. Multiple studies have shown no significant differences in the outcomes of procedures done with either of the particles [9,10], and they are cheap, easy to use and effective [11]. These particles afford consistent controllable embolization at defined levels in the vascular bed and may also be used as drug delivery systems should this be so desired [12].

A prominent characteristic of these materials is their compressibility (more so in TAG particles), allowing for essentially effortless delivery through a catheter [12,13]. It has been shown, however, that many failure mechanisms of embolization therapy such as particle deformation and lack of durable occlusion are directly related to compressible beads [13]. These particles are also radiolucent and permanent, inhibiting visualization of the particles themselves and recanalization, respectively. Recently, patients have expressed concerns about foreign materials remaining in their body indefinitely, and therefore are

more partial to degradable embolic agents. To assess the range of products being developed to address the need for degradable embolic agents, a state of the art review of current preclinical degradable technologies available was conducted and published in the Journal of Functional Biomaterials in January of 2018.

## **1.2. Advances in Degradable Embolic Microspheres: A State of the Art Review**

**Jensen Doucet<sup>1</sup>, Lauren Kiri<sup>2</sup>, Kathleen O’Connell<sup>2</sup>, Sharon Kehoe<sup>3</sup>, Robert J. Lewandowski<sup>4</sup>, David M. Liu<sup>5</sup>, Robert J. Abraham<sup>6</sup>, Daniel Boyd<sup>3</sup>**

<sup>1</sup> School of Biomedical Engineering, Dalhousie University, Halifax, NS Canada

<sup>2</sup> Department of Applied Oral Sciences, Dalhousie University, Halifax, NS, Canada

<sup>3</sup> ABK Biomedical Inc., Halifax, NS Canada

<sup>4</sup> Department of Radiology, Division of Vascular and Interventional Radiology, Fienberg School of Medicine, Northwestern University, Chicago, IL, USA

<sup>5</sup> Department of Radiology, University of British Columbia, Vancouver, BC, Canada

<sup>6</sup> Interventional Radiology and Diagnostic Imaging Department, QEII Health Sciences Center, Halifax, NS, Canada

This manuscript was written by the candidate (Jensen Doucet) under the supervision of Dr. Boyd, who provided guidance and assistance throughout all aspects of the review. Ms. Doucet searched the databases for the determined search terms, reviewed each abstract, filtered abstracts based on the pre-determined inclusion/exclusion criteria, and wrote the preliminary draft of the manuscript based on FDA guidance documentation. Dr. O’Connell and Ms. Kiri aided in the review of the selected articles, as well as with the editing of the manuscript. Dr. Kehoe, Dr. Lewandowski, Dr. Liu, and Dr. Abraham provided clinical and technical oversight, reviewed the final manuscript and proposed suggestions with respect to the clinical significance of the review. Published in the Journal of Functional Biomaterials on Jan 26, 2018.

### **1.2.1. Abstract**

Considerable efforts have been placed on the development of degradable microspheres for use in transarterial embolization indications. Using the guidance of the U.S. Food and Drug Administration (FDA) special controls document for the preclinical evaluation of vascular embolization devices, this review consolidates all relevant data pertaining to novel degradable microsphere technologies for bland embolization into a single reference. This review emphasizes intended use, chemical composition, degradative mechanisms, and pre-clinical safety, efficacy, and performance, while summarizing the key advantages and disadvantages for each degradable technology which is currently under development for transarterial embolization. This review is intended to provide an inclusive reference for clinicians that may facilitate an understanding of clinical and technical concepts related to this field of interventional radiology. For materials scientists, this review highlights innovative devices and current evaluation methodologies (i.e. preclinical models), and is designed to be instructive in the development of innovative/new technologies and evaluation methodologies.

### **1.2.2. Introduction**

Over the past decade, there has been growing interest in the development of degradable microspheres for transarterial embolization (TAE) procedures, especially for applications in trauma, gastrointestinal bleeding, and for the treatment of uterine leiomyoma. Degradable microspheres are intended to provide effective embolization on a transient basis. Ideally, after achieving their clinical outcome, they are removed from the body without interfering with the functionality of other organs. Unlike conventional permanent agents, degradable microspheres should be designed to optimize the window of therapeutic intent (e.g., embolization). In so doing, these agents may then balance therapeutic requirements, while minimizing the potential of long-term sequelae because of permanent alterations in histological architecture, vascular capacitance and/or injury to both ‘on target’ and ‘off target’ deposition of therapy. A significant driver for the development and utilization of degradable microspheres is that “patients commonly express worries about foreign materials remaining in the body”, and while this may not be a physiological problem, it is certainly an important consideration for patients and may

provide competitive marketing advantages for next generation technologies [14].

Although the safety, efficacy, and performance of permanent embolic agents are well established in the clinical literature, degradable microspheres may present new safety concerns. Fortunately, when developing new biomaterials for clinical applications, researchers benefit from the existence of international standards and guidance documents to help address potential risks. With respect to vascular embolization devices, specific guidance documents have been published by regulatory agencies. For example, in 2004 FDA published a document entitled: “Class II Special Controls Guidance Document: Vascular and Neurovascular Embolization Devices”, which lays out special controls for establishing the preclinical safety and efficacy of bland embolic microspheres. This document emphasizes (i) ease of deliverability (from a friction and tortuosity standpoint), (ii) acute complications, (iii) local and systemic foreign body reactions, (iv) recanalization, (v) embolization effectiveness, and (vi) device migration. Given the potential new safety risks that may arise from the use of degradable microspheres, these considerations are critical in the design and evaluation of new microsphere technologies.

Further to such guidance documents, it is also instructive to consider the ideal characteristics of degradable microspheres. These innovative technologies must provide predictable and effective occlusion while also providing:

1. Tailored degradation timeframes—to provide adequate infarction to the target tissues in a variety of indications, subsequently allowing return of flow (e.g., 5–7 h for uterine artery embolization—based on Doppler-guided transvaginal clamping) [15]
2. A variety of tightly calibrated particle size distributions—to optimize particle delivery according to target artery anatomy [16]
3. Ease of delivery through conventional microcatheters—to facilitate adoption of the novel technology into established embolization techniques
4. Full biological compatibility as per the relevant sections of ISO-10993—to minimize safety concerns [17]
5. Multi-modal imageability (e.g., fluoroscopy, CT)—to allow for efficiency and standardization of embolization endpoints [18].

While most of the above points are reasonably self-evident, the last point of multi-modal imageability raises an important and additional design consideration. Specifically, an

understanding of the temporal and spatial distribution of embolic microspheres is clinically beneficial [18], with the assurance that degradation byproducts should not, for instance, generate artifacts arising from degradation.

Prior to developing this article further, readers new to TAE are encouraged to review technical information on techniques and therapies, for example “Transcatheter Embolization and Therapy; Techniques in Interventional Radiology” [16]. It is also important to clarify the definitions and terms utilized in the literature related to degradable microspheres. Terms such as ‘resorbable’ and ‘absorbable’ (with or without the prefix “bio”) are commonly utilized to describe these technologies. However, it must be acknowledged that these terms, which are often used as synonyms for one another, are poorly defined and that despite significant efforts to find consensus about such terms, no agreed consensus in the interventional radiology or broader biomaterials literature exists [19]. Conversely, terms such as ‘degradation’ or ‘degradable’ are scientifically defined throughout the literature. Broadly, degradation refers to “a deleterious change in the chemical structure, physical properties and appearance of materials” [20]. More specifically, and within the context of TAE, degradation may be defined as the cleavage of bonds arising from oxidation, hydrolysis, or enzymatic activity, ultimately culminating in the complete removal of the agent from the human body. Preferably, the degradation mechanism(s) and concomitant byproduct(s) provoke minimal adverse local and systemic responses. For clarity, the remainder of this review will utilize the term ‘degradable’ as per the aforementioned definition.

Based on the special controls described by FDA, as they relate to degradable microspheres for TAE applications, this paper intends to consolidate the highest levels of preclinical evidence relating to the safety, efficacy, and performance of new technologies which are under development as degradable microspheres – specifically, those that are in development for bland embolization procedures. This paper is structured to cross-reference microsphere compositions with the special controls provided by the FDA. This format was deliberately chosen to provide a robust framework for discussing the current state of the art technologies with respect to potential risks that may need to be considered as part of a design control process for the development of new degradable microsphere technologies. Finally, a review of the preclinical models utilized by the identified papers will be provided



to further highlight the current understanding of the safety, efficacy, and performance of degradable microspheres.

### 1.2.3. Methodology

To clearly establish the new materials, which are under development for bland TAE indications, an initial search strategy was completed using search strings with descriptive characteristics for degradable microsphere technologies (e.g., degradable, bioresorbable, bead, microsphere). A summary of the materials identified from this formative analysis is provided in Table 1.2. Subsequently, each material type was cross-referenced with the peer-reviewed literature using the standard search parameters outlined (Table 1.2). ‘Web of Science’ and ‘PubMed’ databases acted as primary sources for peer-reviewed literature. Retrieved abstracts were reviewed by Jensen Doucet, Daniel Boyd, Kathleen O’Connell, and Sharon Kehoe.

**Table 1.2:** Materials reviewed and generalized search parameters for PubMed and Web of Science

Material Type	Acronym (if applicable)	Standard Search Parameters
Poly (lactic-co-glycolic acid)	PLGA	“Material Type” <sup>**</sup> AND “Microsphere” “Material Type” AND “Embolization”
PLGA-Polyethylene Glycol-PLGA	PLGA-PEG-PLGA	“Material Type” AND “Occlusion” “Material Type” AND “Arterial”
Carboxymethylcellulose	CMC	“Material Type” AND “Radiology”
Chitin		“Material Type” AND “Bead”
Hydroxyethyl acrylate	HEA	“Material Type” AND “Resorbable”
Albumin*		“Material Type” AND “Bioresorbable”
Gelatin		“Material Type” AND “Degradable”
Pluronic F127		“Material Type” AND “Bioabsorbable”
Polyvinyl alcohol	PVA	
Starch		

\* “Albumin” + “arterial” was excluded due to the arterial presence of albumin.

\*\*Note: The words ‘material type’ was replaced in each search by a given material of interest from the left-hand column. Each material type was fully searched as per the search parameters in Table 1.

Eligibility of the papers was established in line with the objectives of this work; specifically, the inclusion criteria adhered strictly to (1) preclinical studies with established control articles (i.e., tris-acryl gelatin, gelatin sponge, PVA), which were (2) directly associated with bland embolization indications and having (3) microspherical morphologies. Papers not meeting these criteria were excluded from the review, along with papers associated with *in vitro* studies, degradable microspheres for chemoembolization, and opinion-based articles. Included articles are identified and summarized in Table 1.3. Degradable microspheres intended for use as drug-eluting beads for transarterial embolization have been excluded from this review on the basis that no FDA guidance documents exist with respect to establishing the safety, efficacy, and performance of this type of drug device combinations for TAE.

**Table 1.3:** Initial Returned Searches based on Table 1, with Articles Meeting Inclusion Criteria.

Material Type	Initial Returned Searches	Articles Meeting Inclusion Criteria	Article Title
PLGA	1,662	1	A Preclinical Study of the Safety and Efficacy of Occlusin™ 500 Artificial Embolization Device in Sheep
PLGA-PEG-PLGA	985	2	A Novel Resorbable Embolization Microsphere for Transient Uterine Artery Occlusion: A Comparative Study with Trisacryl-Gelatin Microspheres in the Sheep Model
			Targeting and Recanalization after Embolization with Calibrated Resorbable Microspheres versus Hand-cut Gelatin Sponge Particles in a Porcine Kidney Model
CMC	417	1	Calibrated Bioresorbable Microspheres: A Preliminary Study on the Level of Occlusion and Arterial Distribution in a Rabbit Kidney Model
Chitin	585	1	Chitin-based Embolic Materials in the Renal Artery of Rabbits: Pathologic Evaluation of an Absorbable Particulate Agent
Hydroxyethyl acrylate	65	1	Transcatheter embolization using degradable crosslinked hydrogels
PVA	2,014	0	
Albumin	6,751	0	
Gelatin	2,347	0	
Pluronic F127	41	0	
Starch	2,083	0	
<b>TOTAL</b>	<b>16,950</b>	<b>6</b>	

#### **1.2.4. Current State of the Art**

Based on the search methods, five materials were identified as candidates for review in this paper. The materials are summarized in Table 1.3, and comprise: Polylactic-co-glycolic acid (PLGA), PLGA-Polyethylene glycol (PEG)-PLGA, Carboxymethylcellulose-chitosan (CMC-CCN), Chitosan, and Hydroxyethyl acrylate (HEA). Although Chitin was the search term originally entered, its derivative in microsphere form (Chitosan microspheres) warranted inclusion within the assessment, as the chitin agents were all irregular particles. This paper is structured to deal with each of these materials individually based on (1) their basic chemistry as it pertains to their mechanism(s) of degradation, and (2) their respective safety, efficacy, and performance data tabulated against the specific risk mitigation requirements identified by FDA [17]. Further information on the details of the individual parameters regarding safety, efficacy, and performance, can be found in the Class II Special Controls Guidance Document provided by FDA [17]. Finally, the paper provides a brief commentary on preclinical investigation methodologies utilized by those articles included for review.

##### **1.2.4.1. PLGA**

###### ***1.2.4.1.1. PLGA: Basic Chemistry and Mechanisms of Degradation***

PLGA is a hydrophobic, degradable polymer commonly used in drug delivery and medical sutures [21]. It is a linear co-polymer that can be synthesized with different ratios of lactic and glycolic acids [22]. The monomers are linked with an ester bond and, depending on the ratio of lactic acid to glycolic acid used in polymerization, different forms of PLGA can be obtained with variable degradation rates [23]. These forms are usually identified based on the ratio of monomers used; for example, PLGA 75:25 identifies a copolymer consisting of 75% lactic acid and 25% glycolic acid [24]. In general, low molecular weight PLGA has been found to degrade more quickly than high molecular weight PLGA, most likely due to its decreased entanglements, allowing water to penetrate the structure more readily and hydrolyze the ester bonds [21]. The degradation of PLGA is well understood and described in detail elsewhere [25-27]. Succinctly, PLGA degrades *in vivo* by hydrolysis of the ester bonds between polylactic acid (PLA) and polyglycolic acid

(PGA), yielding PLA and PGA as degradation byproducts [22]. PLA undergoes further hydrolysis to produce monomers, which are metabolized to form lactic acid and then easily excreted through normal cellular activity or converted to glucose to produce adenosine triphosphate [28-30]. The degradation of PGA *in vivo* follows this same process, however the monomer produced is glycolic acid, which is excreted via the kidney or converted to pyruvate for use in the tricarboxylic acid cycle.

#### *1.2.4.1.2. PLGA: Safety, Efficacy and Performance*

This review identified 1662 articles relating to PLGA based on the search parameters identified in Table 1.2. Only one of these papers met the inclusion criteria; the remainder of the articles were substantially focused on *in vitro* studies and materials for chemoembolization. The article that met the inclusion criteria was published by Owen *et al.* in 2012 [31] and provides a comprehensive and detailed analysis of the safety and efficacy of PLGA-based microspheres for TAE. This paper utilized a uterine artery sheep model over a period of 12 months, with animals divided into four cohorts (1, 3, 6, and 12 months). The control article was EmboSphere® (300–500 µm, Merit Medical Systems Inc., South Jordan, UT, USA). A summary of the article's findings versus the specific animal testing requirements to establish safety and efficacy as per FDA are provided in Table 1.4.

**Table 1.4:** Pre-clinical safety summary for hydrolysis mediated degradable PLGA microspheres.

Authors and year of publication	Study Model & Duration	Test Material Information.	Ease of use	Time to Complete Degradation of Test Material	Recanalization	Acute Complications (Vessel rupture / perforation)	Local and Systemic Foreign Body Reactions	Embolization Effectiveness.	Device Migration
Owen et. al. (2012)	Uterine Artery Sheep Model  32 Suffolk cross sheep (Mean weight <i>a.</i> 60kg)  Study duration: 12 months. Cohorts at 1, 3, 6 and 12 months.  Control material: EmboSphere® 300-500 µm	PLGA  150-212 µm  No particle size distribution analysis is provided.	UA selectively catheterized with either 2.3F Rapid Transit or 2.3F Prowler (Cordis Corporation).  Fluoroscopic time to achieve stasis was comparable for the test article (8.9 ± 2.7 min) and EmboSphere® (8.1 ± 3.6 min)  Suspensions in “a solution of normal saline and contrast medium” were noted as being “easily delivered to target vasculature” using a 2.3F catheter.	Test material still present at 1 and 3 months. By 6 months the authors state that no residual material was observed, but occlusion remained persistent due to the presence of fibrous connective tissue.	3/4 animals treated with test article showed recanalization at 12 months. Recanalized vessels showed normal luminal architecture “histologically indistinguishable from the untreated contralateral vessel”  No recanalization in EmboSphere® cohorts.	Vessel rupture not assessed. None reported.	Standard hematology and clinical chemistry parameters were performed prior to procedures and at 1, 7, 14 days, and thereafter at 1, 3, 6 and 12 months. No differences at any time point were reported between the test and control materials.  At 1 month, fibrous connective tissue observed around test material, which by 3 months fully occludes treated vessels and persists at 6 months.  By 12 months vessels treated with test material were fully recanalized and had similar architecture to untreated vessels.  Microspheres of both types were embedded in a thin collagen matrix with small numbers of macrophages and occasional giant cells present in close proximity. However, inflammation was not a significant feature of the reaction to either type of microsphere.	Determined as being equivalent to EmboSphere® up to at least 6 months.	Not directly addressed.  Histology showed test articles present in all 12 (100%) treated uterine arteries and in 1 untreated uterine artery, but not in vaginal, ovarian, or vesical vasculatures of any animal.  Control articles were detected in all 16 (100%) treated uterine arteries, 6 (40%) untreated uterine arteries, as well in the vaginal vasculature of 10 (63%) animals, ovarian vasculature of 2 (13%), and Vesical vesicle vasculature of 1 (6%) animal.

Degradable PLGA microspheres have already been approved by FDA and are available on the market under the brand name Occlusin® 500 Artificial Embolization Device from IMBiotechnologies Ltd. (Edmonton, AB, Canada) [31,32]; however human clinical studies have not been published up to the period leading to literature review. To assess the safety, efficacy, and performance of these microspheres, Owen *et al.* used a particle size distribution of 150–212  $\mu\text{m}$ , comparing this to a conventional product, EmboSphere®, with a size range of 300–500  $\mu\text{m}$  in a sheep model [31]. This PLGA particle size range selected by Owen *et al.* is substantially smaller than that used in most clinical indications, such as hepatic and renal tumor embolization (e.g., 300–500  $\mu\text{m}$ ) and uterine fibroid embolization (e.g., 500–700  $\mu\text{m}$ ), as well as the control article included in this paper [16,31]. However, it is reasonable to assume this small particle size represents a higher risk with respect to biological response (i.e., higher surface area) and migration, and therefore safety risks in this study were evaluated using approximated worst-case conditions. With regards to delivery, Owen *et al.* reported that it was possible to suspend and visualize the PLGA microspheres in conventional contrast media, and that the microspheres were “easily delivered to target vasculature” using a standard 2.3-French microcatheter without clogging the syringe [31]. The authors note, similar to other published literature, that no significant difference in (i) the volume of test and control materials delivered or (ii) the fluoroscopic times required to achieve effective stasis for either product [33].

The PLGA microspheres were shown to degrade in *ca.* six months; however occlusion persisted up to nine months due to the presence of fibrous ingrowth [31]. Initially, occlusion was mechanical in nature due to aggregation of microspheres within the target vessel. This shifted over time to include biological occlusion at one month and three months, as fibrous ingrowth formed “a matrix that held the microspheres in place as they degraded”, maintaining complete occlusion of the treated artery at six months despite the complete degradation of the PLGA microspheres [31]. This is an anticipated biological response given the acidic nature of the degradation byproducts arising from PLGA [34]. By 12 months, normal vessel luminal architecture was observed to be “histologically indistinguishable from the untreated contralateral vessel”, suggesting vessel recanalization (The term ‘recanalization’ is used in a variety of ways in the literature, ranging from re-opening of the occluded vessel to the formation of new vasculature [31]. In this study, the

term appears to refer to the reopening of the vessel that has been embolized) [31]. Although PLGA is considered to be a degradable embolic agent in the literature and does technically degrade *in vivo*, this extended occlusion time may not meet the intended purpose of degradable microspheres or be suitable for the indications proposed for such products (e.g., <24 h for Uterine Artery Embolization (UAE) [35]). Furthermore, based on its contact type and duration (>30 days), PLGA is technically categorized as a permanent agent according to ISO 10993-1, the international standards used to assess the biological performance of medical devices [36].

Acute complications, such as vessel rupture and perforation, were not assessed in this paper. However, it is reasonable to assume that these complications are not likely a risk associated with PLGA given that it has been cleared by FDA. Further to the generation of fibrous tissue as discussed, both the PLGA and control microspheres were associated with a small number of macrophages and occasional giant cells. Nevertheless, the authors state that “inflammation was not a significant feature of the reaction to either type of microsphere” [31] and no significant systemic foreign body reactions were reported on hematological and clinical chemistry analyses.

Although the risk of migration did not appear to be directly assessed by Owen *et al.*, the authors noted that the control microspheres were detected in non-target vasculature including vaginal, ovarian, and vesicle arteries (63%, 13%, and 6% of the animals, respectively). Conversely, PLGA microspheres were not observed in these structures. This difference may be explained by the compressibility of the control microspheres [37], which likely facilitated passage of the material through small diameter anastomoses joining the uterine artery with the vaginal and ovarian arteries [38]. Furthermore, and perhaps more concerning, was the presence of particles in the vesicle artery, as this was likely a result of reflux out of the uterine artery back into the umbilical artery, resulting in possible non-target embolization [38]. The authors attributed the lack of retrograde flow (reflux to vesicle artery) observed with PLGA to its increased density over the control; it is important to point out that biological occlusion (in the form of fibrotic encapsulation) likely secures the PLGA microspheres at the target level [31]. These observations are of import with respect to designing degradable microspheres. Firstly, inherent to the design, the degradation must be predictable and proceed in a manner that avoids complications

associated with non-targeted embolization due passage of smaller particles through the target vascular bed. This may raise safety concerns with respect to the clinical utility of materials designed to degrade in a timeframe shorter than that associated with the development of a sufficient foreign body response (encapsulation of material at the target area), which may mitigate the risk of migration. For example, it is considered in the literature that degradation timeframes of *ca.* 24 h are sufficient for UAE [15]; however, the host response at this time point likely represents transient edema and migration of inflammatory cells without fibrosis. Dichotomously, engineering microspheres that degrade over time periods sufficient to cause biological responses, suitable to mitigating migration risk (i.e., fibrous ingrowth), may contradict the design requirement underpinning the development of degradable microspheres—balancing therapeutic requirements while minimizing collateral damage to adjacent tissue.

#### *1.2.4.1.3. Key Advantages of PLGA Microspheres (Occlusin® 500 Artificial Embolization Device)*

- Approved by FDA for the treatment of unresectable/inoperable hypervascularized tumors (k093813) [32]
- Available in multiple particle size ranges for a variety of applications
- Easily suspended in conventional contrast media and delivered using standard embolization equipment
- Demonstrated full biological compatibility (via testing performed to obtain device clearance)
- Mitigate the risk of migration through biological occlusion (fibrous ingrowth anchoring the particles in place as they degrade).

#### *1.2.4.1.4. Key Limitations of PLGA Microspheres (Occlusin® 500 Artificial Embolization Device)*

- Lack of tailorable degradation timeframes—6 to 12 months occlusion timeframe only
- Lacks multi-modal imageability.



#### 1.2.4.2. PLGA-PEG-PLGA

##### *1.2.4.2.1. PLGA-PEG-PLGA: Basic Chemistry and Mechanisms of Degradation*

The chemical composition of PLGA and the mechanisms by which it degrades are described in the previous Section 1.2.4.1.1. Polyethylene glycols (PEG) are polymers of ethylene oxide with a chemical formula of  $\text{HO}-(\text{CH}_2-\text{CH}_2-\text{O})_n-\text{H}$ , where  $n$  can range from 4 to  $>400$  [39]. From a mechanistic standpoint, the degradation of PLGA-PEG-PLGA begins with hydrolysis of the PLGA crosslinks, yielding PLGA and PEG as the initial degradation byproducts [40]. It is typically regarded that PEG does not degrade, but rather is excreted unchanged in urine, leading to a limited risk of toxicity [39]. However, should PEG degrade, it is metabolized in the kidney and can be evaluated by the presence of ethylene glycol metabolites, such as calcium oxalate and carbon dioxide, which may pose risk of toxicity [39].

##### *1.2.4.2.2. PLGA-PEG-PLGA: Safety, Efficacy and Performance*

This review identified 985 articles relating to PLGA-PEG-PLGA based on the keyword search identified in Table 1.2. Only two of these papers met the inclusion criteria; the remainder of articles were substantially focused on *in vitro* studies and drug eluting materials. Papers meeting the inclusion criteria were published by Verret *et al.* in 2014 [15] and Maeda *et al.* in 2013 [41]. With respect to the former, the study utilized a uterine artery sheep model for a duration of seven days, with tris-acryl gelatin microspheres (500–700  $\mu\text{m}$ ) as a control. The latter study used a porcine kidney model for a period of up to seven days with gelatin sponge particles as a control. Summaries of the articles' findings versus the specific requirements to establish safety and efficacy as per FDA are provided in Table 1.5.

**Table 1.5:** Pre-clinical safety summary for hydrolysis mediated degradable PEG-PLGA-PEG microspheres.

Authors and year of publication	Study Model & Duration	Test Material Information.	Ease of use	Time to Complete Degradation of Test Material	Recanalization	Acute Complications (Vessel rupture / perforation)	Local and Systemic Foreign Body Reactions	Embolization Effectiveness.	Device Migration
Maeda et al. (2013)	Porcine Kidney Model.  Study duration: 7 days.  Control material: gelatin sponge particle (GSP) approx. 1 mm <sup>3</sup>  9 Minipigs (Mean weight 34.9 kg ± 2.1 kg)  Groups comprised two pigs (i.e. four kidneys per group)	PEG-PLGA-PEG  300-500 µm 500-700 µm 700-900 µm  Size distributions determined by sieving only. No particle size distribution analysis is provided.  1:2 ratio of saline/contrast for test article with pure contrast for the control article	A 4-F cobra catheter was utilized for the embolization procedures.  The mean volume of injected material per kidney was 0.48 mL ± 0.17, 0.24mL ± 0.11, 0.24mL ± 0.12 for REM of 300-500 µm, 500– 700 µm, and 700–900 µm.  Mean volume of control article injected was 1.2mL ± 0.2  Authors note, “none of the products clogged in the catheter.”	Proposed as 24hr based on tests in PBS.  At day 7 the test material was not visible, no fragments of materials were observed in histological slides / analysis.  GSP was still present at day 7, though partly degraded. Its presence was associated with foreign body inflammation.	Assessed at 10 minutes and 7 days using angiography. Large variations in measurements due to methodology acknowledged. Assessed at 10 minutes and 7 days using histological analysis. At day 0 test materials were washed out during processing limiting analysis. Fully patent vessel lumens apparent after 7 days post embolization with test article. Recanalization varied based on size of test material: 700-900 µm demonstrated complete recanalization 300-500 µm and 500-700 µm demonstrated partial recanalization.	Numerous patchy arterial lesions, including myointimal proliferation, medial concentric thickening, adventitial fibrosis, and fibrinoid necrosis of the arterial wall, were focally observed.  No excessive pain or abnormal behavior reported	Local histological analysis provided. Hematoxylin-eosin-saffron stain used. GSP (control) had eosinophilic or slightly basophilic appearance at day 7 and partly degraded. Presence associated with foreign body inflammation (macrophages, lymphocytes and fibrocytes). Test materials were washed out during histological processing limiting analysis for day 0. At day 7, test material was not visible, no fragments of materials were observed in histological slides / analysis. Fully patent lumen visible upon histology.	Recanalization demonstrated on angiography  No gross histology to examine presence of long term necrosis	Not addressed.
Verret et. al. (2014)	Uterine Artery Sheep Model  6 adult Préalpes Sheep. (Mean weight 54 kg) (Mean age 48 mo ± 22)  Study duration: 7 days.  Control material: EmboSphere® 500-700 µm  Bilateral UAE successful in all animals.	PEG-PLGA-PEG  500-700 µm  Size distributions determined by sieving only. No particle size distribution analysis is provided.  2:1ration of saline/contrast for test material and 4:5 ratio for control article	Selective embolization of both internal iliac arteries achieved using a 5F “cobra-type” catheter. Superselective embolization of both UAs performed with a 2.7F microcatheter.  Mean volume of test material injected per uterine artery was 1.0mL ± 0.5. For control material mean volume was 1.6mL ± 0.9 No difference in injectability noted between control and test materials.	Proposed as 24hr based on tests in PBS.  At day 7 the test material was not visible, no fragments of materials were observed in histological slides / analysis.	Presence or absence of recanalization assessed based on (i) the presence or absence of vascular lumen with (ii) red blood cells or plasma in the occluded vessel.  For test article “complete recanalization rapidly obtained” and fully patent on angiography at 7 days.	Vessel rupture not assessed. None reported.	Local histological analysis provided. Gross examination showed ischemic damage to endometrium and myometrium for test and control uteri. Hematoxylin-eosin-saffron stain used. No test materials or inflammatory response observed at 7 days for test article. Control material showed evidence of recanalization, and was surrounded by macrophages, neutrophils and foreign body giant cells.	Gross examination showed ischemic damage to endometrium and myometrium for test and control uteri.  The authors suggest that for the test article, full UA recanalization and absence of parenchymal defects were associated with low endometrial alterations.	Not addressed.

The performance, safety, and efficacy of the PLGA-PEG-PLGA microspheres were assessed by Verret *et al.* using a particle size distribution of 500–700  $\mu\text{m}$ , as it represented the “most common diameter used for uterine fibroid embolization in clinical practice” [15]. Maeda *et al.* studied this particle size range as well, also incorporating 300–500  $\mu\text{m}$  and 700–900  $\mu\text{m}$  for comparison [41]. No data confirming actual particle size distribution was listed in either study, thus it may be assumed that the size classifications were based on sieve aperture utilized to produce the microspheres. It is worth noting sieve aperture tolerances allow for a degree of error and the actual particle size distributions may be as low as 286  $\mu\text{m}$  and as high as 585  $\mu\text{m}$  for the 300–500  $\mu\text{m}$  range, 480  $\mu\text{m}$  to 815  $\mu\text{m}$  for the 500–700  $\mu\text{m}$  range, and 670  $\mu\text{m}$  to 970  $\mu\text{m}$  for the 700–900  $\mu\text{m}$  range [42]. With respect to injectability and ease of use, no substantial differences between the test and control articles were reported in either study [15,41]. The reported mean volume of particles delivered by both groups showed variability, suggesting different volumes may have been utilized from one animal to next. For example, Verret *et al.* reported delivering  $1.0 \pm 0.5\text{mL}$  of the test article and  $1.6 \pm 0.9\text{mL}$  of the control [15]. The volumes of test article delivered by Maeda *et al.* were notably smaller ( $0.48 \pm 0.17\text{ mL}$ ,  $0.24 \pm 0.11\text{ mL}$ , and  $0.24 \pm 0.12\text{ mL}$  for the so called ‘REM’ (resorbable embolic microspheres) of 300–500  $\mu\text{m}$ , 500–700  $\mu\text{m}$ , and 700–900  $\mu\text{m}$  respectively). However, the volume of control article delivered was comparable to the volume of test article delivered by Verret *et al.* These discrepancies may be due to variability in animal vasculature—both between and within species but are worthy of note since they may confound the observations.

PLGA-PEG-PLGA microspheres were reported by both Verret *et al.* and Maeda *et al.* to degrade *in vitro* in PBS in  $<24\text{ h}$ , and *in vivo* in less than seven days. Both papers angiographically monitored the animals at three time points, as follows: before delivery of microspheres, 10 min after embolization was achieved, and after seven days. Verret *et al.* characterized degradation and recanalization at day seven using a three-tier graded system: “normal flow, reduced flow (defined as contrast material visible during five heartbeats before disappearing), and stasis (defined as the blockade of the contrast column in the [uterine artery])” [15]. All animals treated with the PLGA-PEG-PLGA regained ‘normal flow’ by day seven and histological analysis showed no remaining fragments and no arterial wall modifications [15]. Conversely, Maeda *et al.* reported recanalization as

‘patency rates’, showing it correlated with particle size, as well as level of occlusion (particle distribution), extent of necrosis, and the total percentage of the embolized vessels that recanalized (‘recanalization rate’). It was observed that decreased particle size distributions resulted in more distal occlusion, greater necrosis, and lower recanalization rates [41]. These investigations were conducted with angiography and the authors made strong efforts to correlate them histologically; however, unfortunately, the test microspheres ‘washed out’ into solvent baths during processing, and so the distribution of PLGA-PEG-PLGA could not be directly observed [15]. Accordingly, with respect to Maeda *et al.*, it is difficult to fully evaluate the safety, efficacy, and performance of PLGA-PEG-PLGA microspheres. However, given the encouraging results, future work will likely buttress and substantiate this early data; it would be of benefit to develop methodologies that make it possible to definitively determine the *in vivo* degradation timeframes of degradable microspheres. Such methodologies would be of immense benefit since it is widely accepted that initial host-material responses, including (but not limited to) protein deposition and cellular interactions, may accelerate or impede the degradation rates of biomaterials [43].

While it may be possible to argue that the degradation byproducts of PLGA-PEG-PLGA (e.g., oxalic acid and its calcium salt) may be a concern with respect to systemic toxicity, evidence for such claims is limited in the literature. Although it is commonly accepted that PEG is excreted unchanged in urine, PEG byproducts can be as large as 20,000 Da, which is significantly larger than the size exclusion of the glomerulus (*ca.* 7265 Da) [39,44,45]. However, no animals treated with PEG-PLGA-PEG suffered any obvious systemic toxicities, pain, abnormal behavior, or atypical blood counts/biochemistry. With regards to necrosis, Verret *et al.* found the PLGA-PEG-PLGA microspheres produced significantly less ischemic damage relative to the control (tris-acryl gelatin), attributing this, in part, to the short degradation timeframe of PLGA-PEG-PLGA [15]. Maeda *et al.* found their control (gelatin sponge) yielded a similar level of necrosis to the smallest PLGA-PEG-PLGA size investigated (300–500  $\mu\text{m}$ ), which was significantly higher than the two larger PLGA-PEG-PLGA particle sizes explored. This group did not comment on degradation time as a factor, rather stated the level of necrosis correlated with the distribution of the microspheres, with those positioned distal to the arcuate artery yielding

significantly more necrosis. Given the variability in the size distribution of gelatin sponge, it is likely the control agent was present both proximal and distal to this anatomical location, resulting in a higher level of necrosis [41].

Neither Verret *et al.* or Maeda *et al.* directly investigated the risk of migration of degradable PLGA-PEG-PLGA microspheres (as pointed out by the FDA special control document), and it would be unreasonable to assume that these studies could fully evaluate the multiplicity of risks identified by FDA. Nevertheless, in consideration of the risk, Verret *et al.* did comment on the absence of observable ovarian damage, concluding migration could not be ruled out solely based on these findings [15]. Given that the predicted degradation timeframe of PLGA-PEG-PLGA is <24 h, embolization would likely be limited to mechanical occlusion (i.e., the material itself) and thrombus formation, without the presence of fibrotic encapsulation (i.e., biological occlusion) to ‘anchor’ the microspheres in places while they degrade. As discussed previously, the absence of this biological occlusion may increase the risk of migration and non-target embolization, as small microsphere fragments may break off and travel forward through small anastomoses, or reflux retrograde into neighboring vasculature [15,41].

#### *1.2.4.2.3. Key Advantages of PLGA-PEG-PLGA Microspheres*

- Limit necrotic damage due to rapid degradation timeframe (*ca.* <24 h)
- Available in multiple particle size ranges for a variety of applications
- Comparable ease of delivery to control article.

#### *1.2.4.2.4. Key Limitations of PLGA-PEG-PLGA Microspheres*

- Lack of tailorable degradation timeframes—*ca.* seven-day timeframe only
- Toxicity concerns related to PEG degradation byproducts not directly addressed, may not offer full biological compatibility
- Lacks multi-modal imageability.

### 1.2.4.3. CMC-CNN

#### 1.2.4.3.1. CMC-CNN: Basic Chemistry and Mechanisms of Degradation

Carboxymethylcellulose-chitosan (CMC-CCN) has been proposed as a material for use in TAE based on its ability to rapidly degrade. CMC-CCN polymers can be created with varying degradation times by altering the degree of oxidation of the carboxymethylcellulose (CMC); however, only two time points have been validated in the literature (14 days for 10% oxidated CMC and 30 days for 25% oxidated CMC) [46,47]. In manufacturing, the two components (CMC and chitosan) are combined in a water-in-oil emulsion to form crosslinked polymers via a Schiff base reaction between the aldehyde groups on oxidized-CMC and the amino groups on chitosan [47]. This two-part system avoids small molecular cross-linking agents, which are usually considered to have higher cytotoxic potential [47]. The macrostructure of the resulting polymer is susceptible to degradation by lysozyme, an enzyme that is abundantly present in most parts of the human body; lysozyme hydrolytically cleaves the Schiff base, separating the material into two components (CMC and chitosan) [47].

The first component, CMC, is a non-toxic, biodegradable polymer that is widely used in the pharmaceutical industry [48]. CMC is not degradable by mammalian enzymes but has demonstrated limited *in vivo* degradation via hydrolysis of its 1,4-glucosidic linkages, producing small amounts of glucose [49,50]. The exact extent of CMC degradation is likely to be determined in future work as the research teams continue to consider the degradation kinetics and compatibility of degradation by-products in future work.

Chitosan is a naturally occurring polysaccharide derived from the exoskeleton of crustaceans that is commonly used in medicine and pharmaceuticals [51]. It is widely considered non-toxic, having been cleared by FDA for use in wound dressing. Chitosan is not one chemical entity but varies in composition depending on manufacturing; during alkaline hydrolysis of chitin to form chitosan, N-deacetylation and depolymerization occur to varying extents. Structurally, chitosan is considered a polymer of glucosamine and N-acetylglucosamine, linked by 1,4-glucosidic bonds [52]. Like CMC-CCN, chitosan is also degraded *in vivo* by lysozyme, which breaks glucosamine-glucosamine, glucosamine-N-acetyl-glucosamine, and N-acetyl-glucosamine-N-acetyl-glucosamine linkages, leaving

only glucosamine. Glucosamine then goes on to produce glycosaminoglycans, proteoglycans, and glycolipids in the body. The rate of degradation is historically believed to depend on the acetylation of chitosan, with more acetylated and thus more crystalline chitosans (like chitin) showing faster rates of degradation [51-54].

#### ***1.2.4.3.2. CMC-CCN: Safety, Efficacy and Performance***

This review identified 417 articles relating to CMC-CCN based on the keyword search identified in Table 1.2. Only one of these papers met the inclusion criteria, the remainder of articles were substantially focused on drug-carrying materials and neuroprotective effects in ischemic brain injury. The paper meeting the inclusion criteria was published by Weng *et al.* in 2013 [55] and provides a detailed analysis of the safety and efficacy of CMC-CCN-based microspheres for TAE, which they call ‘bioresorbable microspheres’ (‘BRMS’). This paper used a renal artery rabbit model over a period of 15 min. The animals were divided into three groups: partial occlusion with BRMS-I (CMC-CCN with a theoretical oxidation degree of 10%), total occlusion with BRMS-I, and total occlusion with BRMS-II (CMC-CCN with a theoretical oxidation degree of 25%). Tris-acryl gelatin microspheres (TGMS) with a particle size range of 100–300  $\mu$ m were included as the control. Angiography was performed before, immediately after, and 15 min after the embolization procedure. A summary of the article’s findings versus the specific requirements to establish safety and efficacy as per FDA are provided in Table 1.6.

**Table 1.6:** Pre-clinical safety summary for hydrolysis mediated degradable CMC microspheres.

Authors and year of publication	Study Model & Duration	Test Material Information.	Ease of use	Time to Complete Degradation of Test Material	Recanalization	Acute Complications (Vessel rupture / perforation)	Local and Systemic Foreign Body Reactions	Embolization Effectiveness.	Device Migration
Weng et. al. (2013)	Renal Artery Rabbit Model  11 New Zealand white rabbits (Weight range 4–5 kg)  3 rabbits (group 1) received partial occlusion with BRMS-I (3, 15, and 25mg of microspheres)  To test the level of occlusion, 4 (group 2) received total occlusion with BRMS-I (10mg/mL), and 4 more (group 3) rabbits received complete occlusion with BRMS-II  Study duration: 15 minutes  Tris-acryl gelatin microspheres (TGMS) (100-300 μm) were used as a control	2 test articles: BRMS-I and BRMS-II  2% (w/v) oxidized carboxymethylcellulose and 2% (w/v) carboxymethyl chitosan  10% oxidized carboxymethylcellulose was used in BRMS-I and 25% oxidized carboxymethylcellulose was used in BRMS-II  100 - 300 μm  Average diameter of the microspheres was 250 μm ± 50 for BRMS-I, and 255 μm ± 45 for BRMS-II  Concentration of microsphere suspension used was 1mg/mL and 5mg/mL for group 1, and 10 mg/mL for groups 2 and 3 all in a 5:5 saline:contrast solution	RA selectively catheterized a 4-F Cobra catheter inside which a 2.8-F microcatheter was placed  Injection was “easily performed without any clogging or clumping”  BRMS were deemed to be less “sticky” than TGMS  BRMS-I required 8.7 mL ± 3.5 to achieve stasis and BRMS-II required 6.3 mL ± 0.8  Fluoroscopic time to achieve the endpoint was 4.5 min ± 1.6 for BRMS-I and 3.8 min ± 0.74	Not Addressed	Not addressed	Not addressed	Not addressed	Determined to achieve the desired goal of embolization similar to commercially available TGMS  Mean diameter of occluded vessels found to be 197 μm ± 23 for BRMS-I, 219 μm ± 36 for BRMS-II and 158 μm ± 21 for TGMS	Not addressed



Beneficially, CMC-CCN microspheres may be produced in a wide variety of particle size distributions ranging from 100 to 1550  $\mu\text{m}$  [47]. For assessment of this technology, Weng *et al.* utilized a size range of 100–300  $\mu\text{m}$ , providing comprehensive details specific to particle size distribution [55]. This selection of particle size may be justified, similarly to Owen *et al.* [31], as representing a worst-case scenario in terms of biocompatibility (i.e., surface area) and risk of migration (Section 1.2.4.1.2). Importantly, and with regards to ease of use, Weng *et al.* stated the injection of CMC-CCN microspheres was “easily performed without any clogging or clumping” using a 2.8-F microcatheter [55]. The control article was deemed significantly more difficult to use as it tended to stick to both the syringe and the microcatheter, substantially reducing the percentage of particles delivered per syringe. The authors attributed the decreased ‘stickiness’ observed for the CMC-CCN microspheres to the low coefficient of surface friction inherent to hydrogels [55].

Degradation rates of CMC-CCN microspheres have been previously demonstrated *in vitro* and depend on the level of oxidation from processing [56]. In the present study, the timeframe of 15 min did not allow for assessment of *in vivo* degradation or recanalization. Nonetheless from a performance standpoint, the authors stated that more cross-linking can provide for a slower rate of degradation [55,56]. The key focus of this paper was related to the acute phase of embolization, focusing on initial particle distribution and level of occlusion. Comparisons regarding material performance were made when total occlusion (effective stasis) was used as an end point (versus a pre-determined dose). Interestingly, microsphere distribution was reported as being dependent on the level of CMC-CCN crosslinking. Weng *et al.* found BRMS-II microspheres (oxidation degree of 25%) occluded slightly more proximal than BRMS-I (oxidation degree of 10%) and the control (which was equal to BRMS-I), likely due to their lower compressibility. Despite these observations, the authors reported no statistical differences in the diameter of occluded vessels or the magnitude of particle deformation between any of the materials [55]. The CMC-CCN microspheres remained intact in all histological specimens; however, 20% of the control particles showed pitting or ‘peeling’. The authors stated this may have been a result of the histochemical processing and agree that it may have obscured their analysis of microsphere deformation [55].

Given the focused and acute scope of this study, it was not possible to comment on acute complications and foreign body reactions. On histological evaluation, the authors discussed the presence of ‘white spaces’ surrounding the microspheres, attributing them to either “dehydration of the microspheres and shrinking during the staining process, or slicing that was not through the cross-section of the vessel diameter” [55]. It may also be possible these spaces resulted from thrombus formation, as the authors noted “visible tissue and blood cells that surrounded the microspheres were erased” prior to analysis [55]. Although risk assessment was limited in this paper due to its short timeframe, the authors have published a subsequent study, which is considerably more focused on the special controls published by FDA; this follow-up study was not included in the present review as it did not meet the inclusion criteria (lack of commercial control), but is cited so as to direct the readers toward additional data for these materials [57].

#### *1.2.4.3.3. Key Advantages of CMC-CNN Microspheres*

- Potentially offers a range of tailorable degradation timeframes based on *in vitro* evaluations
- Available in a wide variety of particle sizes from 100 to 1550  $\mu\text{m}$
- Superior ease of delivery as compared to the control (less adhesive) using conventional embolization equipment.

#### *1.2.4.3.4. Key Limitations of CMC-CNN Microspheres*

- No information on *in vivo* degradation timeframes or recanalization
- Toxicity concerns related to degradation byproducts and their size(s) not addressed, may not offer full biological compatibility
- Lacks multi-modal imageability.

#### **1.2.4.4. Chitosan**

##### *1.2.4.4.1. Chitosan: Basic Chemistry and Mechanisms of Degradation*

Chitin is a biopolymer found in the shells and exoskeletons of animals, such as insects, squids, and crustaceans, and serves a similar structural role to that of cellulose in plants or collagen in higher species [58,59]. Structurally, chitin has a highly-extended

hydrogen bonded semi-crystalline arrangement, which limits its solubility in water [58]. The chemical composition of chitin is poly( $\beta$ -(1-4)-N-acetyl-D-glucosamine). Chitosan is the N-deacetylated derivative of chitin and contains multiple free amino groups, typically with a degree of deacetylation  $> 0.65$  (deacetylation values of 75% and 99% were found in the specific body of literature explored for this paper) [60]. The degradation mechanism and products of chitosan have already been addressed in the section on CMC-CCN (Section 1.2.4.3.1).

#### *1.2.4.4.2. Chitosan: Safety, Efficacy and Performance*

This review identified 585 articles relating to chitin and chitosan based on the keyword search identified in Table 1.2. Only 1 of these papers met the inclusion criteria, the remainder of the articles were substantially focused on *in vitro* studies and drug-loaded materials. The paper meeting the inclusion criteria was published by Kwak *et al.* in 2005 [60] and provides a comprehensive and detailed analysis of the safety and efficacy of chitin- and chitosan-based particles for TAE. While this paper examined many morphologies (e.g., thin, scale-shaped chitin and chitosan plates), the current review focuses solely on data relating to the chitosan microspheres (75% deacetylated). This paper used a renal artery rabbit model over a period of 32 weeks. The animals were divided into nine cohorts: 1 and 3 days, and 1, 2, 4, 8, 16, 24, and 32 weeks, and PVA particles (150–250 m) were used as the control. A summary of the article's findings versus the specific requirements to establish safety and efficacy as per FDA are provided in Table 1.7.

**Table 1.7:** Pre-clinical safety summary for hydrolysis mediated degradable Chitin microspheres.

Authors and year of publication	Study Model & Duration	Test Material Information.	Ease of use	Time to Complete Degradation of Test Material	Recanalization	Acute Complications (Vessel rupture / perforation)	Local and Systemic Foreign Body Reactions	Embolization Effectiveness.	Device Migration
Kwak et. al. (2005)	Renal Artery Rabbit Model  36 New Zealand white rabbits (weight range 2.0–3.5 kg)  Study duration: 32 weeks. Cohorts at 1 and 3 days, and 1, 2, 4, 8, 16, 24, and 32 weeks  Control material: PVA 150-250 $\mu\text{m}$	Chitin particles, 99% deacetylated chitosan particles, and 75% deacetylated chitosan microspheres  150-250 $\mu\text{m}$  The length of chitin particles, chitosan particles, and chitosan microspheres was 335 $\mu\text{m} \pm 56.8$ , 466 $\mu\text{m} \pm 100.2$ , and 271 $\mu\text{m} \pm 37.2$ , respectively	RA selectively catheterized with 4-F angiography cobra catheter.  No fluoroscopic time to achieve stasis given  All four materials were noted as being “easily injected through the catheter without causing any blockage”	All embolic materials maintained their shape until week 8  Chitin particles showed fragmentation and absorption at week 24, absorbed completely at week 32  Chitosan particles showed fragmentation and absorption at week 16, absorbed completely by week 24  Chitosan microspheres showed degradation and absorption at week 24, absorbed completely by week 32	Severe proliferations of the blood vessels by the retroperitoneal fat around the embolized kidney were observed from day 1 to week 1 for PVA, chitin and chitosan microspheres and from day 3 to week 2 for chitosan particles.  Formation of capillaries were observed most frequently with PVA particles, followed by chitosan particles and chitosan microspheres	The degree of vascular injuries was moderately reactive with PVA particles and chitosan microspheres and substantially reactive with chitin particles  No hemorrhage or extravasation for any of the embolic materials.	Giant cell reaction appeared prominently 1–2 weeks after embolization, and lasted until week 32. The degree of reaction was lowest with chitosan microspheres.  As a whole, there was no substantial difference in gross observations among the four groups.	Chitosan microspheres were determined to be potential embolic agents as they block the blood vessels more compactly and with a lower rate of capillary formation than PVA particles.	Not addressed.

To assess the safety, efficacy, and performance of chitosan microspheres, a uniform size distribution of 150–250  $\mu\text{m}$  was used for all test and control agents. The authors provided detailed particle size distributions, reporting the mean  $\pm$  standard deviation of chitosan microspheres as  $271 \pm 37.2 \mu\text{m}$  and non-spherical PVA particles as  $326 \pm 89.1 \mu\text{m}$  [60]. The notable increase in mean PVA particle size as compared to the labelled size range can likely be attributed to the rod-shaped morphology of this material, which enabled passage through 150–250  $\mu\text{m}$  sieves. Spherical agents were not included for control purposes, as the authors reported they were “not available at the time [their] study was performed”. With regards to ease of use, the authors reported both the chitosan microspheres and control were “easily injected through the catheter without causing any blockage” [60]. The distinct morphologies of the two materials lead to varied degrees of occlusion; the chitosan microspheres filled the vessel lumen more compactly than the irregular PVA particles. The authors do not provide the volume of material delivered per injection.

Chitosan microspheres were found to have a degradation timeframe of *ca.* 32 weeks. The first signs of degradation appeared at 24 weeks, with complete absence of the microspheres at 32 weeks [60]. Although PVA is known to be non-degradable and is therefore regarded as a permanent agent in the literature, this group found the size and number of PVA particles decreased over time. This began after eight weeks and persisted for the duration of the study. Unlike the chitosan microspheres, PVA particles were still present in situ after 32 weeks. The authors suggested this observation, along with the presence of PVA fragmentation and foreign body giant cell infiltration, may indicate PVA underwent some sort of degradation process(es) [60]. Recanalization (reopening of occluded blood vessels) was not explicitly studied in this paper, although the authors did comment on the formation of new capillary growth that correlated with the degree of fibrosis [60]. This was present for both chitosan microspheres and PVA particles, though it occurred earlier in the PVA cohort (week two vs. week four) and to a more substantial degree. The presence of fibrosis, in combination with the extended amount of time both embolic agents were present in the vessels, suggest there was a very good chance that particle degradation did not lead to vessel reperfusion in either case [60]. This extended occlusion time lends itself to the same argument as noted above for PLGA (Section

1.2.4.1.2); although both materials may eventually degrade in situ, both chitosan and PVA can essentially be categorized as permanent embolic materials due to their protracted biological occlusion times [36].

Acute complications were discussed effectively in this paper, owing to the use of two additional stains, Victoria blue and Masson trichrome, allowing for thorough examination of elastic lamina damage and fibrosis, respectively. Victoria blue staining demonstrated that vascular injuries became more severe over time in both groups, progressing from damage of only internal elastic lamina to damage of the middle membrane. There was, however, no hemorrhage or extravasation of either material. The authors proposed that the destruction of the elastic lamina occurred because of either “ischemia, direct toxic effects of embolized materials, or focal angionecrosis by embolized materials to the vessel wall” [60]. Inflammation was seen in relation to both particle types to varying degrees, beginning immediately after embolization, and persisting up to roughly one week. The inflammation observed with chitosan microspheres, although more severe than that of the control, was not severe enough to destroy the vessel wall. After approximately one-week, inflammatory infiltrates aggregated into foreign body giant cells, which persisted up to week 32 for both materials; these foreign body giant cells presented before degradation of the material and persisted continuously after the chitosan microspheres were completely degraded [60]. With regards to systemic reactivity, neither material altered blood chemistry. Specifically, the authors emphasized the importance of the low eosinophil count, which suggests chitosan microspheres are unlikely to evoke allergic reactions [60].

Although not formally assessed, the issue of migration arose due to complications seen in this study. One rabbit died following reflux of chitin particles (irregular particles not discussed in detail in this review) from the right renal artery to the left, resulting in occlusion of both renal arteries. The authors discussed this complication in relation to the volume of material, stating this occurred when an excessive number of particles were injected. Unfortunately, the volumes of each material delivered were not provided [60] and the issue of reflux was not discussed any further or specifically in relation to material properties, such as embolic morphology or density. As previously mentioned, the extended timeframe of chitosan microsphere degradation likely mitigates, to a degree, the risk of

embolic migration, as fibrous ingrowth anchors the microspheres in place as they degrade. Nonetheless, this theory merits proper exploration prior to use in human subjects.

#### *1.2.4.4.3. Key Advantages of Chitosan Microspheres*

- Easily delivered through conventional microcatheters and provides for more compact vessel occlusion (relative to irregular PVA particles)
- Low risk of local and systemic toxicity (unlikely a high-risk allergen)—potential to fulfill full biological compatibility
- Extended degradation timeframe potentially mitigates risk of migration through stimulation of fibrous ingrowth.

#### *1.2.4.4.4. Key Limitations of Chitosan Microspheres*

- No information provided on ability to manufacture different particle size ranges
- Lack of tailorable degradation timeframes—24 to 34 week occlusion timeframe only
- Lacks multi-modal imageability.

#### *1.2.4.5. HEA*

##### *1.2.4.5.1. HEA: Basic Chemistry and Mechanisms of Degradation*

Hydroxyethyl acrylate (HEA) is a hydrolytically degradable material that has been proposed for embolization procedures due to its resiliency and lack of dependence on enzymatic degradation [61]. HEA is synthesized to contain two degradation sites using a N,N'-(dimethacryloyloxy)adipamide crosslinker (C<sub>6</sub>NCL) to modulate the rate of degradation while maintaining desired mechanical properties. HEA undergoes degradation in basic conditions, which is an important consideration when designing HEA microspheres, since embolization procedures are intended to produce ischemic events (resulting in acidic conditions) and cessation of flow (preventing elimination of carbon dioxide) [62]. The degradation of hydroxylamines substituted into the material, such as C<sub>6</sub>NCL, is known to lead to production of primary amines (e.g., putrescine) and linear carboxylic acids with the loss of carbon dioxide [61]. Although these degradation byproducts (e.g., putrescine) are often naturally present in the body, they may be toxic in

large quantities [63].

#### ***1.2.4.5.2. HEA: Safety, Efficacy and Performance***

This review identified 65 articles relating to HEA based on the keyword search identified in Table 1.2. Only one of these papers met the inclusion criteria; the remainder of articles were substantially focused on *in vitro* testing and studies related to high environmental ammonia. The paper meeting the inclusion criteria was published by Schwarz *et al.* in 2003 [61]. This paper used both renal artery canine and auricular artery rabbit models over a period of three weeks, with EmboGold microspheres (300–500  $\mu\text{m}$ , Merit Medical Systems Inc., South Jordan, UT, USA) as the control. A summary of the article's findings versus the specific requirements to establish safety and efficacy as per FDA are provided in Table 1.8.



**Table 1.8:** Pre-clinical safety summary for hydrolysis mediated degradable HEA microspheres.

Authors and year of publication	Study Model & Duration	Test Material Information.	Ease of use	Time to Complete Degradation of Test Material	Recanalization	Acute Complications (Vessel rupture / perforation)	Local and Systemic Foreign Body Reactions	Embolization Effectiveness.	Device Migration
Schwarz et. al. (2003)	Renal Artery Canine Model 5 Beagles (Weight range 10-15 kg)  3 Kidneys were embolized with HEA Median auricular artery occlusion model  5 New Zealand rabbits (Weight range 2.5–3.5 kg)  4 central auricular arteries were embolized with HEA microspheres  Study duration: 3 weeks. Monitored immediate and weekly through catheter angiography  Control material: EmboGold microspheres 300-500 µm	Hydroxyethyl acrylate  300-500 µm  No particle size distribution analysis is provided.	RA selectively catheterized with either 4-F or 5-F catheters.  Catheterization of central artery of rabbit ears was performed with radiopaque catheters  No comment made on ease of use	At 3 weeks, microspheres (sometimes intact but encapsulated, most often in various stages of degradation and phagocytosis) could be detected  Occlusion lasted for the critical period at risk for recanalization, typically 10–14 days	Renal arterial occlusions that persisted at 1 week were recanalized at 3 weeks  Experiments performed in the rabbit central auricular arterial model showed that HEA microspheres led to occlusions that persisted at 1 week but that recanalized at 2 weeks  No recanalization in EmboGold cohorts.	Vessel rupture not assessed. None reported.	Only a residual inflammatory reaction and some neointimal thickening could be observed as a witness to the previous presence of these degradable microspheres	Determined as being potentially effective up to 2 weeks	Not addressed.

The safety, efficacy, and performance of HEA microspheres were evaluated by Schwarz *et al.* using a particle size range of 300–500  $\mu\text{m}$ , which was obtained via sieving [61]. The authors did not provide any commentary regarding the ease of use of either product, and no values for average volume delivered per injection were provided. It was, however, mentioned that the transparency of HEA microspheres rendered them practically invisible in a syringe. To mitigate this issue and facilitate easier handling of this product, HEA microspheres were colored orange using small amounts of fluorescein acrylate [61]. Schwarz *et al.* began their study by investigating the degradation rate of synthesized HEA microspheres *in vitro* (pH 7.4, 37°C), demonstrating complete degradation of the material at 22 days. This correlated, to a degree, with what was observed in their *in vivo* investigation; on angiography, embolized vessels were recanalized at three weeks. However, histopathology showed HEA microspheres were often present *in situ* at three weeks in “various stages of degradation and phagocytosis”, indicating (i) that degradation was incomplete at this time point (ii) highlighting potential discrepancies between *in vivo* and *in vitro* degradation findings [61]. In areas where the HEA microspheres had completely degraded, residual inflammation and neointimal thickening were observed. As discussed by Schwarz *et al.*, this discrepancy between *in vitro* and *in vivo* degradation timeframes may be a result of the acidic conditions produced during ischemic events and cessation of blood flow [61]. Nevertheless, the authors effectively showed using both renal and auricular models that temporary arterial occlusion could be achieved using HEA microspheres for up to two weeks [61].

Risks associated with acute complications and systemic toxicity were not reported for HEA microspheres in this work. Little information was provided regarding foreign body reactions other than noting that both HEA microspheres and the control lead to inflammation and tissue infarction, with the permanent agent demonstrating notably higher levels of both. In line with this, the authors stated, “the theoretical advantages of temporary embolization were not convincingly demonstrated in [their] model since temporary renal branch occlusions for the time periods investigated still led to tissue infarction” [61]. It should be noted that a renal artery model is an end vessel model and may not be ideal for correlating infarction and degradation. The ideal degradation timeframe for embolic microspheres remains unclear and likely varies across different clinical indications.

Although HEA yielded ischemic insult to the healthy tissues examined by Schwarz *et al.*, this may not have occurred, to the same degree, in the presence of a tumor/fibroid. Due to the hypervascular nature of tumors/fibroids, these diseased tissues have been shown to preferentially attract blood flow and therefore microspheres, sparing neighboring healthy tissues. Consequently, the ischemia observed by Schwarz *et al.* may not be representative of a true clinical scenario. HEA microspheres reliably degraded, succeeding in providing patients with a dependable material that will be eliminated from their body—a key driver in the development of degradable microspheres for TAE.

The risk of microsphere reflux was briefly mentioned in the methods of this paper as a potential complication to avoid; however, it was not discussed in detail, as unlike Kwak *et al.* (Chitosan, Section 1.2.4.4), no animals died from microsphere migration. The authors alluded to microsphere encapsulation in some tissue samples, but it appears this was not always the case. As such, it is unclear, and perhaps unlikely, a biological mechanism would be reliably in place to anchor HEA microspheres during degradation, suggesting migration would be possible.

#### *1.2.4.5.3. Key Advantages of HEA Microspheres*

- Produced notably lower levels of ischemia relative to control agent

#### *1.2.4.5.4. Key Limitations of HEA Microspheres*

- No information provided on ability to manufacture different particle size ranges
- No information provided on ease of use of microspheres
- Lack of tailorable degradation timeframes—2 to 3 week occlusion timeframe only
- Toxicity of degradation byproducts (e.g., putrescine) not assessed
- Lacks multi-modal imageability.

### **1.2.5. Preclinical Models**

Selecting an appropriate model for the preclinical evaluation of embolization products is critical for accurately assessing safety, efficacy, and performance prior to human use. While some parameters can be assessed *in vitro* (e.g., particle size and ease of use), animal models are required to best evaluate the material in an environment that

approximates the intended clinical scenario [64]. Specifically, with regards to the list of special controls provided by FDA, *in vivo* models are required to assess degradation and recanalization, host response (acute complications and local and systemic reactions), and migration [64]. As no animal model can truly represent the intended clinical conditions in their entirety, it is necessary to match the specific objectives under consideration to the best available model. Unfortunately, this proves to be a complicated process, as several variables are at play that can significantly alter outcomes and distort results – anatomy, vascular distribution, blood flow, and immune and coagulation responses are examples of such [64]. The selected animal, organ, and tissue condition (e.g., tumor vs. healthy) are three key factors that affect these variables, which must be carefully selected to meet a study's objectives [65]. The following section is intended to outline the advantages and disadvantages of the models incorporated in the papers considered in this review.

The kidney and uterus were the two main organs used to carry out the preclinical analyses reviewed in this paper. Embolization procedures are performed clinically in both of these organ structures (e.g., for renal cell carcinoma, uterine fibroids), and thus these models are clinically relevant. Both of these organs act as a filter, in which microspheres may be delivered, and entrapped, as the vascular diameters decrease from the renal/uterine artery down to end arterioles [66]. The uterus is perhaps less straightforward, in that the uterine artery often anastomoses with the contralateral uterine artery, ovarian artery, and/or vaginal artery [66]. In theory, these structures are suitable for evaluating the migration risk associated with degradation, as they allow the material to advance deeper into the vascular bed as it decreases in size, but remain entrapped within the organ (i.e., not shunt elsewhere). In the papers under review, the kidney and uterine models enabled, for the most part, effective evaluation of degradation, recanalization, and host response; however, commentary regarding migration was limited.

Microsphere migration is perhaps the most difficult parameter to investigate, as vascular patterns and blood flow are so variable in different species, organs, and disease states [65]. None of the papers discussed in this review considered a diseased model, and thus the vascular distribution and blood flow dynamics limited the applicability of these results to clinical use for several reasons. Firstly, vascular tumors (including uterine fibroids) tend to show significant increases in blood flow relative to their non-diseased

counterparts, and preferentially draw microspheres from the circulation to the tumor [67]. Secondly, the vasculature of tumors is generally more disorganized, potentiating migration of the material through poorly developed vessels beyond the tumor itself [67]. Finally, a significant complication of uterine fibroid embolization is post-embolization syndrome (PES), which is often seen when small particles (e.g.,  $<500\ \mu\text{m}$ ) are used and thought to result from microspheres reaching arterioles in close proximity to the fibroid [68,69]. As degradable microspheres shrink and likely advance further downstream within the tumor vascular bed, the risk of this complication may be increased. The complicated nature of diseased tissue combined with the novelty of degradable microspheres questions the applicability of the healthy models used in the papers under review as preclinical evaluations prior to clinical use.

Embolization is performed clinically for several different indications not covered by the models explored in this review, such as arteriovenous malformation and hepatocellular carcinoma [19]. It should be noted these indications have a unique set of inherent risks, perhaps the most concerning of which is bypass of the target tissue with shunting to vital organs. The vascular networks of these pathologies, and hypervascular tumors in general, is highly variable and poorly organized, potentially enabling passage of microspheres to the systemic circulation. This may be of extreme clinical importance, especially with degradable materials, which are designed to decrease in size over time; the pressure of the pulsatile flow, coupled with the decreased size and altered compressibility of partially degraded microspheres may push the embolics further downstream. Several groups report pulmonary emboli when particles  $<10\ \mu\text{m}$  are utilized [70], and radioactive Y-90 microspheres are designed to limit pulmonary radiation below a given threshold, indicating migration beyond target tissue is an acceptable event associated with the use of these products. Although the kidney and uterine models discussed above are clinically relevant, they do not address this important issue and therefore the commentary made in relation to migration does not translate to all indications.

### **1.2.6. Conclusions**

This review identified five state of the art materials that have been investigated for use as degradable microspheres for TAE. In considering the FDA's list of special controls

for the preclinical evaluation of bland embolic microspheres, it is evident there are significant gaps in the current understanding of the safety, efficacy, and performance of these materials. More importantly, in reviewing this body of literature, it appears there is little consensus regarding the ideal characteristics of degradable microspheres. Specifically, ideal degradation timeframes, recanalization rates, and host responses (e.g., fibrotic ingrowth) have not been identified, making it difficult to establish precise design controls for the development of these products. Furthermore, the degradability of these microspheres present new and complex risks that have not been previously considered, the most important of which may be migration. As degradable microspheres shrink in size, they may (i) potentially advance beyond the intended level of occlusion resulting in more profound ischemia and necrosis and/or, (ii) reflux into adjacent vessels, resulting in non-target embolization and/or (iii) through capillaries (i.e., shunting) leading to unintended injury of next level organs such as the lung or brain. In the future, degradable embolic materials may be engineered so as to permit repeat embolization procedures with radioactive embolic particles, drug-eluting particles, and bland embolic agents. Doing so will permit physicians to achieve levels of occlusion on repeat procedures, and as a consequence may enhance the overall safety, efficacy, and performance of TAE procedures.

### **1.3. Consolidated Design Inputs**

Based on the information evaluated in Section 1.2, a list of design inputs has been formulated to coincide with the ideal properties of a degradable embolic agent for uterine artery embolization. The ideal material should:

- Maximize CT radiopacity – to allow for visibility upon CT, fluoroscopy, and angiography during and after the procedure.
- Minimize MRI interference – so as not to confound follow up imaging to assess remaining pathology.
- Minimize density – to allow for the best spatial distribution within the target tissue.
- Ability to hydrolytically degrade in 24 to 48 hours – to effectively starve the tumor without causing excessive damage to the healthy tissues, and to minimize unwanted inflammatory effects.

- Be easily manufactured – to allow for sufficient material to be synthesized and processed into spheres.
- Be fully biocompatible - to minimize unwanted adverse effects.

#### **1.4. Glasses as Candidate Embolic Agents**

Based on these design inputs and previous work in the field of bioactive glasses, it is possible that glasses may be strong candidate materials for the development of next generation embolic agents [18]. Their use in dentistry and orthopaedics has illustrated their ability to add radiopacity to medical materials (e.g. restorative dental composites & bone cements) without compromising biocompatibility, and while the indications are substantially different, there is reason to consider their applicability in the embolization of hypervascular tumours including uterine leiomyoma [13]. In particular, glasses allow for radiopacity through the incorporation of heavy elements into the glass network [18], the engineering of variable degradation timeframes by varying the stability of the glass network, and the ability to manufacture different sized particles based on the methods used to grind/sieve the manufactured glass frits.

To understand the remainder of the work enclosed in this thesis, it is first important to understand some vocabulary related to glass science. A glass, in the broadest sense, is an amorphous solid which exhibits “glass transformation behaviour”; essentially glasses are considered solid liquids, as they display comparable properties to solids, but their structure is more similar to that of a traditional liquid [71]. Sun explained that elements with high single bond strength are less able to rearrange during cooling from a liquid to a solid, thereby creating a glass through melt quenching [72]. He then divided glass components into three classes: network formers, network modifiers, and network intermediates. Network formers are the elements which form the network structure of the glass, and typically bond very strongly to oxygen. Network modifiers have a weaker single bond strength, and can therefore rearrange easily and modify the glass network. Network intermediates are elements that can behave either as a network former or a network modifier, depending on the environment in which they are found. The addition of network modifiers or network intermediates can greatly alter the glass structure (or network connectivity) and thereby alter the properties that said glass displays.

### 1.4.1. Borate Glasses

Borate glasses are significantly understudied in the literature due to their hydrolytic instability; *ca.* 2% of glass science literature consists of borate glass compositions, and the majority of this literature relates to the borosilicates (e.g. Pyrex) [71]. Over 20% of the literature focuses on silicates because of their high durability and use in industry [71]. Traditionally, the degradable properties of borate glasses were unfavorable for industrial purposes; however, when considering medical devices, this shortcoming becomes an advantage for potential degradable embolic materials. It is thus important to investigate simple high boron glass compositions to develop better understanding of the structure-property relationship of these networks.

Relative to silicates and phosphates, there is little understood about borate glasses (in particular those where B is the only network forming element). Nevertheless, there are some areas of the literature that are well studied. The basic structure of a borate glass networks has been extensively studied and has identified an interesting phenomenon called the borate anomaly [72]. Pure  $B_2O_3$  consists of trigonal boron, found largely in the form of boroxyl rings; however, boron has the potential to form more than one stable configuration with oxygen, allowing for the formation of super-structural units. Upon the addition of a monovalent network modifier, trigonal  $B\emptyset_3$  (where  $\emptyset$  signifies an oxygen atom bridging two boron atoms) converts to tetrahedral  $B\emptyset_4^-$  up to about 33 mol% as seen in Figure 1.2 [72]. The mole percent at which this conversion is maximized depends on a variety of factors such as the charge density and size of the modifier ion. This conversion stabilizes the glass network and leads to longer dissolution times (i.e. enhanced hydrolytic stability). Thereafter, (> 33 mol% addition of modifier) the network becomes more disrupted leading to non-bridging oxygen and more reactive glass species [72,73]. This feature provides a compositional and structural basis upon which the degradation of borate glasses may be modulated by the inclusion of specific elements, which can themselves modulate critical network properties (e.g. radiopacity).



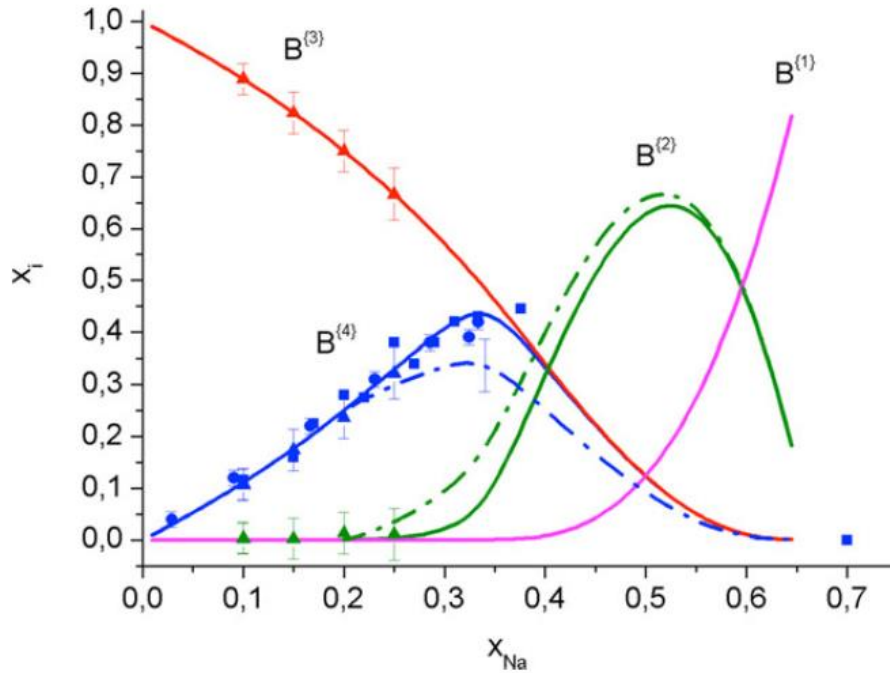
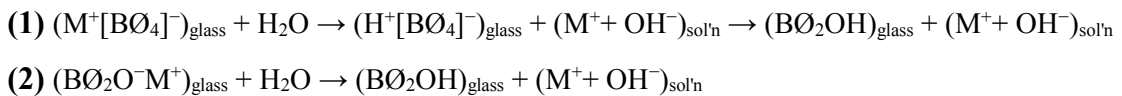


**Figure 1.2:** Distribution,  $x_i$ , of the borate basic structural unit species,  $B^{(n)}$  in monovalent substituted glasses. The solid lines correspond to the model distribution of (super)structural units [74].

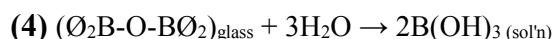
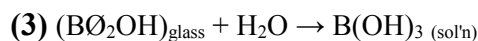
The degradation of borate glass networks is an area that is less well understood. Presently, it is contended that the degradation of borates, in aqueous solutions, occurs via the simultaneous hydration and hydrolysis of the network. Alkali and alkaline earth ions stabilize the charge on the anionic tetrahedral ( $B\text{O}_4^-$ ) and trigonal ( $B\text{O}_2\text{O}^-$ ) borate sites that constitute the borate glass structure. The hydration of these cations from these respective sites can be described by the following reactions [73]:



The replacement of an alkali ion with a proton in the initial hydration reaction **(1)** creates an unstable four-coordinated borate unit, which then converts to a more stable hydroxyl bond on a trigonal site. For both hydration reactions, solution pH will increase because of the consumption of protons by the borate units [72,73].

During hydrolysis, water attacks the bridging oxygen bonds between neighboring three-coordinated borate units to eventually release boric acid via two possible reaction

pathways. Reaction 3 shows the hydrolysis of the hydrated borate sites formed by the hydration reactions described above in Reactions 1 and 2, and Reaction 4 shows the hydrolysis of two trigonal sites that constitute the original glass structure [73]. The release of boric acid to solution by the hydrolysis of the borate sites will decrease the pH of the solution. As there is a much larger number of boron centers than modifier ions, the overall pH of the local environment will decrease with the degradation of the glass system.



The dissolution of borate glasses progresses by the simultaneous hydration of metal ions and the hydrolysis of the borate network [73]. The identity and concentration of the network modifier plays a large role in the dissolution kinetics; however, these dissolution pathways are only fully understood for alkali, and partially understood for alkali earth metals; there is little information on how higher valency ions may modulate structural and degradation characteristics. An understanding of how the modifier ions modulate the borate glass network is crucial to understanding the mechanism by which the glass degrades.

### 1.4.2. Modifier Ions

The role of monovalent (alkali) ions on borate structure has been studied in the literature, with less information available about how divalent ions or trivalent ions modify borate glass networks [76]. When divalent and trivalent ions are studied, the compositions chosen to assess their effects are typically very complex, which inhibits the understanding of the role of individual elements. Assessing the effects of substituting higher valency ions into a simple binary or ternary system will develop our knowledge by providing a clear platform on which to compare the effects of modifier ions, with respect to glass structure and properties.

Glasses intended for human use require additional considerations when choosing a modifier ion. For example, for use as uterine embolic agents, glasses should not cause cytotoxic effects, lead to acute or systemic toxicity, or generally be harmful to the patients.

Additionally, for the intended use as imageable, degradable beads, the modifier ion must modulate the architecture of the glass to allow for degradation, whilst concurrently imparting sufficient mass attenuation on the particle to provide contrast in diagnostic imaging. Furthermore, the glass must be designed so that their degradation by-products will not a) generate artifacts that might complicate follow-up imaging and/or b) provoke inappropriate host responses [18].

NIST mass attenuation coefficients [77] and publications from the Agency for Toxic Substances and Disease Registry (ATSDR) relating to the toxicological characteristics of candidate elements were considered to determine the makeup of a potential new embolic material composition [78,79]. Based on previous work completed in the Boyd lab, the degradable glass utilized for this research will comprise a borate network, with Sr and Ga substituted for Rb to attain the desired properties. Table 1.9 outlines the selection criteria information for each element.

**Table 1.9:** Mass attenuation and toxicity information for B, Rb, Sr and Ga [77-79].

	<b>Z/A</b>	<b>mean excitation energy</b>	<b>Density (g/cm<sup>3</sup>)</b>	<b>NOAEL</b>
<b>Boron</b>	0.46245	76.0	2.370	27 mg/kg/day
<b>Strontium</b>	0.43369	334.0	2.540	110 mg/Kg/day
<b>Rubidium</b>	0.43291	363.0	1.532	-
<b>Gallium</b>	0.44462	366.0	5.904	-

#### 1.4.2.1. Rubidium

Rubidium (Rb) is an alkali metal, which typically exists in an oxidation state of +1 [80]. Rubidium was chosen as the monovalent modifier ion due to its ability to impart radiopacity, as well as its hygroscopic nature which will allow the glasses to degrade quickly [80]. Previous works by Youngman and Zwanziger have shown that borate glasses with a 30 mol% substitution of Rb<sub>2</sub>O as a modifier ion have the highest concentration of B<sub>4</sub> units (38% of the relative population) [81]. Therefore, a binary boron – rubidium glass

with 30 mol% rubidium was chosen as the basis for this study, so as to allow for the highest number of B4 units, theoretically imparting the highest hydrolytic stability of all binary B-Rb glasses. Additionally, rubidium has a high atomic number to mass ratio and excitation energy compared to boron, and as a result will impart radiopacity into the glass [77,82].

Although the exact toxicological specifications on rubidium have not been reported by ATSDR, studies have been done on the potential harmful effects (or lack thereof) of rubidium [83-85]. A Provisional Peer-Reviewed Toxicity evaluation conducted by the U.S. Environmental Protection Agency gives rubidium chloride a LOAEL of between 5.1 and 7.7 mg/kg/day. Rubidium has been shown not to have an effect on glomerular filtration rates in rats, and only demonstrates mild hepatotoxicity in its fluoride salt form (RbF) [86]. It was concluded that the counter ion used in rubidium salts, such as fluoride and carbonate, are primarily responsible for the toxic effects reported, despite having blood serum rubidium concentrations of *ca.* 11 mg/L. Similar results were reported for humans with a blood serum rubidium concentration of 13.7 mg/L [87]. Rubidium is therefore only slightly toxic on an acute toxicological basis, and would need to be ingested in large quantities to pose an acute health hazard [88]. As such, rubidium compounds have been used as both an antidepressant (as rubidium chloride) and as an iodine source for the treatment of goiters (as rubidium iodide) [84]. Additionally, rubidium was found to be readily taken up by tumor cells, as it behaves similarly to potassium [85] in cells whose Na<sup>+</sup>-K<sup>+</sup>-ATPase activities are elevated, which may impart radiopacity into the tumors themselves.

#### 1.4.2.2. Strontium

Strontium (Sr) is an alkali earth metal, typically found in the 2+ oxidation state. The selection of strontium as the divalent modifier ion for this research was done with the intent to impart the highest level of radiopacity, without adding any toxicological concerns. Strontium has a very high NOAEL threshold, allowing for the administration of a large amount of ion in a short amount of time without adverse toxicological effects [78]. However, care should be taken to avoid strontium treatments in children, as Sr is taken up in lieu of calcium, which may lead to bone growth problems. As can also be seen in Table 1.9, strontium has a high atomic number to mass ratio, excitation energy, and density

compared to boron, and as a result will impart radiopacity into the glass [77] whilst providing a means to control degradation.

Strontium is similar to calcium both physiologically in terms of absorption and secretion in the body, but also in effectively controlling the degradation rates of degradable glasses [88]. From a glass structure standpoint, an increasing SrO fraction in a borate glass composition favors the conversion of  $\text{BO}_3$  to  $\text{BO}_4$  units [89] creating a more durable glass by (i) acting as the ionic crosslink between non-bridging oxygens (NBOs) and/or negatively charged tetrahedral boron centers, and (ii) increasing the bond strength of this ionic crosslink. It has also been shown that binary strontium-borate glass exhibit a higher glass transition temperature than binary rubidium-boron glasses, demonstrating an increase in network stability; theoretically this is most likely due to an increase in  $\text{BO}_4$  units [76]. This increase in tetrahedral coordinated boron can stabilize the glass network, thereby modulating the time required to achieve complete hydrolytic degradation.

#### 1.4.2.3. Gallium

Initially, lanthanum was chosen as the trivalent modifier ion to be used in this research due to its nature as a network intermediate; it can act as a network modifier and, due to its high field strength, may also resemble a network former [90]. Substituting an alkali oxide for lanthanum has been shown to increase the number of oxygen atoms within the network, forcing an increase in network volume [91]. This indicates that increasing substitution of La causes the glass network to stabilize and densify, possibly via the formation of  $\text{BO}_4$  [90,91]. The stabilization of the borate network would have been effective in modulating the degradation time frame of the glass, while imparting significant radiopacity on the network. However, upon attempting this substitution into a rubidium-borate glass, it was observed that lanthanum caused rapid crystallization of the glass. Accordingly, alternative trivalent ions were considered; due to the design criteria, limited options are available when searching for trivalent ions. Gallium (Ga) was chosen for its ability to modify the network similarly to lanthanum, and its potential to impart radiopacity.

Gallium is a post-transition metal, commonly found in the 3+ oxidation state (however 1+ oxidation state is also possible). Gallium has been shown to transition from a network modifier to a network former (at *ca.* >6 mol% substitution) and may exist in both

tetrahedral and octahedral co-ordination states [92]. This transition may decrease the  $\text{BO}_4$  concentration by sequestering bridging oxygens away from the boron network, causing the formation of hydrolysable  $\text{BO}_3$  units [92]. Regardless of this decrease in  $\text{BO}_4$ , gallium as a network former appears to stabilize borate networks, and should therefore enable the production of a more stable glass, with increased resistance to hydrolytic degradation (i.e. provide an opportunity to modulate longer degradation timeframes as necessary). The observation of gallium as a substitution for a monovalent ion in a simple ternary system will give better insight to its exact role in the borate glass architecture. As seen in Table 1.9, gallium has a high atomic number to mass ratio, excitation energy, and density compared to both boron and strontium. It can be expected to impart significant radiopacity into the glass, while also offering an ability to modulate network architecture and properties to achieve the desired technological characteristics [77].

Unlike strontium, gallium does not have an accompanying ATSDR document, and therefore its exact toxicological specifications become more difficult to predict. It has no known physiologic function in humans, however it may be able to interact with certain cellular processes and proteins, especially those related to iron metabolism [93]. This introduces a potential risk in the design, which will need considerable further research should proof of principle be delivered with the current work. However, gallium has been increasingly used in the literature as a therapeutic ion for multiple disorders such as pathologic bone resorption, autoimmune disease, allograft rejection, infectious disease, Non-Hodgkin's lymphoma, bladder cancer, and hypercalcemia [93,94], and as such may carry limited risk.

## 1.5. The Problem Statement

Based on a comprehensive review of the literature, it is clear that the ideal requirements for imageable degradable embolic agents may be satisfied by examining modified borate glasses in a way which permits (i) the balance of sufficient radiopacity (to provide angiographic visualization), whilst (ii) altering the structure of the borate network so as to tailor appropriate degradation timeframes. However, the understanding of the composition-structure-property relationship for borate glasses is not well understood. This thesis presents the first investigative analysis into borate based degradable radiopaque embolic agents, while also expanding the compositional palette of borate glasses under consideration in the literature in a fundamental way. In this study, two series of borate glasses will be investigated: 1) the BRS series with the composition  $70\text{B}/30-x\text{Rb}/x\text{Sr}$  (where  $x=2,4,6,8,10$ ), and 2) the BRG series with the composition  $70\text{B}/30-x\text{Rb}/x\text{Ga}$  (where  $x=2,4,6,8,10$ ). Each formulation will be fully characterized, and their imaging and degradation properties examined. Arising from this analysis, a best in class composition will be chosen and designed to evaluate embolization safety and efficacy in a swine renal model. This model will be used to evaluate the risks laid out by FDA in the “Class II Special Controls Guidance Document: Vascular and Neurovascular Embolization Devices” [17]. Additionally, the feasibility of using a benchtop model to examine the risk of migration will be investigated.

## CHAPTER 2

### Overarching Thesis Objectives

The overall objective of this thesis was to investigate glass compositions suitable for use as degradable, radiopaque embolic agents, potentially for use in uterine artery embolization procedures. To do so, two glass series were synthesized and characterized to determine their potential use as embolic agents, and consequently the potential risks associated degradable embolic agents were assessed. The following are the specific objectives of this thesis:

- The first experiment of this work consists of synthesizing and characterizing eleven glasses of composition  $70 \text{ B}_2\text{O}_3 - 30-X \text{ Rb}_2\text{O} - X \text{ Y}$ , where  $\text{Y} = \text{Ga}$  or  $\text{Sr}$ , and  $0 \leq X \leq 10$  (in 2 mol% increments). The aim of this experiment was to contribute to the expansion of the compositional palate for borate glasses by bettering our understanding of the composition-structure-property relationship found in simple borate systems. The objective was to assess the effect of divalent (Sr) or trivalent (Ga) substitutions of monovalent (Rb) network modifiers on the basic properties of the glass systems.
- The second experiment of this work consists of assessing each glass for their the critical, indication specific, performance attributes that would make them effective embolic agents (i.e. degradability and radiopacity). This portion of the work aims to advance potential uses of bioactive glasses outside of the skeletal system, by assessing their potential as TAE materials. These indication specific properties were then compared to target degradation timeframes, CT radiopacities, and MRI susceptibilities collected from the literature and from interventional radiologist opinions, to determine their potential utility as embolic agents.



- The issue of migration remains a concern for regulatory agencies and the development of bench top models may provide a simple mechanism to examine this risk in an objective manner. Accordingly, the first objective of experiment three was to develop an *in vitro* benchtop method to assess the risk of migration. The aim of this section was to determine the feasibility of assessing migration *in vitro*, prior to implantation in an animal model.
- The second objective of experiment three was to choose a best in class (BIC) composition for the intended indication (based on the information collected in experiments one and two). This composition was then used to determine the usefulness of conducting *in vitro* testing on glass frit over microspheres, when microspheres will be used in the final application. The comparison of the properties of both the frit and the microspheres was used to determine if the thermal augmentation of the glass led to changes in the structure and/or properties of the selected glass.
- The final objective of experiment three was to develop a pilot *in vivo* protocol to provide a preliminary assessment of the safety, efficacy, and performance of the chosen composition. This pre-clinical protocol was designed to assess the following criteria (as per FDA guidance): (i) ease of deliverability (from a friction and tortuosity standpoint), (ii) acute complications, (iii) local and systemic foreign body reactions, (iv) recanalization, (v) embolization effectiveness, and (vi) device migration. The aim of this study was to design a pilot model which will demonstrate how safety, efficacy and performance could be established for degradable agents.

## CHAPTER 3

### **Multi-Modal Imageability and Degradation Characteristics of Borate Networks**

**J. Doucet<sup>1</sup>, E. Tonkopi<sup>2</sup>, A. Nuschke<sup>3</sup>, M.L. Tremblay<sup>3</sup>, K. Brewer<sup>1,3</sup>, S. Beyea<sup>1,3</sup>, M. Filiaggi<sup>1,2,4</sup>, R. Abraham<sup>2</sup>, U. Werner-Zwanzinger<sup>5</sup>, D. Boyd<sup>1,2,4\*</sup>**

<sup>1</sup> School of Biomedical Engineering, Dalhousie University, Halifax, NS, Canada

<sup>2</sup> Department of Diagnostic Imaging and Interventional Radiology, QE II Health Sciences Centre, Halifax, NS, Canada

<sup>3</sup> BIOTIC, IWK Health Centre, Halifax, NS, Canada

<sup>4</sup> Department of Applied Oral Science, Faculty of Dentistry, Dalhousie University, Halifax, NS, Canada

<sup>5</sup> Department of Chemistry, Dalhousie University, Halifax, NS, Canada

\* Corresponding Author:

Daniel Boyd, PhD

Department of Applied Oral Science

Faculty of Dentistry

Dalhousie University

Halifax, NS, Canada

This manuscript was written by the candidate (Jensen Doucet) under the supervision of Dr. Daniel Boyd, who provided guidance and assistance to all aspects of the work. Ms. Doucet proposed and conducted all the experiments described, with the exception of the solid-state NMR evaluations, which was designed and performed in collaboration with Dr. Ulrike Werner-Zwanziger from the Chemistry Department. Dr. Werner-Zwanziger provided critical support and manuscript review concerning the solid-state NMR evaluations. Dr. Elena Tonkopi conducted the data collection for the CT radiopacity measurements and provided assistance with the manuscript preparation regarding CT radiopacity experiment. Dr. Kimberly Brewer and her team at BIOTIC conducted the data collection for the MRI radiopacity measurements and provided assistance with the manuscript preparation regarding MR radiopacity experiments. As first author of the manuscript presented in Chapter Two, Ms. Doucet prepared the manuscript and incorporated the suggested edits from the co-authors. All co-authors reviewed the respective manuscripts and provided critical feedback.

The first two experiments of this thesis are enclosed in the following chapter. Experiment one encompasses basic characterization of all eleven glass compositions; the experiments consisted of x-ray diffraction, particle size analysis, solid state  $^{11}\text{B}$  NMR spectroscopy, density, and thermal analysis. Experiment two consisted of specific characterization of the desired properties investigated for uterine artery embolization; the experiments consisted of CT imaging, MRI, and mass loss analysis. The results of these two experiments have been combined into the following manuscript included in Chapter 3. The following statements were hypothesized for experiments one and two:

- $^{11}\text{B}$  NMR will show a higher ratio of four to three coordinated boron structural units upon higher concentration of substituted Sr, however the ratio of four to three coordinated boron will reach a maximum during the Ga series at 6 mol%, and begin to descend, due to the transition of gallium from a network modifier to a network former.
- Due to the large charge densities of  $\text{Sr}^{2+}$  and  $\text{Ga}^{3+}$ , addition of these modifier ions will modulate the super-structural units in the borate network in a way that requires the formation of space to accompany these large ions, thereby decreasing the

density of the borate glass network, and thus of the glass, as the concentration of substituted ions increases.

- Given that the atomic number to mass ratio, excitation energy, and density of gallium exceed that of strontium, it will be possible to extend the CT radiopacity of the gallium containing borate networks to a level above that which is possible for the strontium containing glass of the same range
- Due to gallium's ability to transition from a network modifier to a network former, the gallium substituted glasses will show a change in the rate of mass loss per unit surface area per time from a decrease to an increase upon increasing substitution. The strontium substituted glasses will decrease in degradation rate as the amount of strontium is increased, since the network structure and architecture modulation will lead to increased four-coordinate boron, hindering hydrolytic degradation.
- The stabilizing nature of the modifier ions will balance with the radiopacity they impart to yield a particle that has both a degradable time frame of 48 hours  $\pm$  10 and a radiopacity of at least 2,500 HU (which is suitable for uterine artery embolization) in the middle of one of the series.

### 3.1. Abstract

Two glass series were developed based on the substitution of a monovalent glass modifier for a di- or trivalent ion in a high borate glass system. The BRS series consists of compositions  $0.70 \text{ B}_2\text{O}_3 - 0.30-X \text{ Rb}_2\text{O} - X \text{ SrO}$ , and the BRG series consists of compositions  $0.70 \text{ B}_2\text{O}_3 - 0.30-X \text{ Rb}_2\text{O} - X \text{ Ga}_2\text{O}_3$ , where  $0.00 \leq X \leq 0.10$  in increments of 0.2. All glasses were characterized in order to examine their composition-structure-property relationships, and to assess their potential for use as degradable, radiopaque embolic agents. Glasses were melt quenched and evaluated in terms of structural changes ( $^{11}\text{B}$  MAS-NMR, density, and glass transition temperature), changes in radiopacity (both CT and MRI), and changes in degradation timeframes under simulated physiological conditions. Structural analysis revealed no change in the tetrahedral boron fraction (B4%) of the BRS series, despite a linear increase in density and  $T_g$ . The strontium acts as a crosslinker, creating a more hydrolytically stable network, which leads to longer dissolution times. Conversely, the BRG series displayed a linear decrease in the B4%, a decrease in density ( $T_g$  data not available), yet a slight increase in hydrolytic stability is also observed. Gallium most likely acts more as a glass former than a glass modifier, thereby sequestering oxygens from the tetrahedral boron centers, creating trigonal B3 centers and tetrahedral gallium. All glasses were found to be imageable on CT (intensity  $>3200$  HU at 120 kVp) and invisible on clinical MR imaging modalities.

### 3.2. Introduction

Despite their unique characteristics, including congruent hydrolytic degradation, low processing temperatures, high melt stability, and their potential for biomedical applications, borate glasses are under-represented in the glass science literature. Specifically, less than two percent of the published literature considers borate glass compositions, the majority of which relates to borosilicates (e.g. Pyrex) [73]. Increasing emphasis on the development of degradable biomedical materials, coupled with the philosophy that development of new biomaterials should be directed towards unlocking “the body's innate powers of organization and self-repair” [95], is increasing the popularity of borate glass systems [96]. Contrary to conventional silicate-based bioactive glasses, borates degrade in water at a rate that may be precisely modulated via compositional or

structural modifications [97]. Accordingly, borate glasses have been considered in application such as wound healing, where it is contended that they stimulate angiogenesis, support neovascularization, and direct soft tissue repair [98]. With respect to hard tissue regeneration, objective evidence exists to show that borates support natural healing processes concurrent to providing an osteoconductive and osseointegrative platform suitable for skeletal applications [99].

While the ability of borate networks to degrade hydrolytically offers significant advantages in biomedical engineering, the mechanisms underpinning degradation are poorly understood. Our limited understanding of factors that may modulate degradation, such as ionic radius, field strength, and valency, further complicates this situation. It is understood that pure  $B_2O_3$  glass consists solely of trigonal boron in mostly boroxyl rings [100]; however, boron has more than one stable configuration with oxygen [74]. For example, upon the addition of a monovalent network modifier, trigonal  $BO_3$  (B3) converts to tetrahedral  $BO_4$  (B4) up to *ca.* 33 mol% [74]. The mole percent at which this conversion is maximized depends on a variety of factors such as the charge density and size of the modifier ion(s). This conversion stabilizes the glass network and leads to longer dissolution times (i.e. enhanced hydrolytic stability). Thereafter, (> 33 mol% addition of modifier) the network becomes more disrupted, leading to higher concentrations of non-bridging oxygens, resulting in more reactive glasses [74,75]. This feature, termed the ‘borate anomaly’ [74], provides a unique compositional and structural basis upon which the degradation of borate glasses may be modulated by the inclusion of specific elements which can themselves modulate critical network properties. To date, this anomaly has been highly characterized with alkaline modifier ions, and to a lesser extent alkali-earth ions; the effect of higher valency ions on the properties of simple borate systems is less understood, particularly with respect to degradation [75,76].

From a mechanistic standpoint, it is contended that the degradation of borates in aqueous solutions occurs via the simultaneous hydration and hydrolysis of the network [75]; however, existing models are limited and based largely on alkali-borate glasses. With respect to modulating degradation, it is believed that modifier ions “do not passively occupy sites (cages) formed by the surrounding vitreous network” [74]. Rather, the structure of the local environment surrounding the modifier is altered to suit their

requirements, and thus the size and density of the network is based largely on the modifier ions present [101]. Consequently, for a given compositional palette, it is possible to modulate both the material and host responses of borate glasses for a variety of medical indications.

Recently, glass materials have been increasingly considered for therapeutic applications in oncology [102] and, in particular, as imageable microspheres for the transarterial embolization (TAE) of hypervascular tumors. Briefly, TAE is a minimally invasive, fluoroscopically guided transcatheter procedure that uses microspherical particles to block blood flow to targeted tissues [16]. Glass microspheres for TAE provide the unique clinical advantage of CT imageability under clinical conditions without confounding follow up MRI scans. Specifically, this allows for both intra- and post-procedural feedback regarding the temporal and spatial distribution of microspheres within target tissues [18] and consequently may support personalized treatments, standardization of procedures, and optimized clinical outcomes. In addition to being imageable via CT and X-ray, there is now an increasing emphasis on the development of degradable microspheres for TAE. Degradable microspheres may be preferred over permanent embolics as degradable microspheres could 1) optimize ischemic time to target arteries while 2) minimizing ischemic effects on adjacent normal tissue, thereby balancing therapeutic requirements with excessive ischemia of normal tissue; the latter of which can lead to complications including non-target tissue infarction and post-embolization syndrome [103]. Secondly, patients have expressed “worries about foreign materials remaining in the body”, and the use of degradable microspheres may mitigate patient’s anxiety [14]. However, due to the relative novelty of degradable microspheres, imageability is necessary to accurately and objectively assess their efficacy and risks.

We hypothesize that borate glasses will be ideal candidates for use as degradable embolic agents, as they have tailorable degradation rates as well as the ability to incorporate CT radiopacifying elements without compromising biocompatibility [18,103]. These microspheres will thus be visible using CT, but invisible on MRI to allow for follow up pathological imaging. This study will investigate the multi-modal imageability and degradation of borate networks modified with gallium and strontium. This objective satisfies two functions: firstly, it is intended that the work will provide information on the

influence of monovalent for divalent, and monovalent for trivalent substitutions in borate networks. Secondly, this work is intended to allow for the assessment of critical performance attributes of borate glasses with respect to TAE (i.e. modulation of degradation, and imageability characteristics).

### **3.3. Methods**

#### **3.3.1. Glass Synthesis**

Eleven glasses, separated into two series – one with a monovalent for divalent substitution and the other monovalent for trivalent – were synthesized through melt quenching according to the compositions listed in Table 3.1. The glasses were divided into two series: The BRG series consisting of glasses substituting  $\text{Rb}_2\text{O}$  for  $\text{Ga}_2\text{O}_3$ , and the BRS consisting of glasses substituting  $\text{Rb}_2\text{O}$  for  $\text{SrO}$ . Glass precursor compositions were weighed into high density polypropylene (HDPP) jars and mixed mechanically in a blender for one hour to ensure a homogeneous mixture. Glasses were then melted in 10%Rh /90% Pt crucibles using a high temperature box furnace (Carbolite RHF 1600, UK), programmed to heat at 25 °C/min to an initial dwelling temperature of 600 °C and held for 60 min (to allow calcination). Thereafter the furnace was ramped at 20 °C/min to a final dwelling temperature of 1100 °C and held for 60 min. Each glass melt was quenched between two stainless steel plates and the resulting glasses ground with a planetary micromill (Pulverisette 7), then sieved to retrieve particles of <100  $\mu\text{m}$ , 100-300  $\mu\text{m}$ , and >300  $\mu\text{m}$  (ASTM standard sieves, Cole Parmer, USA). Glasses were stored in labelled glass vials in vacuum desiccators for subsequent analysis. Particle size distribution was verified through laser diffraction of a wet suspension using a Mastersizer 3000 model laser diffraction particle size analyzer using distilled water as the dispersant.



**Table 3.1:** Glass compositions by molar fraction (pre-fired material).

Glass	B <sub>2</sub> O <sub>3</sub>	Rb <sub>2</sub> O	SrO	Ga <sub>2</sub> O <sub>3</sub>
BR 0	0.70	0.30	-	-
BRS 2	0.70	0.28	0.02	-
BRS 4	0.70	0.26	0.04	-
BRS 6	0.70	0.24	0.06	-
BRS 8	0.70	0.22	0.08	-
BRS 10	0.70	0.20	0.10	-
BRG 2	0.70	0.28	-	0.02
BRG 4	0.70	0.26	-	0.04
BRG 6	0.70	0.24	-	0.06
BRG 8	0.70	0.22	-	0.08
BRG 10	0.70	0.20	-	0.10

### 3.3.2. X-Ray Diffraction Analysis

X-ray diffraction (XRD) analysis (Department of Physics, Dalhousie University) was conducted on all glass samples to verify non-crystallinity. A Bruker D-8 Discover diffractometer equipped with a Vantec-500 area detector and a copper target X-ray tube are used for XRD measurements. Powder specimens of each glass (<100  $\mu\text{m}$ ), were pressed into a square hollow steel wafer and scanned between  $10^\circ \leq 2\theta \leq 60^\circ$  with a step size  $2\theta = 0.05$  [90].

### 3.3.3. Solid State NMR Spectroscopy

<sup>11</sup>B magic angle spinning (MAS) NMR spectra were acquired on a 16.4 T Bruker Avance NMR spectrometer (<sup>11</sup>B Larmor frequency = 224.67 MHz) using a 2.5 mm HX probe head. The samples were spun at 10 and 25 kHz to determine center bands and to identify spinning sidebands. The NaBH<sub>4</sub> resonance served as secondary chemical shift standard at -42.1 ppm relative to BF<sub>3</sub>.Et<sub>2</sub>O. For the <sup>11</sup>B NMR spectra 64 scans were accumulated, using a pulse length of 0.56  $\mu\text{s}$  corresponding to a 15 degree pulse angle in the nearly cubic environment of NaBH<sub>4</sub>. The small pulse angle was chosen to allow the comparison of sites with different quadrupole couplings. Rough spin lattice relaxation

times were determined using a saturation recovery sequence and were on the order of 4-5 seconds. The pulse repetition times were chosen to be approximately three times the longest relaxation time. In addition to sample spectra, a spectrum of an empty rotor was acquired under identical conditions. The substantial boron background was removed by subtracting that spectrum of the empty rotor. The intensities of the different sites were determined by integration with shift limits of 23.3 to 6.0 ppm for the B3 range and 6.0 to -6.3 ppm for the B4 resonances [90].

### **3.3.4. Glass Density**

Density measurements were conducted using an AccuPyc 1340 helium pycnometer (Micromeritics, USA) equipped with a 1 cm<sup>3</sup> insert, and packed with 0.9–1.0 g of powdered glass specimens of each glass (n=10 per glass, 100–300 μm). The results are reported as the average ± standard deviation (SD) [90]. Molar density was calculated for each glass composition by  $p_m = p/M$ , where  $p$  is the density of each glass and  $M$  is the molecular weight.

### **3.3.5. Thermal Analysis**

Glass transition temperature ( $T_g$ ) and first crystallization temperature ( $T_{p1}$ ) were analysed by DSC using a simultaneous thermal analysis — STA 409 PC Luxx® (Netzsch-Geratebau-GMBH, USA). Approximately 35mg of powdered glass (n=3 per glass, <100 μm) was packed into a platinum/rhodium crucible and heated at 10 °C/min from 50 to 1000 °C. Prior to heating, the BRG series was baked in an oven at 120°C to ensure no surface water was present to interfere with measurements.  $T_g$  onset,  $T_g$  inflection and  $T_{p1}$  were determined using Proteus Analysis software (VERSION 5.1.1) and are reported as the average ± SD. The glass stability is reported as  $\Delta T = T_{p1} - T_g$  [105].

### **3.3.6. Computed Tomography Imaging**

Quantitative CT radiopacity measurements of each glass composition (n=5) were determined using clinical 128-slice CT scanner Somatom Definition AS+ (Siemens Healthcare, Erlangen, Germany). Glass vials containing particles were imaged at 80 kVp and 120 kVp, 400 mAs, with 1 mm acquisition slice thickness and pitch=0.5. The

radiodensity, or radiopacity, was assessed by placing region of interest (ROI) on axial images at different locations inside the vial. All measurements were performed on 100–300  $\mu\text{m}$  particles. A clinically used contrast agent, Isovue® 370 (Iopamidol; 370 mg of non-ionic iodine per mL, Bracco Diagnostics Inc., Monroe Township, NJ) at half strength (i.e. mixed 50:50 with saline), and a permanent radiopaque embolic agent, ORP5 [105] were scanned under the same CT settings in order to benchmark the radiopacity of the glass compositions. Radiopacity is reported as an average of 5 measurements in Hounsfield Units (HU)  $\pm$  standard deviation (SD) [105].

### **3.3.7. Magnetic Resonance Imaging**

Each particles glass composition (100-300  $\mu\text{m}$ ) was dispersed at varying volume fractions (2.5, 5, 7.5 10 and 12.5% w/w) in an 8% aqueous porcine gelatin for the BRS series. Due to the rapid degradation of the BRG series, these particles were dispersed in a non-aqueous gel made with 1% Evonik Intelimer IPA 13-1 NG polymer (Evonik Industries, Essen, Germany) in peanut oil (Our Compliments, NS, Canada). Prior to addition of the particles, the gels were subjected to magnetic stirring and heating for proper mixture of all components (40° C for gelatin and 50 °C for the oil gel). Melted gels then were added to 5 mm Nuclear Magnetic Resonance (NMR) tubes pre-filled with appropriate amounts of particles. The NMR tubes were then subjected to horizontal rotation to properly distribute particles throughout the tube and to prevent gravitational settling of the microspheres prior to rapid cooling on ice to solidify the gel. Measurements of MRI susceptometry, bulk  $R_2^*$  (full-width at half maximum of the spectral linewidth), bulk  $R_2$  (CPMG) and bulk  $R_1$  (arrayed inversion recovery) [106] were conducted for all samples at room temperature using an Agilent 3T preclinical MRI. Values for a purely glass composition are obtained from linear regression analysis of each imaging parameter and extrapolated to 100% volume fraction ( $V_f$ ).

### **3.3.8. Glass Cylinder Synthesis for Mass Loss Evaluation**

The precursor blends for each composition were prepared and melted as per section 2.1, Glass Synthesis. On removal, each glass melt was quenched into stainless steel moulds (6 mm in length and 4 mm in diameter), which were set between two stainless steel plates.

Excess glass on the resulting quenched glass cylinders was removed by two methods: excessive glass was etched off using a Speedy Sharp utensil and the remaining excess was removed (while placed in the stainless-steel moulds) by using a grinding/polishing wheel equipped with 240 sand paper, and polished with 800 grit sandpaper. Prior to experimental use, the diameter and height of each processed cylinder was measured and recorded 3 times. Cylinders with uneven edges, visible bubbles, and/or noticeable chipping were excluded. The height and diameter are reported as an average  $\pm$  SD. In addition to this, an analytical balance (Mettler Toledo AB104-5/S, Switzerland) was used to measure the mass of each cylinder separately.

### **3.3.9. Mass Loss Evaluation**

Each composition was divided into five different time points (6, 12, 24, 36, 48 hours) and placed separately into 50 ml Falcon tubes (n=5 per time point). 20 ml of 10% FBS/DMEM (Sigma-Aldrich) was then added to each tube as per ISO-10993 Sample Preparation and Reference Materials specifications [107]. The dissolution was performed in a shaking incubator (Thermo Scientific, MaxQ 4000), agitated at 120 rpm and kept at 37 °C. Once the extraction time point had been reached, cylinders were filtered from the extraction solution, washed with cold distilled H<sub>2</sub>O, then placed and dried overnight in a 50 °C oven. Weight, diameter and height of each cylinder was measured and recorded 3 times after drying. The weight, height and diameter are reported as an average  $\pm$  SD.

### **3.3.10. Statistical Analysis**

All statistical analysis was performed using Prism7 software (GraphPad Software Inc., La Jolla, USA). Each calculation of density, T<sub>g</sub>, T<sub>p1</sub>, and CT radiopacity was performed in (minimum) triplicate. Results are expressed as mean  $\pm$  standard deviation of the triplicate determinations. One way analysis of variance (ANOVA) was carried out followed by a Bonferroni post hoc test for comparisons between groups, with the level of significance set at  $p < 0.05$ .

### 3.4. Results

11 glasses of composition  $(70 \text{ B}_2\text{O}_3 - (30-x) \text{ Rb}_2\text{O} - x \text{ Y})$ , where  $x=2, 4, 6, 8$ , and 10%, and  $\text{Y}=\text{SrO}$  or  $\text{Ga}_2\text{O}_3$ , were successfully synthesized and characterized. XRD analysis of all 11 glass compositions revealed amorphous glass structures, free of identifiable crystalline peaks (Fig. 3.1). Particle size analysis (PSA) also showed that the glasses were reproducibly milled to *ca.* 100-300 $\mu\text{m}$  (Fig. 3.2).

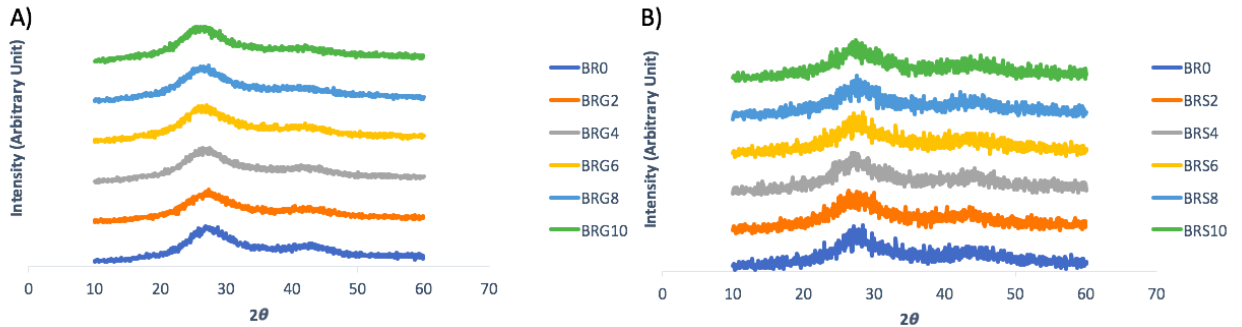


**Figure 3.1:** XRD analysis of A) 5 gallium series glass compositions and B) 5 strontium series glass compositions showing two amorphous peaks, at  $2\theta$  values of approximately 25 and 45, corresponding to 3 and 4 coordinated boron centers in the glass.

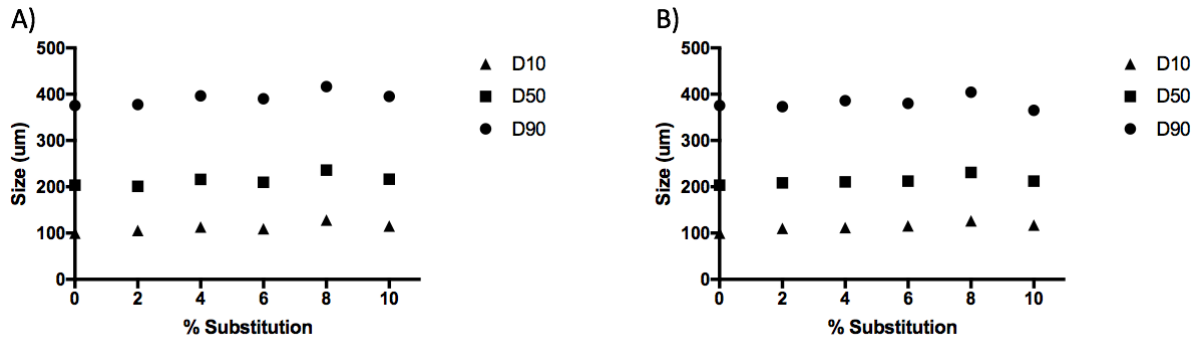


**Figure 3.2:** Particle size analysis of A) BRG series and B) BRS series where D90, D50 and D10 stand for particle diameters at 90%, 50% and 10% cumulative size, respectively. Error bars are plotted for all points, but are contained within the size of the symbol.

The fractional trends of tetrahedral coordinated boron in these glass compositions differed greatly between glass series, as did the line spectra (Fig. 3.3 & 3.4). The unsubstituted binary B-Rb glass (BR0) has a spectrum with two broad peaks – a B3 peak with a quadrupolar broadened resonance from 19 to 9 ppm and a B4 peak which ranges from 3 to -3 ppm, with integral values showing that  $43\pm 5\%$  of the boron centers are

tetrahedral (B4). The BRS series ranged from  $43\pm 5\%$  tetrahedral coordinated boron to  $41\pm 5\%$  with increasing strontium content. The spectra do not show significant changes when  $\text{Rb}_2\text{O}$  is exchanged for  $\text{SrO}$  in either the relative integrals of four coordinate boron vs three coordinate boron, nor in the spectra themselves. The BRG series, conversely, ranges from  $42\pm 5\%$  tetrahedral coordinated boron to  $20\pm 5\%$  with increasing gallium content, with substantial influence on the B4 region of the spectra – the line shapes of the B3 region do not change. Increased Ga substitution led to an increase in the relative integrals of B3 concentrations, and a decrease in B4 intensity despite increased oxygen content.

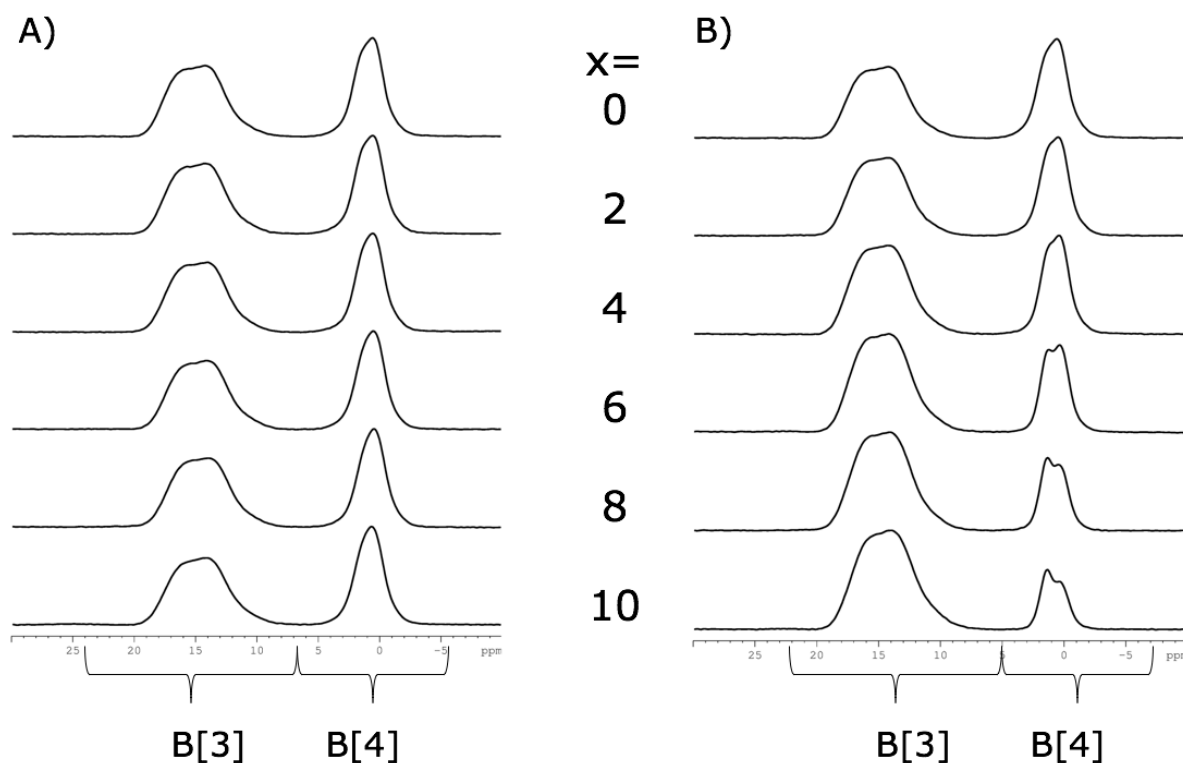


**Figure 3.3:**  $^{11}\text{B}$  MAS NMR line spectra of A) the BRS series, and B) the BRG series. The X value indicated the percentage of Sr or Ga substituted.

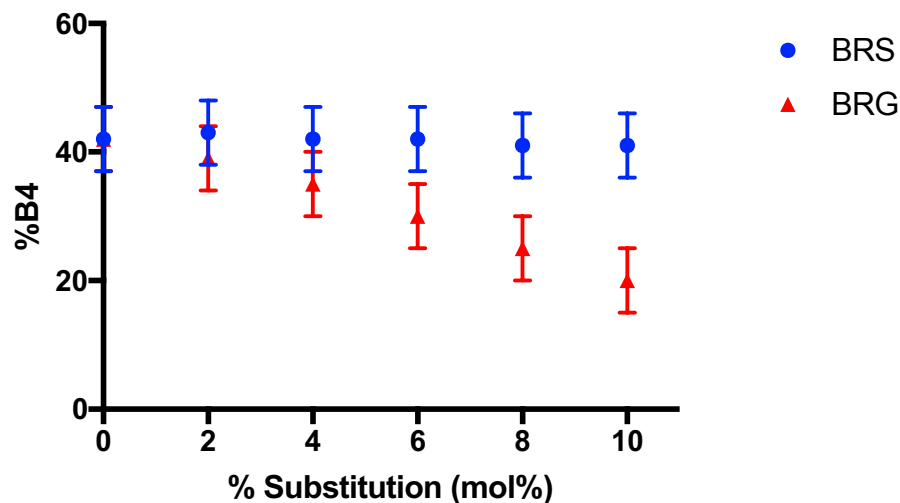


**Figure 3.4:** Fraction of four coordinated boron content by mol% of substituted ion

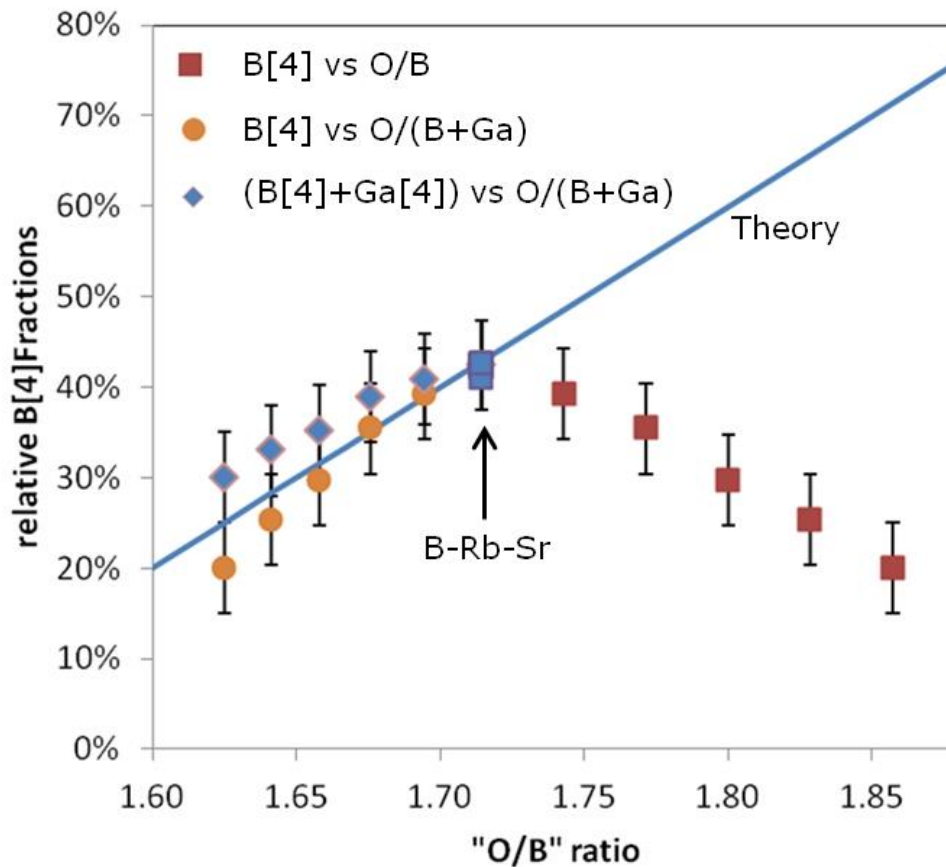


**Figure 3.5:** Plot of B4 concentrations versus oxygen to boron ratios of the BRS series (overlapping blue squares) and the BRG series (red). The blue line marks the theoretical values predicted in alkali modified glasses (see text), and the orange points mark the estimated values when the B4 percentage is compared to both Ga and B as network formers (circle) and when all tetrahedral (B and presumably Ga) are compared to both Ga and B as network formers (diamond).

Density measurements also varied between the glass series. Density increased linearly upon the increased substitution with strontium from 2.82 to 3.03 g/cm<sup>3</sup> (R<sup>2</sup>=0.98), whereas density showed a linear decrease from 2.82 to 2.70 g/cm<sup>3</sup> (R<sup>2</sup>=0.93) upon increased substitution with gallium (Fig. 3.6a). Molar density follows the same trend, with the BRS series ranging from 0.05382 to 0.05664 mol/cm<sup>3</sup> (R<sup>2</sup>=0.97) and the BRG series ranging from 0.05382 to 0.05153 mol/cm<sup>3</sup> (R<sup>2</sup>=0.93) (Fig. 3.6b).

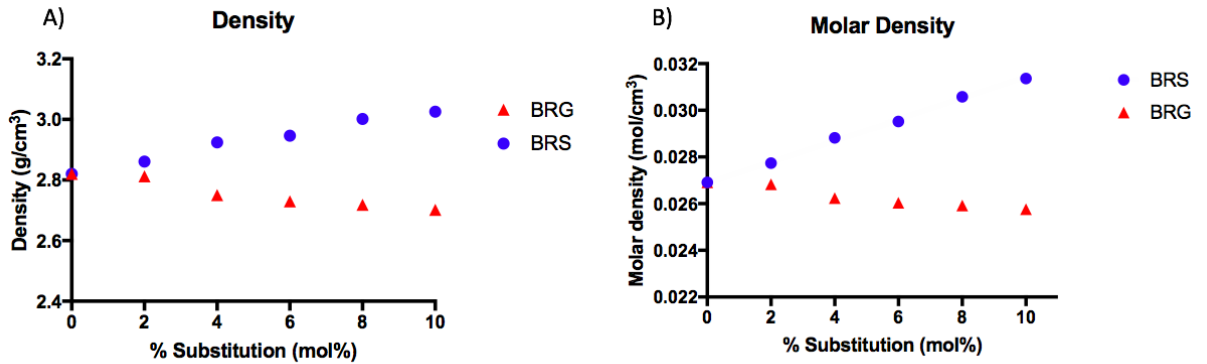


**Figure 3.6:** A) Density and B) molar density analysis of all 11 glass compositions displayed by percentage of ion substitution. Error bars are plotted for all points, but are contained within the size of the symbol.

Similarly, thermal analysis shows a linear increase in  $T_g$ , both onset and inflection, in the BRS series, from 416.2 °C to 489.5 °C (R<sup>2</sup>=0.99) and 431.8 °C to 500.2 °C (R<sup>2</sup>=0.97) respectively (Fig. 3.7). The majority of the values for the BRG series values are missing due to their extreme hygroscopic nature interfering with the spectra.



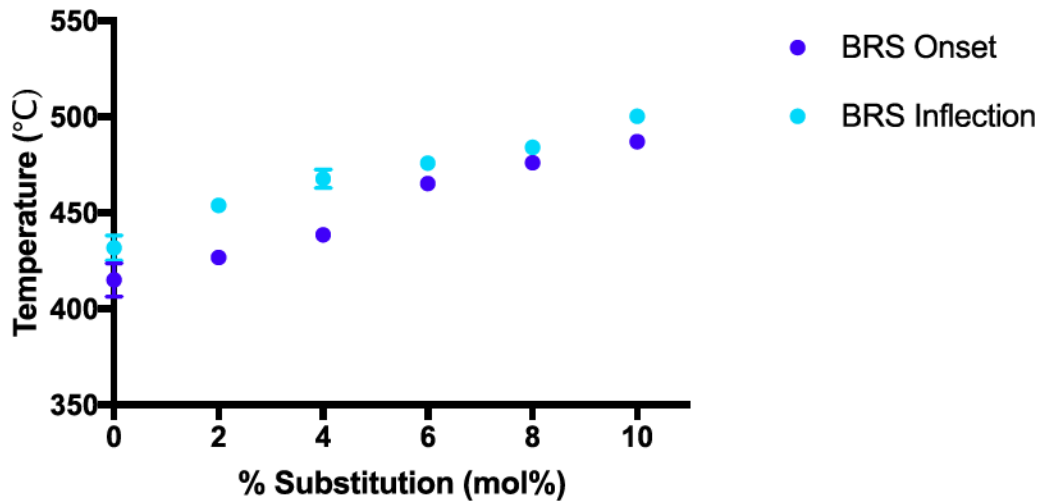


**Figure 3.7:** Glass transition temperatures, both onset and inflection, of the BRS glass compositions.

The first crystalline peak ( $T_{p1}$ ) was determined via DSC, and glass stability was calculated as  $\Delta T = T_{p1} - T_g$ , using both the glass transition onset and inflection points. The BRS series showed a relatively linear increase in glass stability with increasing strontium substitution, from 101.1 °C to 161.1 °C ( $R^2=0.74$ ) when calculated with  $T_g$  onset, and from 84.3 °C to 148.0 °C ( $R^2=0.84$ ) when calculated with  $T_g$  inflection (Fig. 3.8).

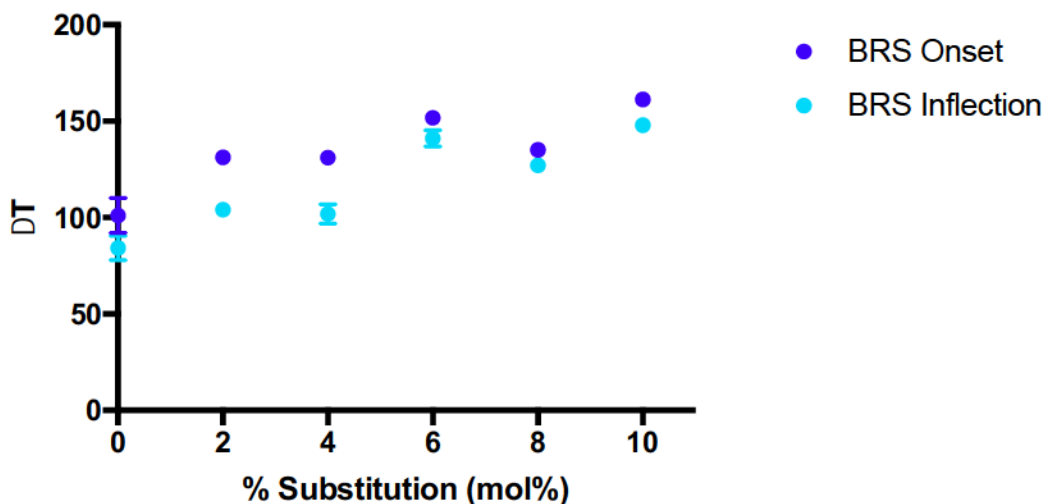


**Figure 3.8:** Glass stability ( $\Delta T = T_{p1} - T_g$ ) of the BRS glass compositions, calculated with both  $T_g$  onset and  $T_g$  inflection

All glass compositions exhibited high radiopacity upon clinical CT imaging (Fig. 3.9). The BRG series slowly decreases in radiopacity from 6022 HU for BR0 to 5398 HU for BRG10 ( $R^2=0.80$ ) at 80kVp and 3721 HU for BR0 to 3179 HU for BRG10 ( $R^2=0.89$ ) at 80 kVp. All data points were between the values recorded for 50:50 contrast media and a permanent radiopaque embolic agent (ORP5) which were used as control data [108]. The trend in the BRS radiopacity seems to be more parabolic, with values ranging from 6237 HU for BRS2 to 6238 HU for BRS6 to 6263 HU for BRS10 ( $R^2= 0.88$ ) and from 3798 HU for BRS2 to 3555 HU for BRS6 to 4072 HU for BRS10 ( $R^2=0.70$ ) at 120 kVp. Error bars are plotted for all points, but are often contained within the size of the symbol.

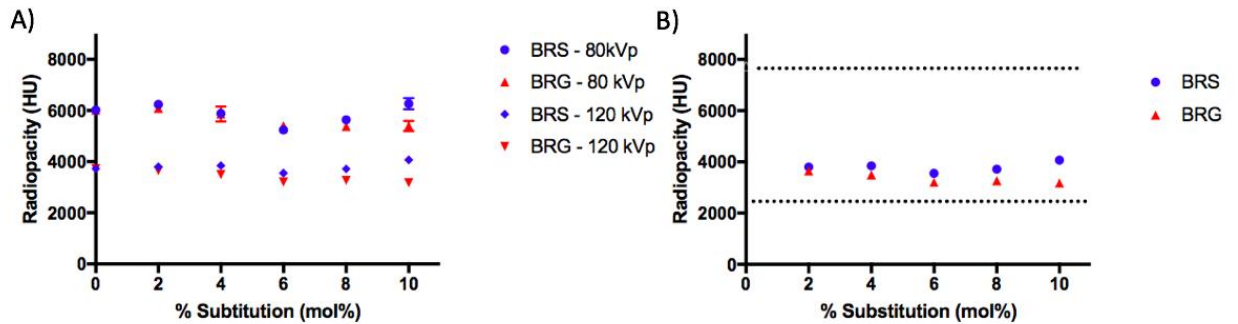


**Figure 3.9:** CT radiopacity values of all 11 glass compositions at (A) 120kVp and 80 kVp, and (B) 120kVp with comparisons. The line at 7733 HU represents 40-150  $\mu\text{m}$  ORP5 radiopacity, and the line at 2455 HU represents the radiopacity of half strength contrast media [105]

All glass compositions show similar outcomes upon magnetic resonance imaging. All exhibit minimal induced  $R_1$  and  $R_2$  contrast changes compared to background, as well as moderate  $R_2^*$  contrast changes (Fig. 3.10). Extrapolated values to 100% volume fraction are found in Table 3.2. The positive slope observed when calculating  $\Delta\chi$  of the materials via susceptometry indicates all samples are mildly paramagnetic (Fig. 3.11).

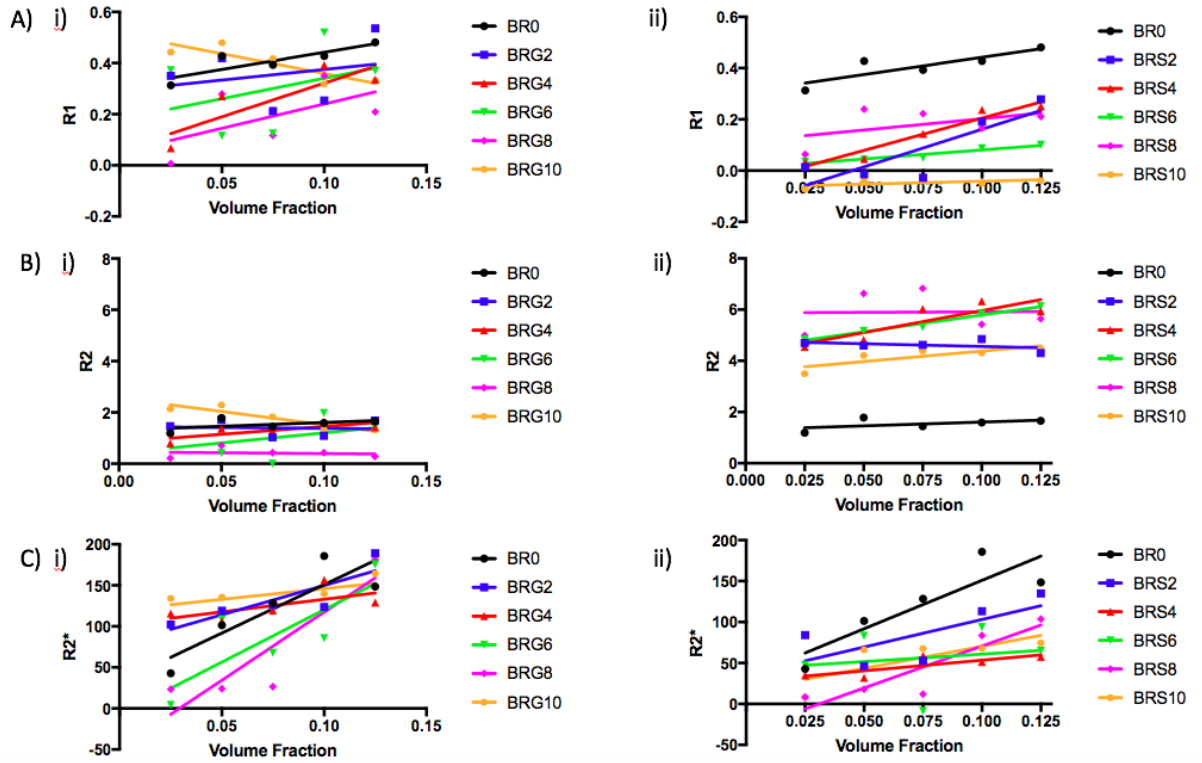


**Figure 3.10:** MRI results for A) R1 values of i) BRG and ii) BRS, B) R2 values of i) BRG and ii) BRS, and C) R2\* values of i) BRG and ii) BRS.

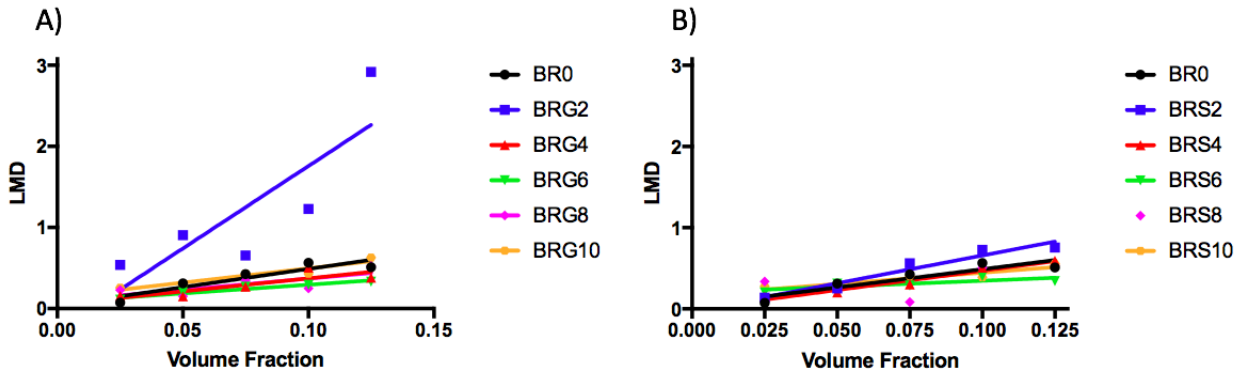


**Figure 3.11:** MRI delta chi ( $\Delta\chi$ ) values for A) BRG compositions, and B) BRS compositions

**Table 3.2:** 100% volume fraction values of R1, R2, and R2\* extrapolated from given data

Composition	R1	R2	R2*	$\Delta\chi$
BR0	1.6518	4.276	1214.71	4.5389
BRS2	2.8003	2.65	709.19	6.8175
BRS4	2.4693	21.441	286.78	4.7464
BRS6	0.7144	17.616	224.92	1.664
BRS8	0.9946	6.263	993.25	-2.0207
BRS10	0.1639	11.727	552.52	2.9366
BRG2	1.1201	0.756	792.65	20.0452
BRG4	2.6902	6.9166	410	3.2598
BRG6	1.7806	8.2808	1269.63	2.2203
BRG8	1.9499	-0.1685	1613.9	2.8497
BRG10	-1.0302	-7.794	379.9	3.6677

Mass loss values were calculated as percentage of total mass lost over time. The BRG series lost all structural integrity within six hours, leaving a white powder at the bottom of the tube. All BRG glasses dissolved quickly; BRG2, BRG4, BRG6, and BRG8 had lost 100% of their boron mass at the 48-hour time point, leaving only insoluble Ga<sub>2</sub>O<sub>3</sub>. Increasing gallium substitution mildly decreased degradation rates, ranging from complete, 100% dissolution for BRG2 to 88 ± 3% dissolved at 48 hours for BRG10 (Fig. 3.12a). The BRS series exhibited slower degradation rates than the BRG series. None of the glass compositions had reached 100% degradation at 48 hours, but even more so than the BRG series, additional substitution of strontium lead to decreased rates of degradation. The glasses degraded linearly over time, with slopes ranging from 0.020 ± 0.001 (R<sup>2</sup>=0.95) for BRS2 reaching 93 ± 3% dissolution at 48 hours, to 0.009 ± 0.001 (R<sup>2</sup>=0.95) for BRS10 which was 40 ± 7% dissolved at 48 hours (Fig. 3.12b). As illustrated in Fig. 3.13, the slope decreased in the BRS series indicating that the glass was dissolving at a lower rate and reaching a lower total percent dissolved at 48 hours with increasing Sr content.

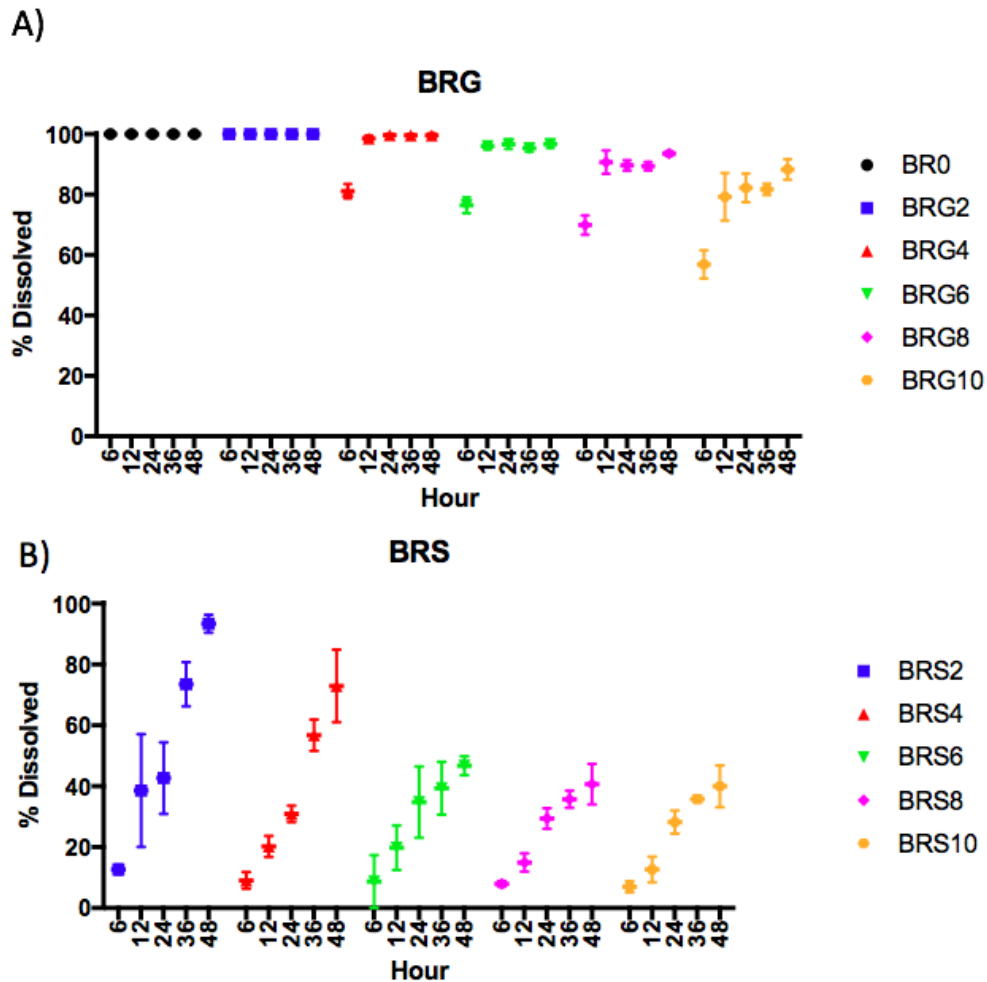


Figure 3.12: Percentage dissolved by mass of A) the BRG series and B) the BRS series over 6, 12, 24, 36, and 48 hours.

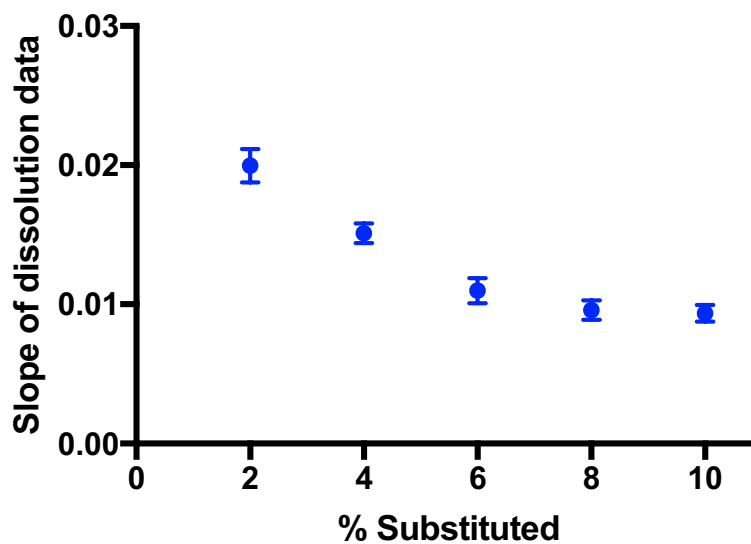


Figure 3.13: Slope of dissolution data vs composition for the BRS series.

### 3.5. Discussion

All 11 glass compositions were found to form a glass through plate quenching with no evidence of crystallization. Interestingly, many properties of both series behaved differently from one another and from what one would expect based on existing literature. It is commonly assumed that an increase in four-fold coordination in borate networks leads to a decrease in dissolution rates under aqueous conditions due to an increase in glass connectivity [74,101]. However, the structural characterization and degradation experiments in this work reinforce the need to consider other components and factors which may influence the properties of borate glasses. The BRS system studied here displayed a fraction of the four-fold coordinated boron which remained constant at the value predicted from theory (Fig 3.5), changing only within the uncertainty limits from  $43\pm 5\%$  to  $41\pm 5\%$  over the series; yet despite this observation, increased Rb substitution by Sr decreased the dissolution rates (Fig. 3.12 and 3.13). This can be understood from several points of view: (i) the alkali ( $\text{Rb}^+$ ) and alkaline-earth ( $\text{Sr}^{2+}$ ) cations both act as glass modifiers, and the replacement ratios were chosen such that the oxygen concentration, and therefore the O/B ratio remains constant, (ii) replacing two singly charged  $\text{Rb}^+$  cations with one doubly charged  $\text{Sr}^{2+}$  cation increases network connectivity and (iii) the substitution range covered is small [74].

In contrast, the substitution of  $\text{Rb}_2\text{O}$  with  $\text{Ga}_2\text{O}_3$  in the BRG series created substantial structural changes within the borate network, which affected the glass properties and demonstrated a decrease in four coordinate boron species. While the line shapes of the B3 regions do not change (Fig. 3.3), the B4 region of the  $^{11}\text{B}$  NMR spectra varies, indicating that  $\text{Ga}^{3+}$  preferentially bonds to B4 tetrahedra. Most importantly, with increased  $\text{Ga}_2\text{O}_3$  content, the relative integrals of B3 species increase, lowering the percentage of B4's (Fig. 3.4). This trend contrasts to what would be expected for alkali modified borated glasses [101,109] represented by the blue line in Figure 3.5; for this compositional range, the theoretical B4 fraction is calculated as  $\text{B4} = x/(1-x)$  at each O/B ratio, for alkali (R) modified glasses with the composition  $x\text{R}_2\text{O} - (1-x)\text{B}_2\text{O}_3$  [110]. The deviation of the BRG system from this theoretical trend suggests that gallium does not act simply as a network modifier, but rather as a network former. These findings can be further understood by examining the crystal structure of gallium oxide,  $\text{Ga}_2\text{O}_3$ , and gallium borate,  $\text{BGaO}_3$ . In  $\text{Ga}_2\text{O}_3$  and

BGaO<sub>3</sub>, gallium finds itself in four- and six-fold coordinated environments, and in order to accommodate these environments, each oxygen atom is triply bonded [111,112]. According to Zachariassen's rule [113], an oxygen atom can only be linked to a maximum of two cations in a glass, and the coordination surrounding that cation is small (four or less). As such, if gallium maintains the four-fold coordination in the glass networks studied in this work, then it cannot provide the necessary oxygens itself (from Ga<sub>2</sub>O<sub>3</sub>) and therefore must sequester them from the surrounding boron network. This conversion may transform BO<sub>4</sub> tetrahedra into BO<sub>3</sub>-groups with the inclusion of GaO<sub>4</sub> tetrahedra and octahedra [92], meaning that gallium is acting more similar to a network former than a network modifier. Treating gallium as a network former allows one to calculate the B<sub>4</sub> fraction against the ratio of "oxygen to total network formers" (labeled "B<sub>4</sub> vs O/(B+G)" in Fig 3.5). Hypothetically assuming further that all of the incorporated gallium assumes tetrahedral coordination, the total amount of tetrahedra can also be plotted as a function of oxygen to total network formers "(B+Ga)[<sub>4</sub>] vs O/(B+Ga)". The relationship between the concentration of B<sub>4</sub> and the ratio of oxygen to network former slightly underestimates the theoretical values, while the relationship between tetrahedral centers (Ga and B) and the ratio of oxygen to network former slightly overestimates the theoretical values (Fig 3.5), but both approximations cover the theoretical percentage within their experimental uncertainties.

The experimentally observed densities further support these conjectures; the density decreases in the BRG series despite the addition of a higher valency element into the glass network, meaning that the network may be expanding to accommodate gallium. While an increase in the percentage of B<sub>3</sub> may lead to lower density by itself, as a trigonal coordinated boron network is assumed to be more open and flexible than one with a high percentage of tetrahedral coordinated boron [74], it is most likely more important that the four (and possibly six) coordinated gallium acts as a glass former in addition to the boron causing the network to expand in order to allow for its incorporation. With respect to the BRS series, an increase in density is observed that is greater than that which would be expected given the marginal differences in atomic mass between Rb and Sr (85.47 g/mol and 87.62 g/mol respectively) [114]. This observation may be attributable to Sr<sup>2+</sup> acting

with higher crosslinking efficiency than two  $\text{Rb}^+$  cations, due to its higher charge density, leading to an increase in density of the glass [76,89].

Unfortunately, and despite several attempts to control water contamination under desiccated conditions, it was not possible to determine the glass transition temperature for all the BRG series due to their extremely hygroscopic nature. The glass transition temperatures for the BRS series were found to increase linearly with increasing strontium substitution despite the constant B4 concentration. The glass stability data (Fig. 2.8) indicate stable glasses for manufacturing processes, with melt stability increasing with increased strontium substitution. Despite stable B4 percentage, the increase in  $T_g$  once again suggests that strontium ions may play a structural role in the glass serving to increase network rigidity. This increased rigidity may potentially be attributable to the increased number of oxygens now surrounding modifier ions, which serves to stabilize the glass network [76,109,92].

One of the most interesting trends observed in this work is that increasing the substitution of  $\text{Rb}_2\text{O}$  for  $\text{SrO}$  or  $\text{Ga}_2\text{O}_3$  stabilizes the glass against hydrolytic degradation. For simple borate glasses, this trend is unexpected based on existing high borate bioglass literature where a higher fraction of tetrahedral boron content is understood to mean a more stable glass [74,75]. It was observed that substituted Sr and Ga do not increase B4 content, but did modify the dissolution via an alternative mechanism to decrease the rate of hydrolytic degradation. For both glass series, a decrease in both rate of degradation and overall mass lost at 48 hours is seen with increasing substitutions. The BRS system dissolves much slower than the BRG system and for each BRS composition the mass loss is linear over time. The BRS series is stabilized by increasing strontium substitution up to a point; the 6, 8 and 10% strontium substituted glasses have similar dissolution patterns with statistically similar mass loss occurring for each formulation at 48hrs (Figures 2.12 & 2.13). They also show statistically different densities, which would theoretically indicate that the 10% strontium should degrade more slowly than the 6% as it is a more compact structure and should make water penetration more difficult; yet this is not demonstrated in the data. Most of the cylinders (except cylinders which fractured early in the dissolution) degraded via surface erosion yielding smaller cylinders at each time point, however an additional white paste was observed as well at the bottom of many of the sample tubes.



The dissolution of the BRG series proceeds very differently; the BRG series glasses lose all structural integrity very quickly – the entirety of the dissolution occurs in the first twelve hours. For all compositions except BRG10 (and perhaps BRG8) no further dissolution is observed after 12 hours. Interestingly, the mass loss after 48 hours agrees within 2% with the borate-rubidium-oxide fraction of the composition. The rubidium-borate glass fraction appears to dissolve very quickly, leaving the gallium oxide portion in the form of a white powder, shown by the structural instability of the cylinders and the deposited powder, as well as the fact that gallium oxide is insoluble in water. Comparing the percent dissolved at 6 hours, one can see a statistically significant difference, which remains the case even when those time points are normalized to the borate-rubidium-oxide fraction of the glass. Further investigation at shorter time points is required to determine the extent to which gallium has stabilized the network. Collectively, the data reported provides valuable information on the influence of monovalent for divalent, and monovalent for trivalent substitutions in borate networks, and further emphasizes the need for expanded research in the area of borate networks.

In addition to providing valuable insights to the composition-structure-property relationship of high borate glasses, this study also provides insight to their usefulness in clinical applications. In clinical scenarios in which embolization is used as a method of treatment, permanent occlusion of target arteries is not a necessary requirement to achieve a satisfactory clinical outcome. The ischemic effect of temporarily occluding arteries can be achieved relatively quickly as tissue does not tolerate loss of blood flow for more than a few hours (5-7 hours for uterine fibroids) [35]. Additionally, allowing the target arteries to re-open soon after clinical effect has been achieved could allow for future retreatment of the region if needed and has the potential to preserve long term function of an underlying target organ such as the uterus, particularly in individuals who may be seeking pregnancy in the future.

Additionally, these glasses display CT radiopacity consistent with use as an embolic agent for the treatment of uterine fibroids. The linear attenuation coefficient data expressed in Hounsfield Units obtained in this study confirms radiopacity levels that would easily be detected by either X-ray fluoroscopy, static X-ray imaging, Cone Beam CT (CBCT) or conventional CT scans for microspheres at a diameter range greater than 40  $\mu\text{m}$ . This would

allow Interventional Radiologists to use these technologies during embolization procedures to truly understand where in the target arteries the microspheres deposit and how adequately the target area is covered. This in turn could allow for the standardization, optimization and personalization of these treatments.

It is also crucial to consider potential effects of treatments on imaging contrast in follow-up imaging, particular in MRI scans. The clinical standard MRI-based assessment of TAE treatment includes  $R_1$ -weighted gradient-echo (where  $R_1 = 1/T_1$ ),  $R_2$ -weighted fast spin-echo (where  $R_2 = 1/T_2$ ), diffusion-weighted imaging, and fat-suppressed  $R_1$ -weighted gradient-echo pre- and post-contrast enhancement using an extracellular gadolinium contrast agent. All of the boron glass compositions studied in this work were shown to induce no additional  $R_1$  contrast and would therefore not interfere with any  $R_1$ -weighted scans. They also induced minimal changes in  $R_2$ , with the maximum realistic change being a  $\Delta R_2$  of  $12 \text{ s}^{-1}$  at 3T from a 60% volume fraction (the maximum volume fraction obtainable due to packing of beads). When this  $\Delta R_2$  is added to a typical average  $R_2$  of liver (about  $23 \text{ s}^{-1}$  at 3T) [115], this would result in a change in  $T_2$  from 42 to 28ms, which is not a significant change compared to normal variability in liver  $T_2$  due to the presence of iron, which can cause typical variations in  $T_2$  from 20-50ms [116]. This means any fluctuations in iron would likely dominate over any effects due to beads.

Interestingly, these boron glass compositions do induce a larger change in  $R_2^*$  contrast (Table 3.2) that may be detectable with an  $R_2^*$ -weighted sequence. It is important to note that  $R_2^*$ -weighted sequences are generally not part of a standard clinical session, although these are increasingly being tested for evaluation of liver disease. However, given the significant amounts of iron that also induce  $R_2^*$  contrast in addition to changes in  $R_2$ , further experiments are necessary to determine if these compositions could be distinguished from effects due to iron. Overall, the bead compositions in this study would have negligible effects on standard MRI clinical scans and would not interfere with physicians' ability to evaluate treatment efficacy.

### **3.6. Limitations**

Limitations exist with any scientific study, and the authors would like to acknowledge the limitations of the present work:

- No compositional verification was done on the post-fired material; the authors assume that the resulting glass has the same composition as the pre-fired materials.
- Although this study aimed to quantify the composition-structure relationships in two different tertiary borate glass series, only the role of borate in the system was probed through the use of  $^{11}\text{B}$  MAS-NMR. Due to the low natural abundance of  $^{87}\text{Sr}$  and relatively low strontium content of the glasses examined, strontium NMR was not a feasible form of analysis to investigate strontium's role in the glass structures. Gallium NMR is feasible, and may be conducted in future works.
- The effect of SrO or  $\text{Ga}_2\text{O}_3$  on the glass structure was not evaluated in a  $\text{Rb}_2\text{O}$  free system; all glasses contained at least 20 mol%  $\text{Rb}_2\text{O}$ . The substitution of SrO for  $\text{Rb}_2\text{O}$  was not stoichiometric; the mole fraction of  $\text{Rb}_2\text{O}$  was replaced with an equal mole fraction of SrO.
- The extreme hygroscopic nature of the BRG series made some testing extremely difficult, and majorly confounded the data collected with the DSC. Future works should process the BRG series in a very dry environment so as to inhibit premature degradation.
- Dissolution profiles did not perfectly match the conditions seen *in vivo*. Due to the hygroscopic nature of the particles, cylinders were used to avoid the error of residual water due to clumping. The use of cylinders, however, made comparing surface area loss and dissolution rates to those expected *in vivo* quite difficult. As such, additional testing on 100-300  $\mu\text{m}$  particles or microspheres may be required to assess the feasibility of using cylinders in place of particles for preliminary testing.
- Radiopacity was measured on irregular particles, with a size range of *ca.* 100-300  $\mu\text{m}$ , resulting in an unknown number of radiolucent voids, which may lead to an artificial reduction in the resulting measured radiopacity.

### 3.7. Conclusion

Substituting strontium or gallium for rubidium in a boron-rubidium binary glass has drastically different effects. The strontium series show a constant percentage of B4 with increasing strontium, yet an increase in density,  $T_g$ , and hydrolytic stability (decrease in dissolution rate). As such, it can be assumed that the Sr ion is crosslinking the network,

thereby creating a higher network connectivity and a more stable glass. The gallium series, shows a decrease in B4 percentage with increasing gallium substitution, however the gallium acts more closely to a network former in this case, also resulting in a more stable glass. The gallium series, however, is less stable than the strontium series, making it unsuitable for use as an embolic agent. The strontium series shows promise as a potential TAE agent due to its high CT radiopacity and degradation rates, although the safety and efficacy of the material must be further assessed. These glass compositions may potentially overcome existing limitations for TAE materials, leading to a standardized, optimized and personalized procedure.

## CHAPTER 4

### Experiment 3: Pilot Benchtop Migration and Pre-Clinical Preparation

The composition-structure-property relationships established in Chapter 3 provide a basis to inform specific clinical performance attributes for the intended indication. Based on these data, experiment 3 was intended to develop pilot protocols for (i) the *in vitro* assessment of migration and (ii) to assess the embolization effectiveness of a preferred composition of borate glass microsphere for the intended indication.

Experiment 3 began the investigation into the safety and efficacy of radiopaque degradable embolic agents. The experiment was divided into two sections: Part 1 examined the feasibility of using an *in vitro* benchtop model to generally assess the migration risk for microspherical embolic agents. Data from experiments one and two informed the selection of a best in class composition for use in part two of experiment 3. This composition was synthesized, re-characterized, and processed into microspheres. A preclinical model was then developed to test the safety and efficacy of this glass composition when used as an embolic agent.

#### 4.1. Part 1: Benchtop Migration Method Development

##### 4.1.1. Objectives

- To develop a method of assessing migration via an *in vitro* benchtop model
- To determine the feasibility of assessing migration via an *in vitro* benchtop model

##### 4.1.2. Rationale

The risk of migration may be increased with degradable particles. As these microspheres degrade, they may potentially advance beyond the intended level of occlusion resulting in more profound ischemia and necrosis. Additionally, they have the potential to reflux into adjacent vessels, resulting in non-target embolization and/or shunt through capillaries leading to unintended injury of next level organs such as the lung or

brain [103]. Currently, the only method of assessing migration is in pre-clinical animal models, and even so there are no widely accepted methods of objectively and effectively observing migration. Furthermore, having reviewed the literature (per Section 1.2) it is obvious that this particular risk is commonly overlooked in pre-clinical embolization efficacy studies, and consequently there are no standardized method of assessing this risk.

In the present study, the feasibility of an *in vitro* benchtop study was assessed to determine if it is possible to assess the risk of migration using a standardized and objective approach. Currently there are no models available to assess migration via benchtop. The University of North Carolina at Chapel Hill has begun some work in particle hemodynamics and the use of an anti-reflux catheters [117]. However, they have focused more on the development of computer simulations as opposed to bench top modeling. A benchtop model is useful for actively visualizing the movement of particles in real time, as well as measuring the number of particles that migrate per unit time. As such, the development of an *in vitro* model may allow for the objective and reproducible assessment migration risk. EmboSphere® particles (500-700  $\mu\text{m}$ ) were selected for use in the development and evaluation of the benchtop model. The compressibility of EmboSphere® allows for the potential for particles to migrate the particle size range of 500-700  $\mu\text{m}$  was chosen to ensure that occlusion was possible in a model that had a terminal diameter of *ca.* 0.7mm. EmboSphere® was suspended in DMEM to act as a ‘contrast’ agent for visualization through the clear tubing. They are typically small, clear, colorless spheres, however the DMEM stained the spaces between the EmboSphere® slightly pink, which allowed for the visualization of the spheres within the model, and visualization of total occlusion.

The A-S-N-002-B model from Elastrat, Switzerland was chosen as it represents a soft abdominal silicon model without any aneurysms. However, since the model ends at the renal artery level, additional modifications were required to ensure that arteriole and capillary level vascular anatomy was captured. After substantive trial a stepwise reduction from the 5mm inner diameter (ID) model to the 0.74mm ID micro-tubing was chosen as it allowed for effective embolization.

### 4.1.3. Materials & Methods

#### 4.1.3.1. Model Set-up

An anatomically correct model (Fig 4.1) of the human abdominal aorta, renal arteries and iliac arteries (Elastrat, Switzerland) was modified to mimic a capillary network. The left renal artery (B) was modified by fitting a 43.4 mm x 5.7 mm connecting tube to the model adaptor, and a reduction adaptor connected the capillary – a tube with an inner diameter of 0.74 mm – to the connecting tube. The remaining return tubing was modified by replacing the t-adaptor with a straight junction adapter that allowed for a continuous flow back to the reservoir tank (A). The reservoir tank was filled with 2.5 L of tap water and the pump was turned on to maximum strength, with a flow rate of  $78.80 \pm 1.96$  mL/s measured with a flowmeter (Omega, Canada).

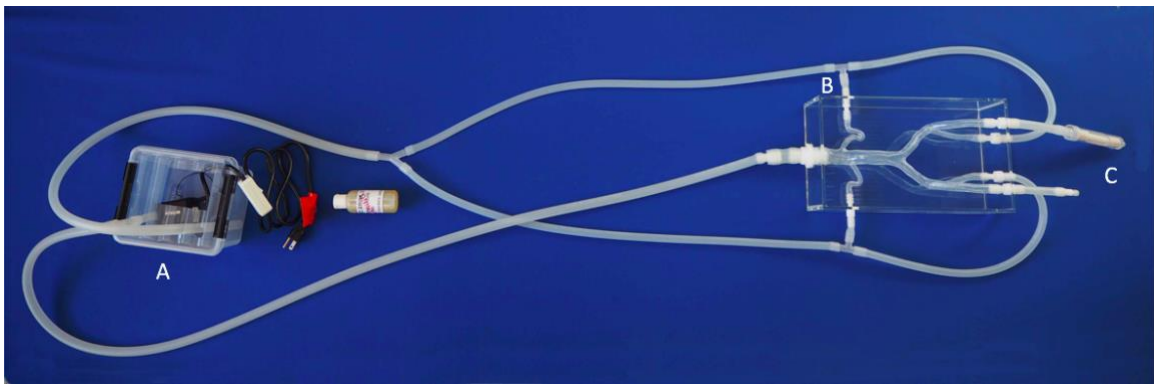


**Figure 4.1:** Benchtop renal artery model. (A) represents the fluid reservoir and the pump which approximates the heart. (B) indicates the area that has been modified to incorporate the capillary bed (C) denotes the percutaneous introducer used to insert the catheter (<20Fr) into the model for embolization.

#### 4.1.3.2. Experimental Design

A micro-catheter (Cook cantata 2.9 4Fr) was inserted into the percutaneous introducer and threaded into the left renal artery and down into the adapter adjacent to the micro-tubing. 500-700  $\mu$ m EmboSphere® suspended in Dulbecco's Modified Eagles Medium (DMEM) were injected until a bolus was formed. The embolization bolus was marked at both the distal and proximal end using a marker directly after embolization occurred. The distal end of the capillary was fed into a filtration system (Filtropur v50, 500 ml) to filter out any EmboSphere® that might have migrated further into the vasculature.

Each trial was run for two hours (n=5). At the completion of each trial the location of the bolus was marked; the pump was turned off and the connecting tube from the renal artery was clamped to prevent reflux of particles into the model. The adaptor and capillary tube were then removed from the model to allow for complete drainage into the reservoir. The entire reservoir tank was then filtered using the Nalgene vacuum filter (Filtropur v50, 500 ml).

#### 4.1.4. Results & Discussion

A total of five runs were completed to test for the success of this model, in addition to the preliminary troubleshooting. The final model can be seen in Figure 4.2, with a close-up on the reduction to the micro-tubing representing the capillary.



**Figure 4.2:** A) Complete setup of the benchtop model, B) stepwise reduction from the 'renal artery' to the 'arteriole' to the capillary bed.

The most effective methods of analyzing migration was with a modified filtration system. This system included a Nalgene vacuum filter (Filtropur v50, 500 ml) adapted to allow for any filtrate to return to the reservoir tank which then can be pumped back into



the model. This adaptation was performed by inserting a tube into the base of the Nalgene and applying sealant (Marine Adhesive Sealant Fast Cure 5200) to the filter device and tubing to ensure a tight seal. A separate filter paper (VWR 415) was placed on the original filter to allow for easy removal for analysis, and the system was vacuum filtered. Of the two methods used to assess the amount of EmboSphere® that had migrated, the most successful was found to be weighing the filter paper before and after the experiment. Counting the individual particles found on the filter paper after the experiment was equally effective but took significantly longer, and was more difficult. Removing the particles from the filter paper was found not to be necessary.

One of five runs demonstrated that particles had migrated through the capillary, indicating migration assessments may be possible using this method; however, four of five runs resulted in no migration of the particles from the bolus. In the successful run, the initial bolus was found to end at 23 mm from the adapter, and following the completion of the run, the end of the bolus was found at 41 mm from the adapter. Unfortunately, during this run the beginning of the bolus could not be measured as it was located within the adapter itself, as seen in Figure 4.3. It was very difficult to get a consistent level of occlusion and a similar number of particles injected. In addition, a method of migration not previously considered was uncovered during this experiment: the migration of individual particles deeper into the vasculature before a bolus has formed. The additional trials did allow for the assessment of bolus position, embolization effectiveness, and determine the number of particles that had migrated prior to bolus formation.



**Figure 4.3:** Reduction adaptor and micro-tubing filled with EmboSphere® suspended in DMEM following completion of one trial.

While the initial pilot work has indicated the potential for the development of *in vitro* test set ups to assess migration, some fundamental areas require considerable attention and development. In particular, due to the nature of the flow paths utilized in this model, when one pathway is obstructed, the flow from the aorta is redirected to the unblocked pathways, causing a strong decrease in pressure in the obstructed vessel. The water around the obstruction appears to be somewhat stagnant, similar to what is seen *in vivo*, however the lack of additional divisions of the renal vasculature makes it difficult to accurately assess fluid flow dynamics. Accordingly, a much larger model with more divisions in the renal artery would be required to accurately assess the risk of migration. The flow rates of these additional divisions should also be dealt with accordingly, to ensure the proper approximation of *in vivo* conditions. Overall, it seems that it may be feasible to assess migration via a benchtop model, were certain limitations addressed. The next section briefly identifies those limitations and provides recommendations to remediate issues, and enhance overall functionality of the model.

#### 4.1.5. Limitations and Future Consideration

- There were no gradual/step-wise reductions from the renal artery to the capillary network. The resistance going from the connector tube and capillary might be higher than expected in an animal. It is recommended that for future work, a single tube with a gradual reduction in size is used, rather than multiple tubes with reduction adapters. Additionally, divisions of the renal artery should be approximated to more similarly reproduce the fluid flow found *in vivo*.
- The pump used for the pilot experimentation was not pulsatile, which would be ideal to mimic the heartbeat of a human. Further works using a pulsatile pump would be more useful than the continuous pump used in this method. BDC laboratories (Colorado, USA) makes a variety of pulsatile pumps that effectively mimic cardiac cycles, with customizable stroke volumes and flow rates.
- Since a flow meter was used, it was difficult to determine the pressure exerted in each vessel of the benchtop model. In future works, pressure gauges should be fitted at the pump, the beginning of the occluded vessel, and on the return tubing to the reservoir tank. This will allow for consistent pressure control, and a more accurate picture of the fluid dynamics within the model.
- Materials used in future work should mimic the compliance of *in vivo* vasculature to properly assess vessel damage. Additionally, fluid used to simulate blood should more accurately approximate dissolved ion concentrations, and potentially clotting ability.
- The basic need for access to a vacuum for the filtering system coupled with the nature of the size of the model itself lead to a very specific need of lab space. The best place found in the lab space available to the authors still resulted in possible hydrodynamic discrepancies in the set-up as some of the tubing was coiled to fit in the space.
- The bench top model is not able to determine the final location of migrated particles, as it is a continuous loop of the abdominal aorta and renal vasculature. It lacks some of the finer conditions (i.e. specific venous vasculature and anastomosis), and therefore cannot predict the severity of harm caused should particles migrate. The severity of harm must be assessed in an animal model.

## **4.2. Part 2: Microsphere Synthesis and Embolization Efficacy**

The second section of experiment three intends to assess the embolization efficacy of a degradable embolic agent in a pre-clinical animal model. First, a best in class material was selected, synthesized, and processed into microspheres. These microspheres were re-characterized, sterilized, and shipped to the Centre Hospitalier de l'Université de Montréal (CHUM) to assess their safety, efficacy, and performance in a pre-clinical porcine renal model.

### **4.2.1. Objectives**

- To choose the best in class material for the intended indication based on the data collected in experiments one and two.
- To melt a new batch of best in class material and process it into microspheres.
- Re-characterize both the irregular frit and microspheres to account for any structure property changes as a result of additional processing.
- To develop a pilot pre-clinical animal model to assess the safety, efficacy and performance of the best in class material against the special controls criteria laid out by the FDA guidance document [17].

### **4.2.2. Hypothesis**

1. If thermal augmentation causes a change in the structure or properties of a glass microsphere, then a significant change in density, glass transition temperature, and glass stability of the frit will be observed after spherical processing.
2. The glass microspheres will be as effective at embolizing the renal arteries of pigs as the control permanent embolic (EmboSphere®), when evaluated based on extent of kidney ischemia and level of occlusion.

### **4.2.3. Rationale**

Taking into consideration the ideal properties for degradable microspheres outlined in Section 1.2.2., the best in class composition was chosen to satisfy the following criteria:

1. Has a degradation timeframe of  $100 \pm 5\%$  in 24-48 hours – so as to adequately address the 5-7 hour total occlusion timeline laid out by Vilos *et al.* [35].
2. Highest possible CT radiopacity – allow for intra- and post-procedural feedback to the clinician
3. No visibility on MRI – so as not to confound clinical follow up scans
4. Minimized density – to eliminate as much as possible concerns related to preferential distribution / flow under the action of gravity.
5. High glass stability –for ease of manufacturing

The BRS2 glass composition (70 B<sub>2</sub>O<sub>3</sub> – 28 Rb<sub>2</sub>O – 2 SrO) was found to fulfill all these criteria. To evaluate their embolization effectiveness, the objective of this phase of the research was to produce microspherical particles of BRS2 to allow the pre-clinical assessment of BRS2 in an accepted model. Spherical particles were chosen for use in this study, as irregular particles tend to clump and clog catheters [12]. To convert glass frit into spherical particles, irregular particles must be passed through a flame at temperatures exceeding 2000°C [118]. However, the melting temperature of these glasses was found to be *ca.* 700 °C, and while the temperature of the flame is sufficient to re-melt the glass and under the action of surface tension form a smooth, spherical particle, this additional process changes the thermal history of the materials. Accordingly, the elevated temperatures necessary to convert glass frit to microspheres may have a significant effect on the structure and properties of the resulting glass. Since glasses are a non-equilibrium system, their properties depend not only on standard thermodynamic variables (i.e. heating and pressure during formation, composition) but also on thermal history [119]. Therefore, additional heat treatments may alter the structure (and thus properties) of the treated glass [120]. If this is the case, any preliminary characterization performed on irregular glass particles may be of limited use, as the glass microspheres may behave differently than the investigated glass frit. If further heat treatments do in fact alter the properties of the resulting microspheres, then preliminary *in vitro* investigations may be required to be conducted on microspheres, to ensure the collected data will translate to *in vivo* applications. To investigate potential structure-property changes as a result of the additional processing step, the glass spheres created by spherical processing were characterized (XRD, PSA, thermal analysis, sphericity, SEM, and CT radiopacity) and the data was compared to both

the original characterization data collected in experiments one and two (in addition, to the newly collected data on the irregular particles).

The particle size distribution selected for this phase of the work was 100-300  $\mu\text{m}$  as this is smallest particle size range used for UAE [37] and therefore represents the worst-case scenario in terms of potential risk. Furthermore, the selection of this particle size represents the highest surface area to volume ratio (for the intended indication), and will thus degrade the most quickly, potentially leading to ineffective occlusion times, or worsening side effects (i.e. post-embolization syndrome). In addition, it is believed that such small particles also increase the risk of migration, as they are lighter and may reflux more easily [121]. Finally, this particle size distribution is likely the most challenging to image using standard imaging modalities (both from a temporal and spatial distribution standpoint [13]), and as such, should these particles prove to be imageable *in vivo* then the more commonly used larger particle size distributions should also be visible under similar conditions. The control article selected for this experiment was EmboSphere®, as it is most commonly used for UAE, and the size range of 100-300  $\mu\text{m}$  was chosen to match that of the test article (TA).

The advantages of degradable embolic agents include limited long-term exposure to foreign bodies, ability for repeat treatments, and peace of mind for patients who “express worries about foreign materials remaining in the body” [14,103]. When considering uterine artery embolization, degradable embolic agents have additional advantages. Specifically, that allow reperfusion of blood to the uterus, potentially preserving fertility in young women who wish to get pregnant later in life. Currently, there are a small number of temporary embolization materials available, each exhibiting substantive limitations in the context of UAE. Gelatin sponge particles are cut by hand prior to injection, leading to inconsistent particle sizes, uncontrollable levels of occlusion, and unpredictable degradation timeframes lasting from 3 weeks to 4 months [122,123,124]. Conversely, starch and PLGA microspheres do have calibrated particle sizes; however their degradation timeframes not suited to most temporary embolization indications. For example, starch microspheres degrade < 40 minutes, which contraindicates their use in UAE and many other TAE procedures [125,126]. PLGA microspheres degrade over several months, which triggers a long-lasting inflammatory and fibrotic reactions [31]. To overcome these

limitations, the preceding chapter discussed the development of two series of borate-based glass composition as potential degradable embolic agents; characterization performed in experiments one and two have shown that these glasses may display critical performance attributes for TAE. However, *in vivo* testing conditions are required to validate some attributes and to evaluate other risks (e.g. embolization effectiveness, inflammatory effects, etc.).

Pre-clinical evaluations are required for new medical devices to demonstrate safety and efficacy with respect to their intended application. The degradable nature of the microspheres developed in this work may presents new patient safety risks which have not been previously considered with permanent embolic agents. The industry guidance document (provided by FDA) to help ensure that all the necessary additional aspects of safety and efficacy of embolization devices are considered is titled “Class II Special Controls Guidance Document: Vascular and Neurovascular Embolization Devices” [17]. However, while this document is thoroughly detailed, it is important to note that the guidance was drafted prior to any substantive work with respect to the development and utilization of degradable embolic agents. Accordingly, many aspects of embolization effectiveness for degradable embolic agents may be overlooked. Therefore, in addition to consulting the required guidance documents, a Design Failure Mode and Effect Analysis (dFMEA) was conducted to evaluate potential risks with the design of the concept and coupled with the literature review, informed the design of an animal study protocol (drafted with the assistance of Lauren Kiri, Dr. Kathleen O’Connell, Dr. Bob Abraham, and Dr. Gilles Soulez).

Originally an ovine uterine model was proposed for this work, as it most closely approximated the human uterus environment, making it an ideal model to test uterine artery embolic agents [127]. However, the porcine renal model was implemented as a backup when the ovine uterine model proved to be unacceptable due to the timing of the study coinciding with lambing season. A non-atherosclerotic swine model was chosen because the model has been used extensively for angiographic/embolization studies resulting in a large volume of data on the vascular response properties and its correlation to human vascular response [128,129,130]. The porcine and human anatomy share important anatomic and physiologic characteristics [128,131]. Furthermore, the porcine kidney

model is accepted for use in preclinical studies by the FDA and as such has been widely used to evaluate embolization agents [130].

The proposed study comprises a pilot investigation to evaluate the effectiveness of biodegradable microspheres and will therefore utilize the minimum number of animals possible to meet the study objectives. The primary outcomes for this study were determined to be the assessment of: (i) embolization effectiveness, and (ii) test article migration. Embolization effectiveness and initial particle distribution will be recorded and compared to the control article. Migration will be assessed from two standpoints: movement of particles deeper into the uterine vasculature, assessed via cone beam CT and histology of the explanted kidneys, and ischemic damage to non-target tissues (i.e. NTE) assessed via full conventional CT and histology (of tissues showing evidence of ischemia on CT). The protocol was then sent for approval by both Dalhousie Animal Ethics and CHUM Institutional Animal Care and Use Committee to ensure compliance with Canadian Council on Animal Care (CCAC) regulations prior to the beginning of the study. For further data on the complete protocol, please see Appendix C.

#### **4.2.4. Materials & Methods**

##### **4.2.4.1. Glass Synthesis & Recharacterization**

300 g of BRS2 was melted, ground and sieved to yield 100-300  $\mu\text{m}$  particles (as per section 3.3.1, pg. 58). Characterization including XRD, PSA, density, thermal analysis,  $^{11}\text{B}$  NMR, mass loss, and CT (full details in Section 3.3, pg. 58) were performed on the newly melted glass frit.

##### **4.2.4.2. Spherical Processing & Recharacterization**

The newly synthesized irregular particles underwent spherical processing at ABK Biomedical (Halifax, NS, Canada) to yield 100-300 $\mu\text{m}$  microspheres. The parameters for the sphere processing process are as follows:

- i. The collection pot was lined with Aluminum foil (Ultra-Clean, premium aluminum foil from VWR International) and placed approximately 30 cm from the burner



- ii. The feeding funnel was positioned with the base directed towards the collection pot at a 45-degree angle.
- iii. The funnel was placed approximately 2.5 cm above the burner (from the center), and 1- 2 cm in front of the burner.

Characterization including XRD, PSA, density, thermal analysis,  $^{11}\text{B}$  NMR, and CT (full details in Section 3.3, pg. 58) was repeated on these microspheres. Additionally, sphericity analysis and scanning electron microscopy (SEM) imaging of the spheres was conducted. In particular, particle size analysis and particle shape (sphericity) were determined using dynamic image analysis (Camsizer XT (Retsch Technology)). A monolayer of the microsphere specimen was placed directly onto the feed chute. The feed rate of the particles was automatically adjusted by the instrument. A total of 976,170 particles were fed into the instrument and through the field of view of the two cameras. Particle size ( $\mu\text{m}$ ) distribution was reported as Dx10, Dx50, and Dx90. Particle shape was reported as the mean sphericity. Once analysis was complete, the microsphere specimens were stored in a desiccated environment.

For SEM, samples were mounted on SEM stubs using carbon paste, and then coated with 20 nm of gold-palladium. Multiple sites of each sample were then inspected using a model No. S-4700 SEM (Hitachi, Chula Vista, CA) operating at an accelerating voltage of 15 kV, a working distance of 12.3mm, and using magnifications up to 3,500.

#### 4.2.4.3. Packaging & Sterilization

Twenty 1g (18x1g for animal study, 2x1g for  $^{11}\text{B}$  NMR analysis) vials of microspheres were sterilized with a *ca.* 30 kGy dose of gamma radiation (Nordion) prior to use in the pre-clinical study. The accompanying required delivery devices (ABK Biomedical, Canada) were sterilized using ethylene oxide gas sterilization (Department of Medicine, Dalhousie University). One control package comprising 100-300  $\mu\text{m}$  EmboSphere® and a traditional delivery stopcock were also prepared for the pilot study. All materials, delivery devices and control microspheres were then delivered to CHUM.

#### 4.2.4.4. Statistical Analysis of Glass Properties

All statistical analysis was performed using Prism7 software (GraphPad Software Inc., La Jolla, USA). Each calculation of density,  $T_g$ ,  $T_{p1}$ , and CT radiopacity was performed in triplicate. Results are expressed as mean  $\pm$  standard deviation of the triplicate determinations. An unpaired parametric t-test was carried out with the level of significance set at  $P < 0.05$ , to compare the microspheres to the glass frit.

#### 4.2.4.5. Pre-Clinical Protocol

The pilot protocol developed intends to utilize bilateral renal artery embolization in 4 non-diseased pigs using methods adapted from the literature [18,129,132,133]. The full protocol is detailed and provided in Appendix C. Briefly, animals will receive the BRS2 (i.e. the TA) as per Table 4.1. Material will be delivered in amounts required to achieve effective stasis in the renal artery. The volume of delivered TA will be recorded for each animal. Three cohorts will be used to analyze embolization effectiveness and distribution at times equal to;  $t=0, 24, 48$  h. Migration will be assessed by assessing ischemic damage to non-target tissues via full conventional CT and histology (of tissues showing evidence of ischemia on CT).

**Table 4.1:** Test and Control Article Allocation

<b>Animal Number</b>	<b>LRA</b>	<b>Embolization Pole (Cranial / Caudal)</b>	<b>RRA</b>	<b>Embolization Pole (Cranial / Caudal)</b>
<b>0-01</b>	Test Article	Cranial	Test Article	Caudal
<b>24-01</b>	Test Article	Cranial	Test Article	Caudal
<b>48-01</b>	Test Article	Cranial	Test Article	Caudal
<b>48-02</b>	Control Article	Cranial	Control Article	Caudal

LRA: Left Renal Artery

RRA: Right Renal Artery

The TA will be delivered using sterile saline to monitor fluoroscopic visibility of the microspheres during injection. 50% of the renal mass will be conserved to preserve renal function; this will be determined angiographically. Fluoro-loops acquired during particle injection will be stored. Microspheres will be injected until effective stasis is reached (stasis of 50% contrast media for 5 or more cardiac pulsations) [18]. The total volume of TA delivered will be recorded for each animal, as well as total duration of the

procedure for each animal, and the ease of use of the material. One shot films and cone beam CT (in the angio suite) acquisitions will be acquired to evaluate the distribution of the radiopaque microspheres in each pig. Post-embolization angiography will be performed to the degree of vessel occlusion and document embolization efficacy. All embolized arteries will be qualitatively evaluated for arterial perforation or rupture and embolization effectiveness.

Immediately prior to the scheduled sacrifice time point, angiography will be performed in each animal to assess the embolization status of the renal vasculature) The following grade scale will be used for qualitative evaluation of recanalization:

- 0=no angiographic visible signs of arterial occlusion
- 1=reduction of parenchymal staining of the dependent territory
- 2=reduction of the parenchymal staining and occlusion of the supplying arcuate artery
- 3=reduction of parenchymal staining, occlusion of the supplying arcuate artery and occlusion of the feeding artery downstream of the catheter tip [18].

All treated animals will be subjected to necropsy, defined as gross examination of the embolized arteries and kidneys, whole body (external surface), all orifices, thoracic and abdominal cavities, and brain. Macroscopic pictures of all kidneys (ventral and dorsal views) and any lesions will be taken with a ruler adjacent to the tissue and properly labeled when possible (study number, animal number, organ). Kidneys will be evaluated macroscopically and measured (length, width and depth) before fixation. Three regions (cranial pole, middle region and caudal pole) will be evaluated individually on both surfaces (ventral and dorsal surfaces) for ischemic changes. An ischemic change score will be attributed to each region according to the following scale [31]:

- 0 = no macroscopic visible change;
- 1= discoloration of renal surface;
- 2 = Surface scars and retractions (corresponding to score 1 and 2);
- 3 = volume shrinkage of the respective area (corresponding to score 1, 2 and 3).

Each kidney with the renal artery (entire length) for each animal will be harvested free of fat and cranial pole properly identified (with ink for example) in a consistent

manner. Upon histological analysis, the number of microspheres in each layer will be recorded. The presence and extent of embolus surrounding each embolic will also be documented, as will the presence of inflammatory reaction and the types of inflammatory cells present (e.g. macrophages, multinucleated giant cells, lymphocytes, eosinophils). Identified microspheres (or microsphere fragments) will be measured and their shape will be qualitatively assessed (spherical vs. irregular). Vessel wall rupture, formation of new endothelium within the embolized vessel, and location of particles within the vessel walls should extravasation occur will be assessed and the degree of vascular injury will be rated as follows [134]:

- 0 = Internal elastic lamina (IEL) intact
- 1 = Disruption of the IEL without medial disruption.
- 2 = Disruption of the IEL with disruption of the media. The external elastic lamina is intact.
- 3 = Disruption of the IEL, media, and external elastic lamina.

Additional sections may be cut and stained with different stains to further assess embolization efficacy at the discretion of the Study Pathologist with the approval of the Study Director.

To assess migration, a selective angiography will be performed to evaluate the branch division into cranial and caudal branches and segmental renal arteries. Hyper-selective catheterization will be performed with a 2.5Fr micro catheter (Cantata, Cook Inc., Bloomington, IN) under fluoroscopic guidance [18,132]. All bifurcations downstream to the cranial and caudal branches will be recorded as D1, D2, D3, etc., where D1 refers to the immediate and largest branches of the cranial or caudal artery, following subsequent branches from this artery will be labelled D2, and further branches will be labelled as D3, etc. [132], similar to what is seen in Figure 4.1. After injection, but before sacrifice, another angiography will be performed and occlusion will again be labelled as per Figure 4.1. After sacrifice, and necropsy, all harvested organs will be fixed in a box containing formaldehyde. Hematoxylin-eosin-saffron staining of specimen will allow observation of occluded vessels and the locations of identified microspheres, which will be labelled according to the different layer of renal vasculature as per Figure 4.4 [132] for comparison

to pre-procedure labelling. Additionally, CBCT will be conducted to assess extent of necrosis arising from non-target embolization due to reflux.



**Figure 4.4:** Division System Method: D1 refers to the immediate and largest branches of the caudal artery, subsequent branches of this artery are labelled D2, further branches labelled D3, etc. [132].

#### **4.2.5. Results**

127.21g of 100-300  $\mu\text{m}$  particles of BRS2 were successfully melted, ground, sieved, and characterized. A summary of both the characterization data collected from experiments one and two, and the data collected from the newly synthesized pre-clinical lot (Lot 5) can be found in table 4.2. The pre-clinical lot was transformed into microspheres to be used in the pre-clinical protocol outlined in Section 4.2.4.5.

**Table 4.2:** Characterization data of BRS2 glass frit.

	B4 Fraction (%)	Density (n=4)	CT Radiopacity (HU)		Glass Transition (°C) (n=4)		Glass Stability (°C) (n=4)		Mass Loss at 48 hours (%)
			80 kVp	120 kVp	O*	I**	O*	I**	
Averaged Melt Data: Lots 1-4 (Exp. 1 and 2)	43 ± 5	2.861 ± 0.002	6236 ± 96	3798 ± 18	426.7 ± 2.7	453.9 ± 2.3	131.2 ± 3.2	104.1 ± 2.1	93.38 ± 2.97
Data for Pre-clinical Lot (Lot 5)***	N/A	2.864 ± 0.004	6414 ± 47	3932 ± 23	432.3 ± 13.3	452.6 ± 1.2	126.4 ± 12.5	99.3 ± 4.2	92.48 ± 0.27

\* O = Onset

\*\* I = Inflection

\*\*\* n=4

XRD analysis of glass frit and of microspheres confirmed that both morphologies were amorphous with no identifiable crystalline peaks evident (Fig. 4.5a). The characteristic broad double peak was visible, representative of three and four coordinated boron centers.

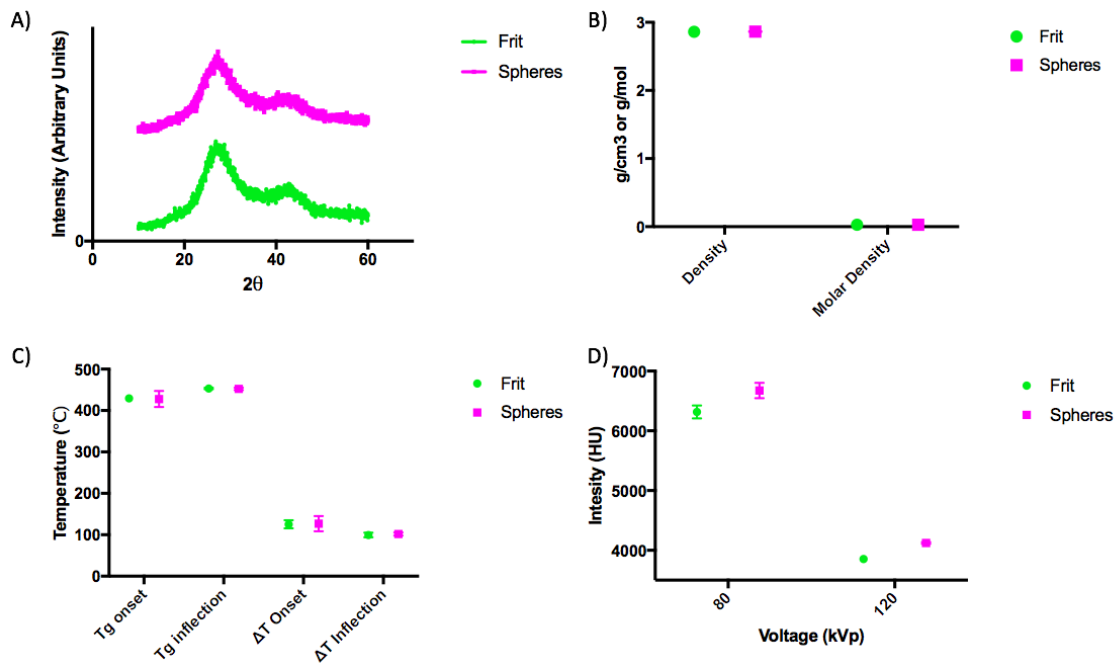


**Figure 4.5:** A) XRD data for the BRS2 glass frit and the microspheres. Two amorphous peaks can be seen at  $2\theta$  values of approximately 25 and 45, corresponding to 3 and 4 coordinated boron centers in the glass. B) Density and molar density data for the original BRS2 glass frit and the microspheres. C) Glass transition temperatures and glass stabilities (both onset and inflection) for the BRS2 glass frit and the microspheres. D) CT radiopacity for the BRS2 glass frit and the microspheres at 80 kVp and 120 kVp.

Density and molar density data (Fig. 4.5b) of the glass frit were recorded as  $2.862 \pm 0.003 \text{ g/cm}^3$  and  $0.02775 \pm 0.00003 \text{ mol/cm}^3$  respectively. After spherical processing, the density was recorded as  $2.863 \pm 0.005 \text{ g/cm}^3$  and  $0.02775 \pm 0.00005 \text{ mol/cm}^3$ , which was not significantly different from the glass frit ( $P=0.7674$ ). Thermal analysis (Fig. 4.5c) data can be found summarized in Table 4.3; no statically significant differences were observed.

**Table 4.3:** Thermal Analysis Data for Frit versus Spheres

	<b>Frit*</b>	<b>Spheres</b>	<b>Statistically Significant?</b>
<b>Tg onset</b>	429.5± 9.12	427.90 ± 19.22	No P=0.8651
<b>Tg inflection</b>	453.3 ± 1.78	452.27 ± 2.84	No P=0.5357
<b>ΔT onset</b>	125.3 ± 9.89	126.87 ± 18.52	No P=0.8718
<b>ΔT inflection</b>	101.6 ± 4.06	101.83 ± 3.60	No P=0.9264

\*Average value of all glass frit data collected

CT radiopacity (Fig.4.5d) of the microspheres demonstrated a significantly different value from the glass frit. The original CT radiopacity reported in experiment two was  $6327 \pm 96$  HU at 80 kVp, and  $3798 \pm 15$  HU at 120 kVp. After spherical processing, the new radiopacity intensity was  $6675 \pm 128$  HU at 80 kVp, and at  $4123 \pm 15$  HU 120 kVp, which is significantly different than the original ( $P=0.0003$  and  $P<0.0001$  respectively).

SEM images of the BRS2 microspheres display spherical particles with a size range of *ca.* 100-300  $\mu\text{m}$  (Fig. 4.6). Their surfaces appear to be essentially smooth; no chipping or cracking is visible on the surface of the spheres. PSA and symmetry analysis of the microspheres confirmed the size range and spherical symmetry of over 90% of the particles, as seen in Table 4.4.

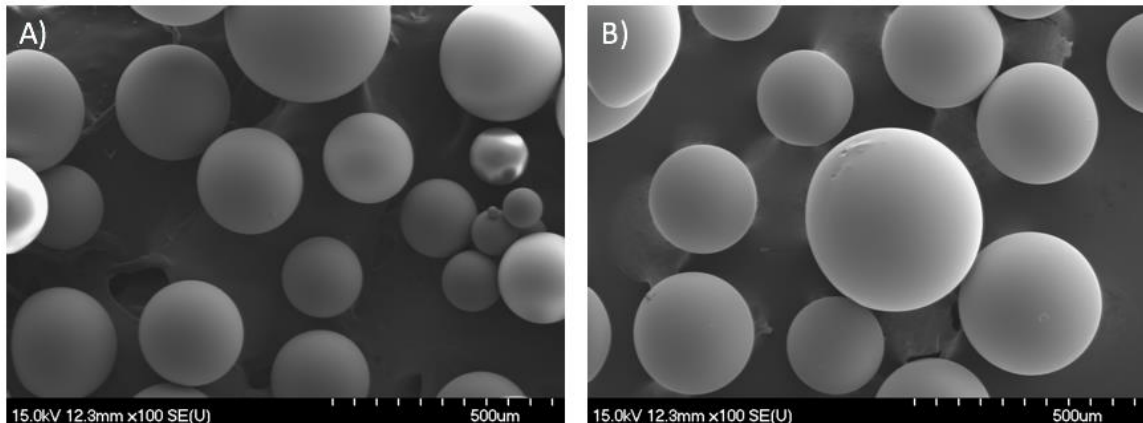


**Figure 4.6:** SEM images of microspherical particles (100x)



**Table 4.4:** Spherical Data and Particle Sizes of BRS2 Microspheres

Symmetry	94.6%
Sphericity	92.0%
D10	103.1
D50	224.5
D90	323.2
Mean value	224.8 ± 93.2

#### **4.2.6. Discussion**

The best in class composition selected for this work was BRS2 (70 B<sub>2</sub>O<sub>3</sub> - 28 Rb<sub>2</sub>O - 2 SrO). BRS2 exhibited the lowest density, second highest radiopacity, and degraded completely in 48 hours. Additionally, BRS2 exhibited high glass stability without any susceptibility to T1 or T2 weighted MRI scans. BRS2 was successfully melted, ground and sieved to yield 127.21g of 100-300 μm irregular particles, and a summary of the property data for BRS2 frit can be found in Table 4.2. No significant differences were found between the data collected in experiments one and two, and the characterization data collected on glass frit synthesized in experiment 3 (Table 4.2).

In order to understand the significance of the re-characterization data collected, one must first consider the fundamentals of glass science. A glass is a solid having a structure that displays the long-range atomic disorder typical of liquids, and as such, the heating and cooling history of glasses can have a significant impact on their properties [71]. This can most easily be understood by considering a volume-temperature (V-T) diagram as displayed in Figure 4.7.

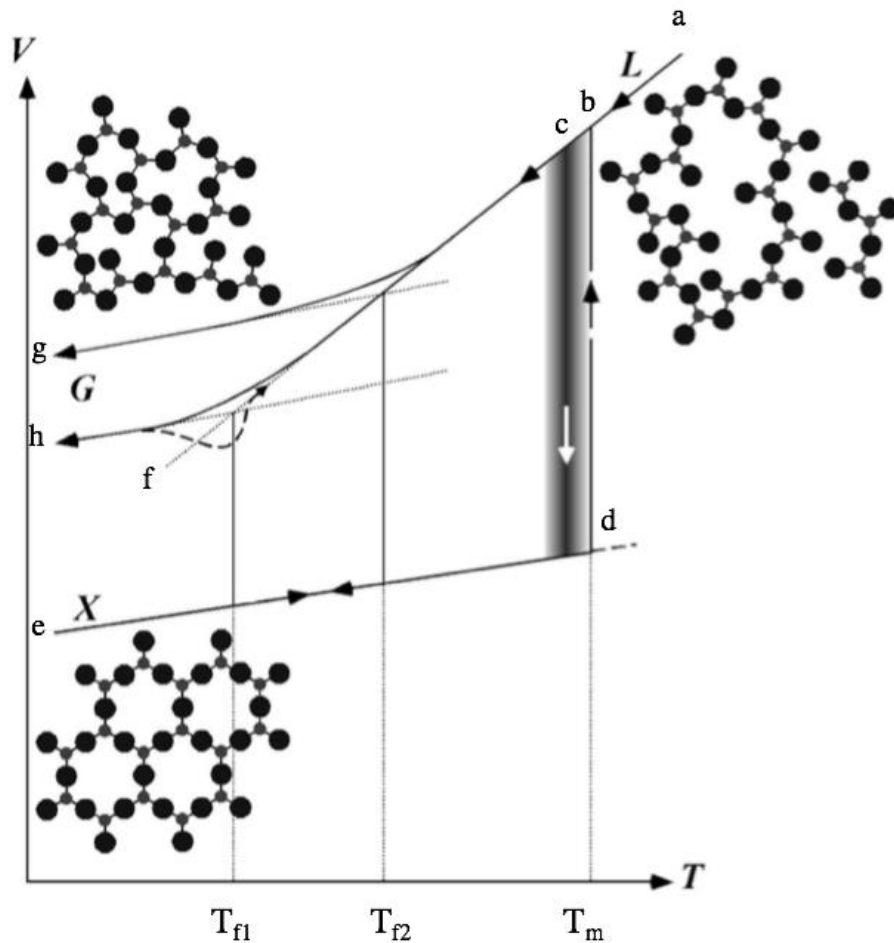


**Figure 4.7:** The volume-temperature diagram for a glass-forming liquid, superimposed with the accompanying atomic structure. “L” signifies liquid phase, “G” signifies glass, and “X” signifies crystal. [Modified from 71]

Before becoming a glass, a high temperature liquid must gradually cool along the ‘abc’ path (where ‘b’ is the melting point of the corresponding crystal,  $T_m$ ). If a large crystal growth rate exists, and there are a large number of crystal nuclei present, crystallization will occur at point ‘c’, and the crystal will continue to cool with a contiguous reduction in volume to point ‘e’ [71]. If crystallization does not occur (i.e. liquid is cooled at too high a rate), then the liquid follows the line of a “super-cooled liquid” (i.e. the ‘bcf’ path). As cooling continues, the viscosity increases as the molecules become less mobile. Eventually, the viscosity of the liquid becomes so high that the molecules cannot rearrange fast enough to attain the crystalline structure and volume characteristics associated with that temperature, and transition into the glassy state. Which end-point is attained (‘g’ or ‘h’)

depends on the cooling rate of the super-cooled liquid (fast cooling and slow cooling, respectively) [71].

Since the transition to the glassy state does not occur at a single temperature, and can follow two different paths, the thermal history of a glass has a large effect on the final structure and resulting properties [71,118,119]. Since spherical processing is done over a flame hot enough to melt the glass frit, there is a chance that the resulting microspheres do not have the same structure and/or properties as the frit. Thermal augmentation after formation may lead to a different heating or cooling rate than that undergone upon formation, thereby changing the final state of the glass from fast cooling ('g') to slow cooling ('h'), or vice versa. It is only by confirming the structure and properties of the thermally augmented glass that one can confirm that data collected on the original glass frit will translate to the intended application.

The characterization data of the newly melted BRS2 irregular particles and microspheres confirm the reproducibility of the results obtained in experiments one and two. Both density and molar density values are statistically equivalent before and after spherical processing. Molar density was calculated to remove the variation that molar mass has on density. However, it was found in experiment one that molar mass has very little effect on density for the BRS compositions, as Sr and Rb have very similar atomic weights. The re-characterization data of the glass frit suggests that the same composition was synthesized in this melt as in the original. The spherical data indicates that there is a good chance that no structural or property changes have occurred in the 100-300  $\mu\text{m}$ , compared to the irregular particles.

Thermal analysis data (Fig. 4.5c) of the microspheres and the irregular particles are not statistically different. A summary of the glass transition temperature and melt temperature (both onset and inflection) data collected is provided in Table 4.4. These data, combined with the consistent densities, allows for the provisional conclusion that the new glass synthesized matches the glass characterized in experiments one and two. Since  $T_g$  is defined as "the intersection of the glassy state line with the tangent to the steep portion of the state curve in the transition range" [71], it can therefore give valuable information regarding the thermal history and structure of a glass. Again, the comparable results seen in the original, the new glass frit, and the spheres reinforces the conclusion drawn from the

density data; that no structural changes have occurred from the thermal augmentation undergone during spherical processing. Therefore, there may be reason to believe that at the 100-300  $\mu\text{m}$  particle size range, spherical processing does not impact structure or properties for BRS2. However, this does not mean that structure and/or property changes may not occur at a smaller or larger particle size range, where different cooling kinetics inside the microsphere may occur, or for alternative compositions

A distinct increase in radiopacity is seen from the original test frit, to the preclinical frit, to the spheres (3798 HU, 3932 HU, and 4123 HU respectively). This increase in radiopacity, however, is more likely due to the random packing of the irregular particles, and the more efficient packing of the microspheres over the irregular particles, rather than an increase in the radiopacity of the glass itself. Radiopacity is calculated by averaging the intensity of multiple voxels within the imaged vial over five different sections. Inefficient packing leads to a large number of air filled spaces (i.e. voxels with a value of 0 HU) between the radiopaque particles, thereby lowering the average intensity. The more efficient packing of the microspheres will therefore increase the radiopacity of the vial as there is less radiolucent air present per measurement area.

SEM, PSA, and sphericity testing have proven that 100-300  $\mu\text{m}$  sized particles have been synthesized, and that over 92% of these particles are spheres. This sphericity value, however, may be higher than reported due to the inclusion of particle agglomerations in the test (which will not be used in the pre-clinical study) which do not display spherical symmetry. Therefore, spherical processing was successful in creating smooth spheres from the clear majority of the glass frit supplied, without altering the structure or properties displayed.

Since the data collected in experiments one and two have been confirmed as transferable to the glass spheres, these microspheres will next be tested *in vivo*, to assess their embolization effectiveness. Pre-clinical animal testing is necessary as not all safety concerns can be tested *in vitro*, and those which can are relying on a certain amount of approximation. The primary benefit of the technology is enhanced patient safety coupled with the ability to ameliorate chronic inflammation whilst permitting subsequent procedures to be performed at the same target level of occlusion. This study is required to demonstrate the embolization effectiveness of the technology per FDA guidance on the

evaluation of embolization particles [17]. All safety concerns for embolic agents laid out by FDA have been addressed in this protocol: (i) ease of deliverability, (ii) acute complications, (iii) local and systemic foreign body reactions, (iv) recanalization, (v) embolization effectiveness, and (vi) device migration. This investigation was performed as a pilot animal study, in an aim to gain better insight into the appropriateness of this design to test the efficacy of strontium substituted rubidium-borate systems as degradable and imageable embolic agents.

Part 2 of experiment 3 was successful in synthesizing BRS2 microspheres which displayed the same properties as those collected on glass frit in experiments one and two. A protocol was successfully designed and approved (by both Dalhousie and CRCHUM) to assess the embolization efficacy of the BRS2 microspheres in a porcine renal model. No results have been collected from the pre-clinical animal study as of yet; it is set to begin June 11<sup>th</sup>, 2018. Upon completion of the study, a Draft Report will be provided to the Sponsor and any revisions to the study report mutually agreed upon by the Sponsor and Study Director and/or Pathologist will be incorporated in the Final Report. At the end of the revision process, the Report will be signed and considered final. The study Final Report will include a summary of the objectives and procedures of the study, description of the TA used, the methods used for histological processing, and a discussion of any circumstances that may have altered or affected the integrity of the data. Any corrections or additions to the Final Report will be in the form of a report amendment.

#### **4.3. Conclusion**

Experiment 3 outlines pilot protocols to be used in both *in vitro* and *in vivo* models. As no *in vitro* models exist to assess the safety issues outlined in the Class IIB Special Controls document provided by FDA, part one attempted to determine the feasibility of implementing an *in vitro* benchtop model to assess the effectiveness of degradable particles and the risk of migration. It was found that although it is possible, much more work must be done before meaningful results can be attained. Part two focused on developing a protocol to assess the embolization effectiveness of a preferred composition of borate glass microsphere in a pre-clinical animal model. It was found that spherical processing of 100-300  $\mu\text{m}$  particles does not seem to affect their structure or properties, and therefore

validated the data collected in experiments one and two on glass frit. The composition BRS2 was chosen for investigation, the microspheres of this composition will be used in the developed pre-clinical protocol found in Appendix C. Successful completion of this study may support the deployment of a larger, pre-clinical protocol in support of full ISO 10993 tests and performance evaluations to further de-risk the technology towards clinical use.

## CHAPTER 5

### Conclusions

Uterine leiomyomas, also referred to as uterine fibroids, are the most common benign tumor of the female reproductive tract [1]. They are found in over 70% of women of reproductive age and cause a variety of debilitating symptoms, such as heavy bleeding, pain, subfertility, urinary frequency and urgency, and pelvic pressure [1,2]. Until recently, their only effective treatment was complete or partial removal of the uterus. However, in 1995 a uterine-sparing procedure was introduced called uterine artery embolization (UAE) [6]. UAE offered (and continues to offer) the potential to preserve fertility in young women with uterine leiomyomas. The minimally invasive nature of UAE also provides additional benefits, including reduced hospital stays, reduced health care costs, and shorter recovery times [6]. Currently, the commercially available microspheres for use in UAE are permanent implants. However, more recently there has been a push from both physicians and from patients for degradable microspheres: products which can effectively occlude the uterine artery, but will subsequently be eliminated safely from the body when their intended function is complete [14].

The nascent nature of degradable products in this application requires diligent assessment of risk, as well as evidence of efficacy, to help drive concept development and design engineering. Evidence based medicine teaches that there are three intersecting spheres of influence to consider when selecting treatment options for patients. These are: (i) the best available research evidence, (ii) individual clinical expertise, and (iii) patient values & expectations [135]. Unfortunately, due to the novelty of degradable embolic agents, clinical evidence to support the physiological benefits of degradable microspheres over their permanent counterparts is limited. It is believed, however, that degradable embolic agents may have particular advantages over permanent agents in UAE, as they allow for the complete reperfusion of blood flow to the uterus after the leiomyoma has been treated [15,56,103]. To support this position, it is contested in the literature that while UAE maintains uterine patency, the presence of permanent agents may impact pregnancy. Specifically, a study completed in 2007 showed that of 164 women who desired future

pregnancy (at the time of their UAE procedure with permanent agents), only 21 were able to get pregnant, resulting in 24 pregnancies. Of those 24 pregnancies, 18 live births occurred, and 33% of those babies were born with low or very low birth weights [136]. In addition, based on studies with sheep, this low birth weight is thought to be the result of uterine lesion and/or a persistent blockage of uterine blood flow [137]. It is believed that extended ischemia to the uterus could potentially inhibit the development of a large-sized placenta, leading to spontaneous abortion or newborns of very low birth weight [137]. Additionally, the remaining permanent embolic agents may lower uterine blood flow during gestation, as the middle uterine artery supplies the bulk of the blood supply to the fetus. If the uterine artery is fully (or partially) occluded, then the reduction in blood flow to the uterus will decrease fetal growth and survival [137].

Although it is believed that degradable embolic agents will provide some physiological benefit over permanent embolic agents, the exact outcomes following embolization with degradable particles are unknown. It is assumed that once the particles degrade and are safely removed from the body, that the recanalized vessel will allow for reperfusion of blood to the uterus. However, outcomes with respect to the downstream vasculature are currently unknown, and degradable agents may present new safety risks. The only information available on the nature of recanalized vessels after TAE with degradable agents is provided by Owen *et al.* However, they do not specify if recanalization means the reopening of the previously occluded vessel, or angiogenesis (and there appears to be much confusion in the literature with respect to the use of this term). As such, limited conclusions can be drawn from the literature in terms of the usefulness of recanalization, and/or the appropriate time frames within which recanalization should occur. However, with this said, it is important to note that evidence does exist which conclusively shows that permanent occlusion is detrimental to the future fertility of patients [136,137].

Due to the lack of high level clinical information available regarding the performance of degradable embolic microspheres, no specific timeframes for degradation are provided for UAE. One can reference the surgical outcomes provided by Vilos *et al.* [35] of total occlusion of 5-7 hours for effective treatment of uterine leiomyomas; however the difference in reperfusion rates must be accounted for. In surgical evaluations, reperfusion of blood to the uterus is instant and complete; with degradable embolic agents,



reperfusion may occur gradually as the particles degrade. Therefore, it is contended that the design requirement for degradable embolic agents for UAE is that they can provide total occlusion for 5-7 hours before degradation sufficient to allow reperfusion of blood to the uterus. Additionally, inflammation causing additional biological occlusion may not be favorable and may prolong ischemic time. This prolonged occlusion contradicts the specific engineering of a particle that degrades at the appropriate timeframe to maximize treatment outcomes while minimizing necrosis to healthy tissues. Although there is a significant amount of evidence outlining the potential harm of permanent embolics, and pre-clinical animal trials demonstrating the potential safety of degradable embolics, sufficient evidence at the clinical level is missing. The current evidence is therefore not suitable to effectively guide physicians in this section of evidence based medicine.

However, despite the lack of evidence and clinical expertise, there is a clear drive in the evidence based medicine paradigm for degradable embolic agents for TAE, which is that patients now want degradable products and physicians want to recommend them. Patients commonly express concerns about “foreign materials remaining in the body” [14] thus there is a need to continue down this path, even if the current clinical evidence regarding degradable embolics is not satisfactory. On the basis of the published (Journal of Functional Biomaterial) review in Chapter 1 (Section 1.2) [103], it has been identified that the following design inputs are important when considering degradable embolic agents for TAE. These innovative technologies must provide predictable and effective occlusion while also providing:

1. Tailored degradation timeframes—to provide adequate infarction to the target tissues in a variety of indications, subsequently allowing return of flow (e.g., 5–7 h for uterine artery embolization—based on Doppler-guided transvaginal clamping) [15]
2. A variety of tightly calibrated particle size distributions—to optimize particle delivery according to target artery anatomy [16]
3. Ease of delivery through conventional microcatheters—to facilitate adoption of the novel technology into established embolization techniques
4. Full biological compatibility as per the relevant sections of ISO-10993—to minimize safety concerns [17]
5. Multi-modal imageability (e.g., fluoroscopy, CT)—to allow for efficiency and

standardization of embolization endpoints [18].

Currently, five materials are being developed for use as degradable embolic microspheres for TAE. None of these materials satisfy all the design inputs published in the literature. The most common limitations are lack of variable degradation timeframes, and lack of multi-modal imageability. Given these design input requirements, there are several material classifications that could be considered for the development of an implantable, degradable, and imageable embolic microsphere. Glasses are currently being investigated for use in neuromuscular repair (fibrous constructs for muscle and nerve regeneration), artificial cornea, orbital implants, epithelial and cardiac tissue engineering, treatment of gastric ulcers and non-osseous cancer therapy [138]. A small variation in glass composition can greatly modify the features of the material, thereby extending the potential applications which glasses can fill in the medical field. Glasses present an attractive option in this instance because not only do they allow for inherent radiopacity through the incorporation of ions with sufficient NIST mass attenuation coefficients, they can be manufactured to exhibit variable degradation timeframes and particle size ranges.

This thesis explored the potential of borate glasses for use in TAE (with particular consideration toward UAE). Borate glasses are excellent glass formers for manufacturing purposes, can accommodate several elements, and offer complete degradation in aqueous environments, potentially allowing for multi-modal imageability, and the complete recanalization of vessels at various degradation timeframes. This work examined two series of glasses: (i) the BRS series with the composition 70B/30-xRb/xSr (where  $x=2,4,6,8,10$ ), and (ii) the BRG series with the composition 70B/30-xRb/xGa (where  $x=2,4,6,8,10$ ). Simple borate systems were chosen for this work so as to better understand the composition-structure-property relationship of monovalent for divalent, or monovalent for trivalent substituted borate networks. For borate systems, it is commonly assumed that an increase in four-fold coordination in borate networks leads to a decrease in dissolution rates under aqueous conditions due to an increase in glass connectivity [74,101]. Interestingly, the opposite of this assumption was observed in the glass systems examined in this work. The BRS series displayed a constant B<sub>4</sub> fraction, while the percentage of B<sub>4</sub> in the BRG series significantly decreased with increasing substitution. Surprisingly, despite the lack of increase in B<sub>4</sub> fractions, an increase in hydrolytic stability and glass transition temperature

were seen in both glass series. Additionally, an increase in density was observed in the BRS series with increasing strontium substitution. In contrast, a significant decrease in density was observed for the BRG series. Essentially, these data indicate that the literature poorly understands these glass systems, and as a result their structure-property relationships are unpredictable. This statement is exemplified by the data collected in experiments one and two of this thesis. Despite the commonly accepted theory that the ratio of B3 to B4 present in glasses has the largest influence on glasses properties, this work determined that this theory does not always accurately explain the structure-property relationships of simple high borate glass systems. Accordingly, continued directed work in this field is important to broaden our knowledge for such glass systems.

While the work conducted in this thesis considered rubidium and gallium containing compositions, toxicological information on these elements exists only at the most basic level (e.g. no ATSDR documents exist) which increases the risk profile of these glasses as an actual medical device. These elements are likely safe in small doses, based on toxicological studies previously published [83-88], and their clinical use to treat a variety of diseases [93, 94]. However considerable further research into the exact toxicity of these ions is required should they be considered in formulations for actual medical grade microspheres. Additionally, the structural nature of the network modifiers should be considered when discussing these glass networks. As previously mentioned, when considering borate glasses, most of the property predictions are based on the borate structure in the network (i.e. 3- vs 4-fold coordinate boron). However, it has been observed in this thesis that modifier ions play an important role in predicting the properties of the resulting glass (and not necessarily in traditionally understood ways). Despite no increase in B4 concentration (i.e. borate glass network structure), the addition of Sr to the BRS series increases density,  $T_g$ , and glass stability, thereby decreasing degradation rates. The role of gallium in the BRG series is even more pronounced;  $^{11}\text{B}$  NMR indicates that gallium has a significant effect on the boron structure, forming tetrahedral gallium centers, and modulating the network to increase hydrolytic stability (as seen in Figure 3.5). When Ga is considered a network former, rather than a network modifier, the theoretical values more closely approximate the accepted O/B ratios for the composition. Therefore, not only do network modifiers affect clinically important properties (i.e. radiopacity and degradation

timeframes), they also have a direct effect on the structure itself and should therefore be given an equal value in the literature when discussing composition-structure-property relationship.

Once the clinically relevant attributes of the glasses assessed in this thesis had been determined *in vitro*, the next step of the work was to conduct some provisional evaluations to examine the safety, efficacy, and performance of one of these glass compositions as a degradable embolic agent. The BRS2 composition was chosen as it exhibited the lowest density, second highest radiopacity, and degraded completely in 48 hours. Additionally, BRS2 exhibited high glass stability without any susceptibility to T1 or T2 weighted MRI scans. Experiment three began by investigating the utility of using glass frit for preliminary evaluation of glass compositions. No significant changes were observed between the properties of the glass frit and the processed microspheres. This discovery was useful from a manufacturing standpoint, as it allows for reliable synthesis of consistent glass compositions. Additionally, since spherical processing is time consuming, has a relatively low yield, and is not readily available, the ability to use glass frit for investigative experiments will make the research process more efficient.

Once a best in class composition was chosen for use in experiment three, the drafting of an appropriate pilot protocol began to test the safety, efficacy, and performance of degradable glass microspheres for TAE. FDA provides a guidance document which outlines the criteria that requires pre-clinical investigation prior to approval of new medical devices for transarterial embolization [17]. One of those criteria is embolization effectiveness. This parameter can be evaluated by multiple measures, including ease of delivery, recanalization of the vessels/durability of occlusion, local foreign body reactions, and level of ischemia when compared to the control [17]. The durability of the occlusion and vessel recanalization are essential when considering effectiveness of degradable embolic agents, as the occlusion is temporary. If ischemic time is too short, full therapeutic benefits of the treatment may not be attained [125,126]. However if the ischemic time is too long, the potential benefits of having a degradable product may be reduced. Additionally, local body reactions must be considered when assessing embolization effectiveness, as biological occlusion resulting from local inflammatory effects may hinder reperfusion of target tissue. For some applications that require longer occlusion times, this

body reaction may be favorable to prolong ischemia; however for uterine artery embolization, a very short occlusion time is desired, and biological occlusion may hinder the early reperfusion of blood to the uterus. Lingering biological occlusion defeats the purpose of engineering the particle to degrade in 24-48 hours, and thereby may impact the effectiveness of the embolic agent for this application.

Another important risk to consider with respect to degradable microspheres is migration; it has been presented by FDA as a requirement to be investigated prior to approval of new medical devices for transarterial embolization [17]. In discussions with interventional radiologists regarding the clinical implications of the risk of migration, there is a general consensus that migration may occur, but if it does, there is little clinical evidence to indicate that it causes clinical complications. It is not clear from the literature the rate of complications associated with migration, and there is limited evidence to support that this is a major risk or a small risk. A review of the Manufacturer and User Facility Device Experience (MAUDE) database for the last 10 years, using the search strings “Migration” and “EmboSphere” revealed only 3 cases. These cases included examples of an arteriovenous shunt leading to cerebral infarction, as well as a reflux of particles to non-target areas, specifically leading to ischemic pancreatitis and postoperative cholecystitis [139]. Although the rate of clinical complications appears to be quite low, there is a chance that it is not being properly assessed. Since all currently investigated materials are radiolucent, very little work has been done to assess the migration risk of degradable embolic agents, apart from the work done by Owen *et. al* [31]. A secondary search of the MAUDE database using only the search string “EmboSphere” revealed an additional 20 cases that although not directly labeled as migration, may easily have been caused by non-target embolization. These cases included instant blindness and vision impairment, necrosis of the gallbladder, and even death. An attempt at further understanding the risk of migration was started in part one of experiment three. Ideally, the risk of migration will one day be assessable via *in vitro* methods prior to any pre-clinical animal studies.

To assess migration, the use of radiopaque particles may be of particular benefit as it may allow for the direct visualization of the embolic agent through CT or fluoroscopy. Although imageability is not necessarily crucial for uterine artery embolization, it is a convenient attribute. Imageability may be more useful when considering applications such

as drug eluting bead transarterial chemoembolization (DEB-TACE) for the treatment of hepatocellular carcinoma. In this application, the spatial distribution of particles is crucial for regulating the local concentration of chemotherapy and if the particles are inappropriately spaced, inappropriate dosing of tumor tissue may occur [140].

Once embolization effectiveness and migration have been assessed in a preclinical animal model, a sufficient level of clinical evidence must be amassed to give physicians the confidence to employ degradable embolics as a mainstream option for TAE. Ideally, a meta-analysis of several multi-centered, randomized, and appropriately powered prospective clinical trials would occur to definitively assess the safety, efficacy, and performance of degradable microspheres in TAE. However, this level of evidence does not exist for most day-to-day procedures. These procedures have become trusted as safe because the occurrence of harm associated with that procedure is low, and the severity of that harm is also low (or if it is high, it occurs so infrequently that it's an acceptable risk). Therefore, since the occurrence of the highest level of clinical evidence is rare and takes a long time to acquire, the question must be asked, 'what is a reasonable level of evidence for physicians to accept prior to suggesting this treatment to their patients?'.

Pre-clinical models do not register on the 6S pyramid of evidence for evidence based medicine [141], however FDA states in the clinical testing section of the Class II Special Controls guidance document [17] that it will rely heavily on benchtop and pre-clinical testing when determining potential safety and efficacy approval. Specifically, "FDA will rely upon well-designed bench and/or animal testing rather than requiring clinical studies for new devices unless there is a specific justification for asking for clinical information to support a determination of substantial equivalence" [17]. This may potentially lead to the approval of materials that are not effective at their intended application. For example, Contour SE was approved by FDA for use in uterine artery embolization, however when compared to conventional PVA and tris-acryl gelatin microspheres (TAGM), it was found to leave substantial portions of tumors uninfarcted [142]. This ineffective treatment led to the premature ending of a large clinical trial, and called into question the "quality of the evidence we accept" before approving a novel material for integration into practice. Therefore, there is a chance that FDA approval is not a reasonable level of evidence for mainstream implementation of an embolic agent.

The intent of the pilot animal study developed as part of this thesis is to demonstrate in a pilot model how safety, efficacy and performance could be established for degradable agents (e.g. processing, post processing, sacrifice procedures, etc). Successful completion of this study will support the deployment of a larger, pre-clinical protocol in support of full ISO 10993 tests and performance evaluations to further de-risk the technology towards clinical use. Should the larger animal study prove successful, and the product can (i) be produced safely, non-pyrogenic, and sterile, (ii) be delivered and perform per all the requirements laid out by FDA, and (iii) pass all biocompatibility tests, then all pre-clinical risks have been managed as fully as possible, before moving to human trials. When considering human trials, the implementation of a small pilot study is the logical first step. However, the population that should be examined is less clear; should the product be tested on women who will have a hysterectomy regardless of the outcome of the procedure, or on women who may benefit from the UFE procedure? Increased discussion on both the acceptable level of evidence required to adopt new embolic products into clinical practice, and the quality of that evidence is required before degradable embolic agents become common practice.

Despite much of the work that being conducted on the development of degradable products, high level clinical evidence is currently missing. Despite the lack of evidence, there is an overwhelming requirement by patients to have materials used for embolization procedures that will be eliminated safely from their body. Therefore, in the world of evidence based medicine, it would seem reasonable that prior to the broader deployment of these materials, we should be considering whether or not there is a significant benefit to degradable particles beyond the desire demonstrated by patients. Patient expectations are only one section of evidence based medicine, and must be supported by both the experienced physician and the highest level of acceptable clinical evidence. As this evidence does not currently exist, this thesis has attempted to address some of the initial uncertainties related to uterine artery embolization, while also expanding the use of glass biomaterials outside the scope of the skeletal system.

Finally, this thesis attempted to expand the understanding of the significantly understudied field of borate glass systems. It succeeded in contributing to the expansion of the compositional palate for borate glasses, and endeavored to better our understanding of

the composition-structure-property relationship found in simple borate systems. By assessing the effect of divalent (Sr) or trivalent (Ga) substitutions of monovalent (Rb) network modifiers on the basic properties of the glass systems, it has been concluded that these glasses behave unpredictably. As such, continued directed work is crucial to reach a sufficient understanding of these unconventional glass systems. Regardless, the BRS glass series exhibits desirable characteristics as degradable and imageable embolic agents for TAE procedures due to its tailorable degradation timeframes and significant radiopacity.



## REFERENCES

1. Goodwin, S. C.; Spies, J. B. Uterine fibroid embolization. *N. Engl. J. Med.* **2009**, *361*, 690–697, doi:10.1056/NEJMct0806942.
2. Gupta, J. K.; Sinha, A.; Lumsden, M. A.; Hickey, M. Uterine artery embolization for symptomatic uterine fibroids. *Cochrane Database Syst Rev* **2012**, CD005073, doi:10.1002/14651858.CD005073.pub3.
3. Kashani, B. N.; Centini, G.; Morelli, S. S.; Weiss, G.; Petraglia, F. Role of Medical Management for Uterine Leiomyomas. *Best Pract Res Clin Obstet Gynaecol* **2016**, *34*, 85–103, doi:10.1016/j.bpobgyn.2015.11.016.
4. Pelage, J.-P.; Cazejust, J.; Pluot, E.; Le Dref, O.; Laurent, A.; Spies, J. B.; Chagnon, S.; Lacombe, P. Uterine fibroid vascularization and clinical relevance to uterine fibroid embolization. *Radiographics* **2005**, *25 Suppl 1*, S99-117, doi:10.1148/rg.25si055510.
5. Cardozo, E. R.; Clark, A. D.; Banks, N. K.; Henne, M. B.; Stegmann, B. J.; Segars, J. H. The Estimated Annual Cost of Uterine Leiomyomata in the United States. *Am J Obstet Gynecol* **2012**, *206*, 211.e1-211.e9, doi:10.1016/j.ajog.2011.12.002.
6. REST Investigators. Uterine-Artery Embolization versus Surgery for Symptomatic Uterine Fibroids. *New England Journal of Medicine* **2007**, *356*, 360–370, doi:10.1056/NEJMoa062003.
7. Beinfeld, M. T.; Bosch, J. L.; Isaacson, K. B.; Gazelle, G. S. Cost-effectiveness of uterine artery embolization and hysterectomy for uterine fibroids. *Radiology* **2004**, *230*, 207–213, doi:10.1148/radiol.2301021482.
8. Vaidya, S.; Tozer, K. R.; Chen, J. An Overview of Embolic Agents. *Semin Intervent Radiol* **2008**, *25*, 204–215, doi:10.1055/s-0028-1085930.
9. Spies, J. B.; Allison, S.; Flick, P.; McCullough, M.; Sterbis, K.; Cramp, M.; Bruno, J.; Jha, R. Polyvinyl alcohol particles and tris-acryl gelatin microspheres for uterine artery embolization for leiomyomas: results of a randomized comparative study. *J Vasc Interv Radiol* **2004**, *15*, 793–800, doi:10.1097/01.RVI.0000136982.42548.5D.

10. Abramowitz, S. D.; Israel, G. M.; McCarthy, S. M.; Pollak, J. S.; White, R. I.; Tal, M. G. Comparison of four embolic materials at uterine artery embolization by using postprocedural MR imaging enhancement. *Radiology* **2009**, *250*, 482–487, doi:10.1148/radiol.2502080574.
11. Guimaraes, M.; Arrington, D.; MacFall, T.; Yamada, R.; Schonholz, C. Does Material Matter? Particular Embolics. *Endovascular Today*. April 2013, pp. 70–74.
12. Worthington-Kirsch. Do Particle Size and Type Matter? Lessons learned from experience with uterine artery embolization. *Endovascular Today*. June 2008, pp. 39–42.
13. Kehoe, S.; Kilcup, N.; Abraham, R.; Boyd, D. Chapter 20: Glass Materials in Interventional Radiology and Interventional Oncology. In *Bioactive Glasses*; 2016; pp. 471–495.
14. Forster, R. E. J.; Thürmer, F.; Wallrapp, C.; Lloyd, A. W.; Macfarlane, W.; Phillips, G. J.; Boutrand, J.-P.; Lewis, A. L. Characterisation of physico-mechanical properties and degradation potential of calcium alginate beads for use in embolisation. *J Mater Sci Mater Med* **2010**, *21*, 2243–2251, doi:10.1007/s10856-010-4080-y.
15. Verret, V.; Pelage, J. P.; Wassef, M.; Louguet, S.; Servais, E.; Bédouet, L.; Beaulieu, T.; Moine, L.; Laurent, A. A novel resorbable embolization microsphere for transient uterine artery occlusion: a comparative study with trisacryl-gelatin microspheres in the sheep model. *J Vasc Interv Radiol* **2014**, *25*, 1759–1766, doi:10.1016/j.jvir.2014.06.025.
16. *Transcatheter Embolization and Therapy*; Kessel, D., Ray, C., Eds.; Techniques in Interventional Radiology; Springer-Verlag: London, 2009; ISBN 978-1-84800-896-0.
17. FDA Guidance Documents: Class II Special Controls Guidance Document: Vascular and Neurovascular Embolization Devices - Guidance for Industry and FDA Staff 2004.
18. Kehoe, S.; Amensag, S.; Looney, M.; Abraham, R. J.; Boyd, D. “Imageable” Zinc-Silicate Glass Microspheres For Transarterial Embolization: A Renal Artery Embolization Study. *Biomedical glasses* **2015**, *1*, doi:10.1515/bglass-2015-0007.
19. Bohner, M. Resorbable Biomaterials as Bone Graft Substitutes. *Mater Today* **2010**, *13*, 24–30, doi:10.1016/S1369-7021(10)70014-6.

20. Williams, D. *Essential Biomaterials Science*; Cambridge University Press, 2014; ISBN 978-0-521-89908-6.
21. Gupta, B.; Revagade, N.; Hilborn, J. Poly(lactic acid) fiber: An overview. *Prog Polym Sci* **2007**, *32*, 455–482, doi:10.1016/j.progpolymsci.2007.01.005.
22. Gentile, P.; Chiono, V.; Carmagnola, I.; Hatton, P. V. An overview of poly(lactic-co-glycolic) acid (PLGA)-based biomaterials for bone tissue engineering. *Int J Mol Sci* **2014**, *15*, 3640–3659, doi:10.3390/ijms15033640.
23. Makadia, H. K.; Siegel, S. J. Poly Lactic-co-Glycolic Acid (PLGA) as Biodegradable Controlled Drug Delivery Carrier. *Polymers (Basel)* **2011**, *3*, 1377–1397, doi:10.3390/polym3031377.
24. You, Y.; Lee, S. W.; Youk, J. H.; Min, B.-M.; Lee, S. J.; Park, W. H. In vitro degradation behaviour of non-porous ultra-fine poly(glycolic acid)/poly(l-lactic acid) fibres and porous ultra-fine poly(glycolic acid) fibres. *Polymer Degradation and Stability* **2005**, *90*, 441–448, doi:10.1016/j.polymdegradstab.2005.04.015.
25. Houchin, M. L.; Topp, E. M. Chemical degradation of peptides and proteins in PLGA: a review of reactions and mechanisms. *J Pharm Sci* **2008**, *97*, 2395–2404, doi:10.1002/jps.21176.
26. Grayson, A. C. R.; Voskerician, G.; Lynn, A.; Anderson, J. M.; Cima, M. J.; Langer, R. Differential degradation rates in vivo and in vitro of biocompatible poly(lactic acid) and poly(glycolic acid) homo- and co-polymers for a polymeric drug-delivery microchip. *J Biomater Sci Polym Ed* **2004**, *15*, 1281–1304.
27. Xu, Y.; Kim, C.-S.; Saylor, D. M.; Koo, D. Polymer degradation and drug delivery in PLGA-based drug-polymer applications: A review of experiments and theories. *J. Biomed. Mater. Res. Part B Appl. Biomater.* **2017**, *105*, 1692–1716, doi:10.1002/jbm.b.33648.
28. Rasal, R. M.; Janorkar, A. V.; Hirt, D. E. Poly(lactic acid) modifications. *Prog Polym Sci* **2010**, *35*, 338–356, doi:10.1016/j.progpolymsci.2009.12.003.

29. Boland, E. L.; Shine, R.; Kelly, N.; Sweeney, C. A.; McHugh, P. E. A Review of Material Degradation Modelling for the Analysis and Design of Bioabsorbable Stents. *Ann Biomed Eng* **2016**, *44*, 341–356, doi:10.1007/s10439-015-1413-5.
30. Nagarajan, S.; Reddy, B. S. R. Bio-absorbable polymers in implantation-An overview. *JSIR Vol.68(12) [December 2009]* **2009**.
31. Owen, R. J.; Nation, P. N.; Polakowski, R.; Biliske, J. A.; Tiege, P. B.; Griffith, I. J. A preclinical study of the safety and efficacy of Occlusin™ 500 Artificial Embolization Device in sheep. *Cardiovasc Intervent Radiol* **2012**, *35*, 636–644, doi:10.1007/s00270-011-0218-7.
32. Revised 501(k) Summary for IMBiotechnologies Ltd. Occlusin 500 Artificial Embolization Device (Per 21CFR 807.92) 2010.
33. Stuart, S.; Mayo, J. R.; Ling, A.; Schulzer, M.; Klass, D.; Power, M. A.; Roberton, B. J.; Wan, J. M.; Liu, D. M. Retrospective study of the impact of fellowship training on two quality and safety measures in uterine artery embolization. *J Am Coll Radiol* **2014**, *11*, 471–476, doi:10.1016/j.jacr.2013.09.020.
34. Anderson, J. M.; Rodriguez, A.; Chang, D. T. Foreign body reaction to biomaterials. *Semin. Immunol.* **2008**, *20*, 86–100, doi:10.1016/j.smim.2007.11.004.
35. Vilos, G. A.; Vilos, E. C.; Romano, W.; Abu-Rafea, B. Temporary uterine artery occlusion for treatment of menorrhagia and uterine fibroids using an incisionless Doppler-guided transvaginal clamp: case report. *Hum. Reprod.* **2006**, *21*, 269–271, doi:10.1093/humrep/dei299.
36. Food and Drug Administration Use of International Standard ISO 10993-1, 'Biological evaluation of medical devices--Part 1: Evaluation and testing within a risk management process'; Guidance for Industry and Food and Drug Administration Staff; Availability Available online: <https://www.regulations.gov/document?D=FDA-2013-D-0350-0037> (accessed on Apr 4, 2018).
37. EmboSphere®® Microspheres Available online: <https://www.merit.com/interventional-oncology->

- spine/embolotherapy/microspheres/EmboSphere®-microspheres/ (accessed on Apr 4, 2018).
38. Swielim, G. E. A. *Atlas: Anatomy of Sheep*; ktab INC.: Cairo, Egypt, 2006; ISBN 977-281-292-4.
39. Webster, R.; Elliott, V.; Park, B. K.; Walker, D.; Hankin, M.; Taupin, P. PEG and PEG conjugates toxicity: towards an understanding of the toxicity of PEG and its relevance to PEGylated biologicals. In *PEGylated Protein Drugs: Basic Science and Clinical Applications*; Milestones in Drug Therapy; Birkhäuser Basel, 2009; pp. 127–146 ISBN 978-3-7643-8678-8.
40. Magnon, L.; Laurent, A.; Wassef, F.; Bedouet, L.; Louguet, S.; Verret, V.; Servais, E. Implantable swellable bio-resorbable polymer 2012.
41. Maeda, N.; Verret, V.; Moine, L.; Bédouet, L.; Louguet, S.; Servais, E.; Osuga, K.; Tomiyama, N.; Wassef, M.; Laurent, A. Targeting and recanalization after embolization with calibrated resorbable microspheres versus hand-cut gelatin sponge particles in a porcine kidney model. *J Vasc Interv Radiol* **2013**, *24*, 1391–1398, doi:10.1016/j.jvir.2013.05.058.
42. ASTM Compass Int. Standard Specification for Woven Wire Test Sieve Cloth and Test Sieves 2017.
43. Agrawal, C. M.; Ong, J. L.; Appleford, M. R.; Mani, G. *Introduction to Biomaterials: Basic Theory with Engineering Applications*; 1 edition.; Cambridge University Press: New York, 2013; ISBN 978-0-521-11690-9.
44. Haraldsson, B.; Nyström, J.; Deen, W. M. Properties of the glomerular barrier and mechanisms of proteinuria. *Physiol. Rev.* **2008**, *88*, 451–487, doi:10.1152/physrev.00055.2006.
45. NSP Nanosoft Polymers Available online: <https://www.nanosoftpolymers.com/product/plga-peg-plga/> (accessed on Apr 4, 2018).
46. Rosca, C.; Popa, M. I.; Lisa, G.; Chitanu, G. C. Interaction of chitosan with natural or synthetic anionic polyelectrolytes. 1. The chitosan–carboxymethylcellulose complex. *Carbohydrate Polymers* **2005**, *62*, 35–41, doi:10.1016/j.carbpol.2005.07.004.

47. Weng, L.; Le, H. C.; Talaie, R.; Golzarian, J. Bioresorbable hydrogel microspheres for transcatheter embolization: preparation and in vitro evaluation. *J Vasc Interv Radiol* **2011**, *22*, 1464–1470.e2, doi:10.1016/j.jvir.2011.06.010.
48. Bajpai, A.; Shrivastava, J. In vitro enzymatic degradation kinetics of polymeric blends of crosslinked starch and carboxymethyl cellulose. *Polymer International* **2005**, *54*, 1524–1536, doi:10.1002/pi.1878.
49. Reeves, R.; Ribeiro, A.; Lombardo, L.; Boyer, R.; Leach, J. B. Synthesis and Characterization of Carboxymethylcellulose-Methacrylate Hydrogel Cell Scaffolds. *Polymers (Basel)* **2010**, *2*, 252–264, doi:10.3390/polym2030252.
50. Lee, S. Y.; Bang, S.; Kim, S.; Jo, S. Y.; Kim, B.-C.; Hwang, Y.; Noh, I. Synthesis and in vitro characterizations of porous carboxymethyl cellulose-poly(ethylene oxide) hydrogel film. *Biomaterials Research* **2015**, *19*, 12, doi:10.1186/s40824-015-0033-3.
51. Kean, T.; Thanou, M. Biodegradation, biodistribution and toxicity of chitosan. *Adv. Drug Deliv. Rev.* **2010**, *62*, 3–11, doi:10.1016/j.addr.2009.09.004.
52. Zhang, H.; Neau, S. H. In vitro degradation of chitosan by bacterial enzymes from rat cecal and colonic contents. *Biomaterials* **2002**, *23*, 2761–2766.
53. Zhang, Y.; Wang, Z.; Zhang, J.; Chen, C.; Wu, Q.; Zhang, L.; Zhang, X. Quantitative determination of chitinolytic activity of lysozyme using half-deacetylated chitosan as a substrate. *Carbohydrate polymers* **2011**.
54. Yang, Y. M.; Hu, W.; Wang, X. D.; Gu, X. S. The controlling biodegradation of chitosan fibers by N-acetylation in vitro and in vivo. *J Mater Sci Mater Med* **2007**, *18*, 2117–2121, doi:10.1007/s10856-007-3013-x.
55. Weng, L.; Rusten, M.; Talaie, R.; Hairani, M.; Rosener, N. K.; Golzarian, J. Calibrated bioresorbable microspheres: a preliminary study on the level of occlusion and arterial distribution in a rabbit kidney model. *J Vasc Interv Radiol* **2013**, *24*, 1567–1575, doi:10.1016/j.jvir.2013.06.009.
56. Weng, L.; Rostamzadeh, P.; Nooryshokry, N.; Le, H. C.; Golzarian, J. In vitro and in vivo evaluation of biodegradable embolic microspheres with tunable anticancer drug release. *Acta Biomater* **2013**, *9*, 6823–6833, doi:10.1016/j.actbio.2013.02.017.

57. Weng, L.; Seelig, D.; Rostamzadeh, P.; Golzarian, J. Calibrated Bioresorbable Microspheres as an Embolic Agent: An Experimental Study in a Rabbit Renal Model. *J Vasc Interv Radiol* **2015**, *26*, 1887–1894.e1, doi:10.1016/j.jvir.2015.01.014.
58. Pillai, C. K. S.; Paul, W.; Sharma, C. P. Chitin and chitosan polymers: Chemistry, solubility and fiber formation. *Prog Polym Sci* **2009**, *34*, 641–678, doi:10.1016/j.progpolymsci.2009.04.001.
59. Usman, A.; Zia, K. M.; Zuber, M.; Tabasum, S.; Rehman, S.; Zia, F. Chitin and chitosan based polyurethanes: A review of recent advances and prospective biomedical applications. *Int. J. Biol. Macromol.* **2016**, *86*, 630–645, doi:10.1016/j.ijbiomac.2016.02.004.
60. Kwak, B. K.; Shim, H. J.; Han, S.-M.; Park, E. S. Chitin-based embolic materials in the renal artery of rabbits: pathologic evaluation of an absorbable particulate agent. *Radiology* **2005**, *236*, 151–158, doi:10.1148/radiol.2361040669.
61. Schwarz, A.; Zhang, H.; Metcalfe, A.; Salazkin, I.; Raymond, J. Transcatheter embolization using degradable crosslinked hydrogels. *Biomater* **2004**, *25*, 5209–5215, doi:10.1016/j.biomaterials.2003.12.022.
62. Ohta, S.; Nitta, N.; Takahashi, M.; Murata, K.; Tabata, Y. Degradable Gelatin Microspheres as an Embolic Agent: an Experimental Study in a Rabbit Renal Model. *Korean J Radiol* **2007**, *8*, 418–428, doi:10.3348/kjr.2007.8.5.418.
63. Jänne, J.; Alhonen, L.; Pietilä, M.; Keinänen, T. A. Genetic approaches to the cellular functions of polyamines in mammals. *Eur. J. Biochem.* **2004**, *271*, 877–894.
64. Conn, M.; J Parker *The Animal Research War*; Palgrave Macmillan: New York, NY, USA, 2008; ISBN 978-0-230-61199-3.
65. Davidson, M. K.; Lindsey, J. R.; Davis, J. K. Requirements and selection of an animal model. *Isr. J. Med. Sci.* **1987**, *23*, 551–555.
66. Standring, PhD, DSc, S. *Gray's Anatomy: The Anatomical Basis of Clinical Practice*; 41 edition.; Elsevier Canada: New York, NY, USA, 2015; ISBN 978-0-7020-5230-9.

67. Nagy, J. A.; Chang, S.-H.; Dvorak, A. M.; Dvorak, H. F. Why are tumour blood vessels abnormal and why is it important to know? *Br J Cancer* **2009**, *100*, 865–869, doi:10.1038/sj.bjc.6604929.
68. Al-Fozan, H.; Tulandi, T. Factors affecting early surgical intervention after uterine artery embolization. *Obstet Gynecol Surv* **2002**, *57*, 810–815, doi:10.1097/01.OGX.0000040427.23658.1D.
69. Bilhim, T.; Pisco, J. M.; Duarte, M.; Oliveira, A. G. Polyvinyl alcohol particle size for uterine artery embolization: a prospective randomized study of initial use of 350-500  $\mu\text{m}$  particles versus initial use of 500-700  $\mu\text{m}$  particles. *J Vasc Interv Radiol* **2011**, *22*, 21–27, doi:10.1016/j.jvir.2010.09.018.
70. van Es, R. J.; Franssen, O.; Dullens, H. F.; Bernsen, M. R.; Bosman, F.; Hennink, W. E.; Slootweg, P. J. The VX2 carcinoma in the rabbit auricle as an experimental model for intra-arterial embolization of head and neck squamous cell carcinoma with dextran microspheres. *Lab. Anim.* **1999**, *33*, 175–184, doi:10.1258/002367799780578372.
71. Varshneya, A. *Fundamentals of Inorganic Glasses*; Elsevier, 1994; ISBN 978-0-08-057150-8.
72. Sun, K.-H. Fundamental Condition of Glass Formation. *Journal of the American Ceramic Society* **1947**, *30*, 277–281, doi:10.1111/j.1151-2916.1947.tb19654.x.
73. Mauro, J. C.; Philip, C. S.; Vaughn, D. J.; Pambianchi, M. S. Glass Science in the United States: Current Status and Future Directions. *Int J Appl Glass Sci* **2014**, *5*, 1–15, doi:10.1111/ijag.12058.
74. Wright, A. C. My Borate Life: An Enigmatic Journey. *Int J Appl Glass Sci* **2015**, *6*, 45–63.
75. George, J. L.; Brow, R. K. In-situ characterization of borate glass dissolution kinetics by  $\mu$ -Raman spectroscopy. *Journal of Non-Crystalline Solids* **2015**, *Complete*, 116–124, doi:10.1016/j.jnoncrysol.2015.07.003.
76. Yiannopoulos, Y. D.; Chryssikos, G. D.; Kamitsos, E. I. Structure and properties of alkaline earth borate glasses. *Physics and Chemistry of Glasses* **2001**, *42*, 164–172.



77. Suplee, C. X-Ray Mass Attenuation Coefficients Available online: <https://www.nist.gov/pml/x-ray-mass-attenuation-coefficients> (accessed on Apr 4, 2018).
78. ATSDR - Toxicological Profile: Strontium 2015.
79. ATSDR - Toxic Substances - Boron 2011.
80. Lenk, W.; Prinz, H.; Steinmetz, A. Rubidium and Rubidium Compounds. In *Ullmann's Encyclopedia of Industrial Chemistry*; Wiley-VCH Verlag GmbH & Co. KGaA, Ed.; Wiley Online Library, 2010; Vol. 1 ISBN 978-3-527-30673-2.
81. Youngman, R. E.; Zwanziger, J. W. On the Formation of Tetracoordinate Boron in Rubidium Borate Glasses. *J Am Chem Soc* **1995**, *117*, 1397–1402, doi:10.1021/ja00109a026.
82. Kaster, T.; Mylonas, I.; Renaud, J. M.; Wells, G. A.; Beanlands, R. S. B.; deKemp, R. A. Accuracy of low-dose rubidium-82 myocardial perfusion imaging for detection of coronary artery disease using 3D PET and normal database interpretation. *J. Nucl. Cardiol.* **2012**, *19*, 1135–1145, doi:10.1007/s12350-012-9621-y.
83. Tuoni, M.; Marchitello, M.; Paternoster, G.; Gerace, S.; Palla, R.; Placidi, G. F.; Lenzi, A.; Toschi, D.; Meltzer, H. L. Renal tolerance of rubidium chloride: short-term clinical evaluation. *J Clin Pharmacol* **1987**, *27*, 503–507.
84. U.S EPA Provisional Peer-Reviewed Toxicity Values for Rubidium Compounds (Rubidium Iodide). 2016.
85. Ando, A.; Ando, I.; Katayama, M.; Sanada, S.; Hiraki, T.; Mori, H.; Tonami, N.; Hisada, K. Biodistributions of radioactive alkaline metals in tumor bearing animals: comparison with <sup>201</sup>Tl. *Eur J Nucl Med* **1988**, *14*, 352–357.
86. Usuda, K.; Kono, R.; Ueno, T.; Ito, Y.; Dote, T.; Yokoyama, H.; Kono, K.; Tamaki, J. Risk Assessment Visualization of Rubidium Compounds: Comparison of Renal and Hepatic Toxicities, In vivo. *Biol. Trace Elem. Res.* **2014**, *159*, 263–268, doi:10.1007/s12011-014-9937-3.

87. Fieve, R. R.; Meltzer, H. L.; Taylor, R. M. Rubidium chloride ingestion by volunteer subjects: Initial experience. *Psychopharmacologia* **1971**, *20*, 307–314, doi:10.1007/BF00403562.
88. Johnson, G. T.; Lewis, T. R.; Wagner, W. D. Acute toxicity of cesium and rubidium compounds. *Toxicology and Applied Pharmacology* **1975**, *32*, 239–245, doi:10.1016/0041-008X(75)90216-1.
89. Hasan, M. S.; Werner-Zwanziger, U.; Boyd, D. Composition-structure-properties relationship of strontium borate glasses for medical applications. *J Biomed Mater Res A* **2015**, *103*, 2344–2354, doi:10.1002/jbm.a.35361.
90. O’Connell, K.; Hanson, M.; O’Shea, H.; Boyd, D. Linear release of strontium ions from high borate glasses via lanthanide/alkali substitutions. *J Non-Cryst Solids* **2015**, *430*, 1–8, doi:10.1016/j.jnoncrysol.2015.09.017.
91. Angeli, F.; Charpentier, T.; Molières, E.; Soleilhavoup, A.; Jollivet, P.; Gin, S. Influence of lanthanum on borosilicate glass structure: A multinuclear MAS and MQMAS NMR investigation. *Journal of Non-Crystalline Solids* **2013**, *376*, 189–198, doi:10.1016/j.jnoncrysol.2013.05.042.
92. O’Connell, K.; Werner-Zwanziger, U.; O’Shea, H.; Boyd, D. High Borate Networks as a Platform to Modulate Temporal Release of Therapeutic Metal Ions Gallium and Strontium. *Biomedical Glasses* **2017**, *3*, 18–29, doi:10.1515/bglass-2017-0002.
93. Chitambar, C. R. Medical Applications and Toxicities of Gallium Compounds. *Int J Environ Res Public Health* **2010**, *7*, 2337–2361, doi:10.3390/ijerph7052337.
94. Kretsinger, R. H.; Uversky, V. N.; Permiakov, E. A. Gallium Therapeutic Effects. In *Encyclopedia of metalloproteins*; 2013 ISBN 978-1-4614-1533-6.
95. Place, E. S.; Evans, N. D.; Stevens, M. M. Complexity in biomaterials for tissue engineering. *Nature Materials* **2009**, *8*, 457–470, doi:10.1038/nmat2441.
96. Gu, Y.; Huang, W.; Rahaman, M. N.; Day, D. E. Bone regeneration in rat calvarial defects implanted with fibrous scaffolds composed of a mixture of silicate and borate bioactive glasses. *Acta Biomater* **2013**, *9*, 9126–9136, doi:10.1016/j.actbio.2013.06.039.

97. Shelby, J. E. *Introduction to Glass Science and Technology*; 2005; ISBN 978-0-85404-639-3.
98. Rahaman, M. N.; Day, D. E.; Bal, B. S.; Fu, Q.; Jung, S. B.; Bonewald, L. F.; Tomsia, A. P. Bioactive glass in tissue engineering. *Acta Biomater* **2011**, *7*, 2355–2373, doi:10.1016/j.actbio.2011.03.016.
99. O’Connell, K.; Pierlot, C.; O’Shea, H.; Beaudry, D.; Chagnon, M.; Assad, M.; Boyd, D. Host responses to a strontium releasing high boron glass using a rabbit bilateral femoral defect model. *J. Biomed. Mater. Res. Part B Appl. Biomater.* **2017**, *105*, 1818–1827, doi:10.1002/jbm.b.33694.
100. Joo, C.; Werner-Zwanziger, U.; Zwanziger, J. W. The Ring Structure of Boron Trioxide Glass. *J. Non-Cryst. Solids* **2000**, *261*, 282–286, doi:10.1016/S0022-3093(99)00609-2.
101. Wright, A. C.; Dalba, G.; Rocca, F.; Vedishcheva, N. M. Borate versus silicate glasses: why are they so different? *Physics and Chemistry of Glasses - European Journal of Glass Science and Technology Part B* **2010**, *51*, 233–265.
102. Salem, R.; Lewandowski, R.; Roberts, C.; Goin, J.; Thurston, K.; Abouljoud, M.; Courtney, A. Use of Yttrium-90 glass microspheres (TheraSphere) for the treatment of unresectable hepatocellular carcinoma in patients with portal vein thrombosis. *J Vasc Interv Radiol* **2004**, *15*, 335–345.
103. Doucet, J.; Kiri, L.; O’Connell, K.; Kehoe, S.; Lewandowski, R. J.; Liu, D. M.; Abraham, R. J.; Boyd, D. Advances in Degradable Embolic Microspheres: A State of the Art Review. *J Funct Biomater* **2018**, *9*, doi:10.3390/jfb9010014.
104. Reynolds, A. Diagnosis and management of uterine fibroids. *Radiol Technol* **2007**, *79*, 157-178-182.
105. Kilcup, N.; Tonkopi, E.; Abraham, R. J.; Boyd, D.; Kehoe, S. Composition-property relationships for radiopaque composite materials: pre-loaded drug-eluting beads for transarterial chemoembolization. *J Biomater Appl* **2015**, *30*, 93–103, doi:10.1177/0885328215572196.

106. Abraham, R.; Basseri, H.; Davis, C.; Tonkopi, E.; Kehoe, S.; Boyd, D.; Bowen, C. Magnetic resonance imaging characteristics of imageable embolic microspheres. *Journal of Vascular and Interventional Radiology* **2015**, *26*, S80, doi:10.1016/j.jvir.2014.12.222.
107. Food and Drug Administration Use of International Standard ISO 10993-12, 'Biological Evaluation of Medical Devices. Part 12: Sample Preparation and Reference Materials'; Guidance for Industry and Food and Drug Administration Staff Available online: <https://www.iso.org/standard/53468.html> (accessed on Feb 4, 2018).
108. Kehoe, S.; Tonkopi, E.; Abraham, R. J.; Boyd, D. Predicting the thermal responses and radiopacity of multicomponent zinc–silicate bioglasses: A focus on ZnO, La<sub>2</sub>O<sub>3</sub>, SiO<sub>2</sub> and TiO<sub>2</sub> - ScienceDirect. *J Non-Cryst Solids* **2012**, *358*, 3388–3395, doi:10.1016/j.jnoncrsol.2012.08.024.
109. Lower, N.; McRae, J. L.; Feller, H. A.; Betzen, A. R.; Kapoor, S.; Affatigato, M.; Feller, S. A. Physical properties of alkaline-earth and alkali borate glasses prepared over an extended range of compositions. *J Non-Cryst Solids* **2001**, *293*, 669–675, doi:10.1016/S0022-3093(01)00768-2.
110. Bray, P.; O'Keef, J. Nuclear Magnetic Resonance Investigations of the Structure of Alkali Borate Glasses. *Physics and Chemistry of Glasses* **1963**, *4*, 37–46.
111. Wang, S.; Ye, N.; Poeppelmeier, K. R. Flux Growth and Crystal Structure Refinement of Calcite Type Borate GaBO<sub>3</sub>. *Crystals* **2015**, *5*, 252–260, doi:10.3390/cryst5020252.
112. Åhman, J.; Svensson, G.; Albertsson, J. A Reinvestigation of β-Gallium Oxide. *Acta Cryst C* **1996**, *52*, 1336–1338, doi:10.1107/S0108270195016404.
113. Zachariasen, W. H. The Atomic Arrangement In Glass. *J Am Chem Soc* **1932**, *54*, 3841–3851, doi:10.1021/ja01349a006.
114. Atomic Weights and Isotopic Compositions for All Elements Available online: [https://physics.nist.gov/cgi-bin/Compositions/stand\\_alone.pl](https://physics.nist.gov/cgi-bin/Compositions/stand_alone.pl) (accessed on Apr 2, 2018).
115. Stanisz, G. J.; Odrobina, E. E.; Pun, J.; Escaravage, M.; Graham, S. J.; Bronskill, M. J.; Henkelman, R. M. T<sub>1</sub>, T<sub>2</sub> relaxation and magnetization transfer in tissue at 3T. *Magnetic Resonance in Medicine* **2005**, *54*, 507–512, doi:10.1002/mrm.20605.

116. Pierre, T. G. S.; Clark, P. R.; Chua-anusorn, W.; Fleming, A. J.; Jeffrey, G. P.; Olynyk, J. K.; Pootrakul, P.; Robins, E.; Lindeman, R. Noninvasive measurement and imaging of liver iron concentrations using proton magnetic resonance. *Blood* **2005**, *105*, 855–861, doi:10.1182/blood-2004-01-0177.
117. Xu, Z.; Jernigan, S.; Kleinstreuer, C.; Buckner, G. D. Solid Tumor Embolotherapy in Hepatic Arteries with an Anti-reflux Catheter System. *Ann Biomed Eng* **2016**, *44*, 1036–1046, doi:10.1007/s10439-015-1411-7.
118. Watkins, I. G.; Prado, M. Mechanical Properties of Glass Microspheres. *Procedia Materials Science* **2015**, *8*, 1057–1065, doi:10.1016/j.mspro.2015.04.168.
119. Smedskjaer, M. M.; Bauchy, M.; Mauro, J. C.; Rzoska, S. J.; Bockowski, M. Unique effects of thermal and pressure histories on glass hardness: Structural and topological origin. *The Journal of Chemical Physics* **2015**, *143*, 164505, doi:10.1063/1.4934540.
120. Zheng, Q.; Mauro, J. C. Variability in the relaxation behavior of glass: Impact of thermal history fluctuations and fragility. *The Journal of Chemical Physics* **2017**, *146*, 74504, doi:10.1063/1.4975760.
121. Kennedy, A. S.; Nutting, C.; Coldwell, D.; Gaiser, J.; Drachenberg, C. Pathologic response and microdosimetry of (90)Y microspheres in man: review of four explanted whole livers. *Int. J. Radiat. Oncol. Biol. Phys.* **2004**, *60*, 1552–1563, doi:10.1016/j.ijrobp.2004.09.004.
122. Katsumori, T.; Kasahara, T. The Size of Gelatin Sponge Particles: Differences with Preparation Method. *Cardiovasc Intervent Radiol* **2006**, *29*, 1077–1083, doi:10.1007/s00270-006-0059-y.
123. Jander, H. P.; Russinovich, N. A. Transcatheter gelfoam embolization in abdominal, retroperitoneal, and pelvic hemorrhage. *Radiology* **1980**, *136*, 337–344, doi:10.1148/radiology.136.2.6967615.
124. Goldstein, H. M.; Wallace, S.; Anderson, J. H.; Bree, R. L.; Gianturco, C. Transcatheter Occlusion of Abdominal Tumors. *Radiology* **1976**, *120*, 539–545, doi:10.1148/120.3.539.

125. Yoshikawa, T.; Kokura, S.; Oyamada, H.; Iinuma, S.; Nishimura, S.; Kaneko, T.; Naito, Y.; Kondo, M. Antitumor Effect of Ischemia-Reperfusion Injury Induced by Transient Embolization. *Cancer Research* **1994**, *54*, 5033–5035.
126. Kennedy, A. S.; Nutting, C.; Coldwell, D.; Gaiser, J.; Drachenberg, C. Pathologic response and microdosimetry of (90)Y microspheres in man: review of four explanted whole livers. *Int. J. Radiat. Oncol. Biol. Phys.* **2004**, *60*, 1552–1563, doi:10.1016/j.ijrobp.2004.09.004.
127. Laurent, A.; Wassef, M.; Namur, J.; Martal, J.; Labarre, D.; Pelage, J.-P. Recanalization and particle exclusion after embolization of uterine arteries in sheep: a long-term study. *Fertil. Steril.* **2009**, *91*, 884–892, doi:10.1016/j.fertnstert.2007.12.015.
128. Giraud, S.; Favreau, F.; Chatauret, N.; Thuillier, R.; Maiga, S.; Hauet, T. Contribution of Large Pig for Renal Ischemia-Reperfusion and Transplantation Studies: The Preclinical Model. *J Biomed Biotechnol* **2011**, *2011*, doi:10.1155/2011/532127.
129. Stampfl, S.; Stampfl, U.; Rehnitz, C.; Schnabel, P.; Satz, S.; Christoph, P.; Henn, C.; Thomas, F.; Kauffmann, G. W.; Richter, G. M. Experimental evaluation of early and long-term effects of microparticle embolization in two different mini-pig models. Part I: kidney. *Cardiovasc Intervent Radiol* **2007**, *30*, 257–267, doi:10.1007/s00270-005-0309-4.
130. Swindle, M. M.; Makin, A.; Herron, A. J.; Clubb, F. J.; Frazier, K. S. Swine as models in biomedical research and toxicology testing. *Vet. Pathol.* **2012**, *49*, 344–356, doi:10.1177/0300985811402846.
131. Pereira-Sampaio, M.; Favorito, L. A.; Henry, R.; Sampaio, F. J. B. Proportional analysis of pig kidney arterial segments: differences from the human kidney. *J. Endourol.* **2007**, *21*, 784–788, doi:10.1089/end.2006.0318.
132. Zehtabi, F.; Ispas-Szabo, P.; Djerir, D.; Sivakumaran, L.; Annabi, B.; Soulez, G.; Mateescu, M. A.; Lerouge, S. Chitosan-doxycycline hydrogel: An MMP inhibitor/sclerosing embolizing agent as a new approach to endoleak prevention and treatment after endovascular aneurysm repair. *Acta Biomater* **2017**, *64*, 94–105, doi:10.1016/j.actbio.2017.09.021.

133. Saeed Kilani, M.; Zehtabi, F.; Lerouge, S.; Soulez, G.; Bartoli, J. M.; Vidal, V.; Badran, M. F. New Alcohol and Onyx Mixture for Embolization: Feasibility and Proof of Concept in Both In Vitro and In Vivo Models. *Cardiovasc Intervent Radiol* **2017**, *40*, 735–743, doi:10.1007/s00270-016-1559-z.
134. Siskin, G. P.; Dowling, K.; Virmani, R.; Jones, R.; Todd, D. Pathologic evaluation of a spherical polyvinyl alcohol embolic agent in a porcine renal model. *J Vasc Interv Radiol* **2003**, *14*, 89–98.
135. Masic, I.; Miokovic, M.; Muhamedagic, B. Evidence Based Medicine – New Approaches and Challenges. *Acta Inform Med* **2008**, *16*, 219–225, doi:10.5455/aim.2008.16.219-225.
136. Singh, S. S.; Bordman, R.; Leyland, N. Pregnancy after uterine artery embolization for fibroids. *Can Fam Physician* **2007**, *53*, 293–295.
137. Laurent, A.; Pelage, J.-P.; Wassef, M.; Martal, J. Fertility after bilateral uterine artery embolization in a sheep model. *Fertility and Sterility* **2008**, *89*, 1371–1383, doi:10.1016/j.fertnstert.2007.03.058.
138. Baino, F.; Novajra, G.; Miguez-Pacheco, V.; Boccaccini, A. R.; Vitale-Brovarone, C. Bioactive glasses: Special applications outside the skeletal system. *Journal of Non-Crystalline Solids* **2016**, *432*, 15–30, doi:10.1016/j.jnoncrysol.2015.02.015.
139. Food and Drug Administration. MAUDE - Manufacturer and User Facility Device Experience. Available online: <https://www.accessdata.fda.gov/scripts/cdrh/cfdocs/cfmaude/textResults.cfm?q=RW1ib1NwaGVyZQ==&sc=&pf=&pn=500>
140. Sharma, K. V.; Dreher, M. R.; Tang, Y.; Pritchard, W.; Chiesa, O. A.; Karanian, J.; Peregoy, J.; Orandi, B.; Woods, D.; Donahue, D.; Esparza, J.; Jones, G.; Willis, S. L.; Lewis, A. L.; Wood, B. J. Development of “imageable” beads for transcatheter embolotherapy. *J Vasc Interv Radiol* **2010**, *21*, 865–876, doi:10.1016/j.jvir.2010.02.031.
141. Haynes, R. B. Of studies, syntheses, synopses, and systems: the “4S” evolution of services for finding current best evidence. *BMJ Evidence-Based Medicine* **2001**, *6*, 36–38, doi:10.1136/ebm.6.2.36.

142. Spies, J. B.; Allison, S.; Flick, P.; Cramp, M.; Bruno, J.; Jha, R. C.; Ascher, S. A. Spherical Polyvinyl Alcohol versus Tris-acryl Gelatin Microspheres for Uterine Artery Embolization for Leiomyomas: Results of a Limited Randomized Comparative Study. *Journal of Vascular and Interventional Radiology* **2005**, *16*, 1431–1437, doi:10.1097/01.RVI.0000179793.69590.1A.



# APPENDIX A

Chapter 1, Section 2 is published in the Journal of Functional Biomaterials with permission

<http://www.mdpi.com/about/openaccess>

## MDPI Open Access Information and Policy

All articles published by MDPI are made immediately available worldwide under an open access license. This means:

- everyone has free and unlimited access to the full-text of *all* articles published in MDPI journals, and
- everyone is free to re-use the published material if proper accreditation/citation of the original publication is given.
- open access publication is supported by the authors' institutes or research funding agencies by payment of a comparatively low Article Processing Charge (APC) for accepted articles.

## External Open Access Resources

MDPI is a RoMEO green publisher — RoMEO is a database of Publishers' copyright and self-archiving policies hosted by the University of Nottingham

Those who are new to the concept of open access might find the following websites or 'Open Access 101' video informative:

Wikipedia article on 'Open Access'

Peter Suber's 'Open Access Overview'


Information Platform Open Access [in English, in German]

SHERPA's 'Authors and Open Access'

## Meaning of Open Access

In accordance with major definitions of open access in scientific literature (namely the Budapest, Berlin, and Bethesda declarations), MDPI defines *open access* by the following conditions:

- peer-reviewed literature is freely available without subscription or price barriers,
- literature is immediately released in open access format (no embargo period), and
- published material can be re-used without obtaining permission as long as a correct citation to the original publication is given.

Until 2008, most articles published by MDPI contained the note: "© year by MDPI (<http://www.mdpi.org>). Reproduction is permitted for noncommercial purposes". During 2008, MDPI journals started to publish articles under the Creative Commons Attribution License  and are now using the latest version of the CC BY license, which grants authors the most extensive rights. All articles published by MDPI before and during 2008 should now be considered as having been released under the post-2008 Creative Commons Attribution License.

This means that all articles published in MDPI journals, including data, graphics, and supplements, can be linked from external sources, scanned by search engines, re-used by text mining applications or websites, blogs, *etc.* free of charge under the sole condition of proper accreditation of the source and original publisher. MDPI believes that open access publishing fosters the exchange of research results amongst scientists from different disciplines, thus facilitating interdisciplinary research. Open access publishing also provides access to research results to researchers worldwide, including those from developing countries, and to an interested general public. Although MDPI publishes all of its journals under the open access model, we believe that open access is an enriching part of the scholarly communication process that can and should co-exist with other forms of communication and publication, such as society-based publishing and conferencing activities.

**Important Note:** some articles (especially *Reviews*) may contain figures, tables or text taken from other publications, for which MDPI does not hold the copyright or the right to

re-license the published material. Please note that you should inquire with the original copyright holder (usually the original publisher or authors), whether or not this material can be re-used.

# APPENDIX B

Chapter 3 is submitted for publication in the Journal of Non-Crystalline Solids with permission

## Article Sharing

<http://www.elsevier.com/about/company-information/policies/sharing>

Authors who publish in Elsevier journals can share their research in several ways. Researchers who have subscribed access to articles published by Elsevier can share too. There are some simple guidelines to follow, which vary depending on the article version you wish to share. Elsevier is a signatory to the [STM Voluntary Principles](#) for article sharing on Scholarly Collaboration Networks and a member of the [Coalition for Responsible Sharing](#).

## Preprint

- Authors can share their preprint anywhere at any time.
- If accepted for publication, we encourage authors to link from the preprint to their formal publication via its Digital Object Identifier (DOI). Millions of researchers have access to the formal publications on ScienceDirect, and so links will help your users to find, access, cite, and use the best available version.
- Authors can update their preprints on arXiv or RePEc with their accepted manuscript .

## **Please note:**

- [Cell Press](#), [The Lancet](#), and some society-owned titles have different preprint policies. Information on these is available on the journal homepage.
- Preprints should not be added to or enhanced in any way in order to appear more like, or to substitute for, the final versions of articles.

---

## Accepted Manuscript

Authors can share their accepted manuscript:

### **Immediately**

- via their non-commercial personal homepage or blog
- by updating a preprint in arXiv or RePEc with the accepted manuscript
- via their research institute or institutional repository for internal institutional uses or as part of an invitation-only research collaboration work-group
- directly by providing copies to their students or to research collaborators for their personal use
- for private scholarly sharing as part of an invitation-only work group on commercial sites with which Elsevier has an agreement

### **After the embargo period**

- via non-commercial hosting platforms such as their institutional repository
- via commercial sites with which Elsevier has an agreement

### **In all cases accepted manuscripts should:**

- link to the formal publication via its DOI
- bear a CC-BY-NC-ND license – this is easy to do, [click here](#) to find out how
- if aggregated with other manuscripts, for example in a repository or other site, be shared in alignment with our [hosting policy](#)
- not be added to or enhanced in any way to appear more like, or to substitute for, the published journal article

---

## Published Journal Article

Policies for sharing published journal articles differ for subscription and gold open access articles:

### **Subscription articles**

- If you are an author, please share a link to your article rather than the full-text. Millions of researchers have access to the formal publications on ScienceDirect, and so links will help your users to find, access, cite, and use the best available version
- If you are an author, you may also share your Published Journal Article privately with known students or colleagues for their personal use
- Theses and dissertations which contain embedded PJAs as part of the formal submission can be posted publicly by the awarding institution with DOI links back to the formal publications on ScienceDirect
- If you are affiliated with a library that subscribes to ScienceDirect you have additional private sharing rights for others' research accessed under that agreement. This includes use for classroom teaching and internal training at the institution (including use in course packs and courseware programs), and inclusion of the article for grant funding purposes
- Otherwise sharing is by agreement only
- The Published Journal Article cannot be shared publicly, for example on ResearchGate or Academia.edu, to ensure the sustainability of peer-reviewed research in journal publications.

# Appendix C

Preclinical Research Protocol: Embolization effectiveness of degradable embolic microspheres in a swine renal artery model.

**D. Boyd and J. Doucet,  
Dalhousie University.**

**March 2018**

## 1.0 Study Summary

**Study Title:** Evaluation of the embolization effectiveness of degradable embolic microspheres in a swine renal artery model.

**Study Number (Testing Facility):** TBD with CHUM

**Study Compliance:** Compliance with aspects of 21 CFR Part 58 GLP under consideration.

**Testing Facility:** Research Center of Centre Hospitalier de l'Université de Montréal (CRCHUM)

**Study Director:** Hélène Héon

**Veterinary Services Director:** Hélène Héon

**Interventional Radiologist:** Dr Bob Abraham, Dr Gilles Soulez.

**Animal Facility Director:** Hélène Héon

**Sponsor:**

Daniel Boyd, PhD.

Applied Oral Sciences, Faculty of Dentistry, Dalhousie University

PO Box 15000, 5981 University Ave.

Halifax, Nova Scotia, Canada B3H 4R2

Telephone: (902) 494-6347

**Sponsor Representative:**

Jensen Doucet, BSc. (Master's Candidate),

Biomedical Engineering, Dalhousie University

Telephone: (902) 863-8535

Email: doucet.jensen@dal.ca

**Test Articles:** Degradable boron-based glass microspheres 100-300 um.

**Control Articles:** EmboSphere® (Merit Medical), 100-300 um.

**Duration of Exposure:** 3x cohorts, exposures of 0h, 24h, and 48h.

**Proposed Study Dates:** TBD with CRCHUM

**Test System:** Female Hybrid Farm pigs (n=4 animals, plus 1 spare animal)



## 2.0 Signatures

Study Director

---

Date

Testing Facility Management

---

Date

Sponsor Representative

---

Date

### **3.0 Introduction**

Dalhousie University researchers have developed a degradable embolic microsphere indicated for the transarterial embolization of hypervascular tumors including uterine leiomyoma. The product is targeted for commercialization as a Class IIb special control medical device [1] and is subject to design control regulations pertaining to CFR 820.30 [2]. The primary benefit of the technology is enhanced patient safety coupled with the ability to ameliorate chronic inflammation whilst permitting subsequent procedures to be performed at the same target level of occlusion. This study is required to demonstrate the embolization effectiveness of the technology, while also monitoring for particle migration, per FDA guidance on the evaluation of microspherical embolization particles [1].

### **4.0 Definitions**

- a. Recanalization: reopening of a previously embolized vessel
- b. Effective stasis: stasis of 50% contrast media for 5 or more cardiac pulsations

### **5.0 Purpose and Objectives**

The primary objective of this study is to evaluate the embolization effectiveness of the test article in a swine bilateral partial renal artery embolization model. This study will use microspheres with a particle size distribution of 100-300  $\mu\text{m}$ . The primary outcomes for this study will be the assessment of; (i) embolization effectiveness, and (ii) test article migration.

### **6.0 Test Materials**

#### **6.1 Description of the Test Article and Control Articles**

The test article is a proprietary degradable glass microsphere developed by Dalhousie researchers, and is indicated for the embolization of hypervascular tumors and arteriovenous malformations including uterine leiomyoma. The test article will be supplied in sterile individual packages (gamma sterilization, Nordion), having a particle size distribution of 100-300  $\mu\text{m}$ . The test article is designed to undergo hydrolytic degradation in *ca.* 48h under physiological conditions. It is required that such pre-clinical evaluations

represent an elevated risk clinical scenario; accordingly, the particle size selected represents the highest risk product for human use, with respect to particle migration and non-target tissue embolization. The control article will be EmboSphere®® (100-300um).

## **6.2 Test Article Preparation**

The Sponsor will supply the Test Article (TA) in a sterile and ready to deliver form. The TA will be delivered using an ABK delivery device, which will also be provided in a sterile, ready to use state.

## **6.3 Test Article Accountability**

While at the Testing Facility, accountability of the TA and delivery device equipment will be maintained using the Facility's standard operating procedures (SOP).

## **6.4 Test Article Characterization**

The Sponsor assumes responsibility for characterization of the TA.

## **6.5 Reserve Samples**

No reserve samples of the TA will be retained by the Testing Facility.

## **6.6 Test Article Disposition**

Unused TA and delivery device equipment will be returned to the Sponsor at the end of the study.

## **6.7 Storage Conditions**

The TA will be stored at room temperature (below 25°C), **desiccated**, and in a secure location.

## 7.0 Animals

### 7.1 Model Description

**Species:** *Sus scrofa domesticus*

**Strain:** Hybrid farm pigs

**Condition:** Non-diseased

**Source:**

Ferme Triporc

3250, rang Haut-de-la-Rivière

Sainte-Élizabeth, Qc

**Age at implant:** Age commensurate with weight.

**Weight at implant:** *ca.* 75-85kg

**Sex:** Female

**Number:** 4 animals (3 animals to receive TA, 1 animal to receive EmboSphere® control)

### 7.2 Justification

#### 7.2.1 Selection of Animal Species and Model

A non-atherosclerotic swine model was chosen because the model has been used extensively for angiographic/embolization studies resulting in a large volume of data on the vascular response properties and its correlation to human vascular response [3,4,5]. It is widely accepted that this type of study should be conducted *in vivo*, since no *in vitro* model currently exists that can mimic the complex biological responses to embolization. The porcine and human anatomy share important anatomic and physiologic characteristics [4,6]. Furthermore, the porcine kidney model, recommended for use in preclinical studies by the FDA has been widely used to evaluate embolization agents [7].

#### 7.2.2 Number of Animals

This study comprises a pilot investigation to evaluate embolization effectiveness and migration risk associated with biodegradable microspheres and will therefore utilize the minimum number of animals possible to meet the study objectives. Three different time cohorts will be analyzed:  $t=0$ , 24, and 48 h, to capture (i) embolization effectiveness and initial particle distribution, (ii) particle distribution after partial degradation, and (iii)

recanalization and residual material at the degradation time of the material (t=48 h), respectively. 1 animal, treated bilaterally will be included in each time cohort for the TA. 1 animal, treated bilaterally with the control article will be sacrificed at the 48h time point.

### **7.3 Animal Welfare and Institutional Animal Care and Use Committee Review**

The protocol will be reviewed and approved by the Testing Facility's Institutional Animal Care and Use Committee. The review will insure compliance with Canadian Council on Animal Care (CCAC) regulations. If an animal entered on the study is found to have contracted a condition or disease that might interfere with the purpose of the study, that animal may be isolated and treated as prescribed by the Facility Veterinarian in consultation with the Study Director.

### **7.4 Animal Husbandry**

#### **7.4.1 Environmental Acclimation**

Prior to the interventional procedure, animals will have had environmental acclimation for at least 7 days.

#### **7.4.2 Testing Facility Housing**

In the Testing Facility, animals will be housed in a room with suspended floors. Pens and the room are washed daily with water and Virex ® (quaternary-based disinfectant cleaner). All housing conditions meet or exceed the standards set forth in the Guide for the Care and Use of Laboratory Animals [8].

#### **7.4.3 Food**

Standard dehydrated food pellets will be given to the animal. Fresh vegetables and certified treats may be given at the facilities discretion.

#### **7.4.4 Water**

The animals receive reverse osmosis water. A bacterial load test (aerobic and anaerobic heterotrophic bacterial count) is conducted every 4-6 weeks on the reservoir water. Twice a year, a microbial burden tests (coliform, aerobic bacteria, total count) is conducted on production water and end of distribution line. Once a year, a specific search for pseudomonas and fungi is conducted as well as a determination of inorganic contaminants such as heavy metals. Results of these analyses are on file at the Testing Facility and are available to the Sponsor on request.

#### **7.4.5 Contaminants**

Certified diet will be fed daily to the animals. The food manufacturer will routinely analyze the diet for nutritional components and environmental contaminants. Results of the manufacturer's analyses are retained on file at the Testing Facility. Details of nutritional components and other manufacturing information will be made available to the Sponsor on request.

#### **7.4.6 Testing Facility Environment**

Temperature and humidity will be monitored. Light cycle will be controlled by an automated system.

### **7.5 Animal Identification**

The animals will be identified using unique Testing Facility number, which will be indicated on its back with a marker and posted on the animals' enclosures with cage cards. At implantation the animals will be attributed a study number composed of the scheduled time point and sequential number (e.g. 24-01 for 24 h animal #1). Ear tag number will be recorded at implantation. If no tag is present, an ear tag with the same number as listed above will be installed.

## 8.0 Experimental Methodology

### 8.1 Experimental Design

Bilateral renal artery embolization will be conducted in 4 non-diseased pigs using methods adapted from the literature [5,9,10,11]. 50% of the renal mass will be conserved so as to preserve renal function; this will be determined on angiography. All animals will receive the TA in amounts required to achieve effective stasis (defined in Section 4.0) in the renal artery. The volume of delivered TA will be recorded for each animal. Three cohorts will be used to analyze embolization effectiveness and distribution/migration at time equal to;  $t=0, 24, 48$  h. Migration will be assessed by assessing ischemic damage to non-target tissues assessed *via* full conventional CT and histology (of tissues showing evidence of ischemia on CT).

**Table A.1:** Insert Table of Proposed Test and Control Article Allocation

Animal Number	LRA	Embolization Pole (Cranial / Caudal)	RRA	Embolization Pole (Cranial / Caudal)
<b>0-01</b>	Test Article	Cranial	Test Article	Caudal
<b>24-01</b>	Test Article	Cranial	Test Article	Caudal
<b>48-01</b>	Test Article	Cranial	Test Article	Caudal
<b>48-02</b>	Control Article	Cranial	Control Article	Caudal

LRA: Left Renal Artery

RRA: Right Renal Artery

### 8.2 Animal Acceptance on Study

A physical examination of the animals will be performed under supervision of the Facility Veterinarian during acclimation. Cardiac and pulmonary auscultations will be performed by the Veterinarian.

### **8.3 Procedures Following Acceptance on the Study**

#### **8.3.1 Animal Monitoring and Examination**

Upon assignment on the study and until sacrifice, animals will be monitored and observed at least twice a day by a trained employee (cage side observation).

### **8.4 Pre-Interventional Procedures**

#### **8.4.1 Fasting**

Fasting (food, including any dietary supplements) will be conducted prior to interventional procedures and scheduled sacrifice. Water will not be withheld. After anesthesia and appropriate recovery, animals may have access to food and water.

#### **8.4.2 General Anesthesia and Fluid Therapy**

Animals will be anesthetized with 25 mg/kg ketamine and 2 mg/kg xylazine administered intramuscularly (IM). Animal weight will be recorded. Anesthesia induction for tracheal intubation will be achieved with 1.66 mg/kg propofol injected intravenously (IV) via a catheter in a vessel of the left or right ear or another appropriate vessel. Upon induction of anesthesia, the subject animal will be intubated and supported with mechanical ventilation. Isoflurane in oxygen will be administered to maintain a surgical plane of anesthesia. Blood samples will be collected for clinical pathology (blood hematology and serum biochemistry analysis described in the Clinical Pathology section). Pre-implant and pre-euthanasia samples will be harvested during anesthesia for implant and terminal procedures. Blood will be sampled prior to heparin administration and prior to initiation of intravenous fluid therapy.

**Clinical Pathology Samples:** Harvested from the arterial sheath

An appropriate volume of blood will be collected as follows:

- Whole blood samples for hematology will be collected in EDTA tubes.
- Blood samples for biochemistry will be collected in serum clotting activator tubes, processed, and the serum extracted.

All clinical pathology samples will be analyzed on collection day. IV fluid therapy will be



initiated and maintained throughout the procedure as per Operator's judgment.

### **8.4.3 Antibiotic Therapy Preemptive Analgesia**

Animals will be injected (IV) with one dose of antibiotic Cefazolin® (22mg/kg) at the beginning of the procedure, and every 2 hours during the procedure to prevent postoperative infections (excluding the t=0 cohort). Additional doses may be administered at the discretion of the Facility Veterinarian in consultation with the Study Director but will be reported to the Sponsor in the final report. To prevent pain sensitization and minimize postoperative pain, a starting IV bolus of fentanyl (0.005 mg/kg), ketamine (0.2 mg/kg), and lidocaine (1 mg/kg) will be administered. A bag of 500 mL saline will then be prepared with 0.5 mg fentanyl, 30 mg ketamine, and 300 mg lidocaine. This bag will be administered during the entire surgical procedure at a flow rate of 5 mL/kg/h, corresponding to a dose of 0.005 mg/kg/h fentanyl, 0.3 mg/kg/h ketamine, and 3 mg/kg/h lidocaine.

### **8.4.4 Animal Positioning, Monitoring, and Surgical Site Preparation**

The animal will be placed in dorsal recumbence, and the hair will be removed from the access area (inguinal area). A rectal temperature probe will be inserted, and the temperature will be monitored regularly. Electrocardiography limb-leads will be placed and electrocardiography will be established. The access site will be prepared with topical application of chlorhexidine, 70% isopropyl alcohol. The area will then be appropriately draped to maintain a sterile field. A urinary catheter may be installed.

## **8.5 Interventional Procedures**

### **8.5.1 Local Anesthesia, Vascular Access, Monitoring and Anticoagulant Therapy and Surgical Approach**

Parameters including blood oxygen saturation, heart rate, blood pressure (at least before and after embolization), and temperature will be regularly monitored and manually recorded in the raw data for each animal. Electrocardiogram will be monitored but not recorded or retained. After induction of anesthesia, the left or right femoral artery will be accessed under ultrasound guidance (echography, non-GLP). A 5 French introducer sheath

will be inserted. The introducer will be perfused with heparinized saline at 2 IU/mL, during the procedure. A 4 French Cobra catheter (Cook medical) will be introduced and advanced in the proximal portion of the right and left renal artery under fluoroscopic guidance.

Before any contrast injection, a cone-beam CT will be performed in the angio suite to evaluate the size and morphology of both kidneys [9]. A selective angiography will be performed to evaluate the branch division into cranial and caudal branches and segmental renal arteries. Hypersselective catheterization of caudal branch will be performed with a 2.5Fr micro catheter (Cantata, Cook Inc., Bloomington, IN) under fluoroscopic guidance [9,10]. All bifurcations downstream to the cranial and caudal branches will be recorded as D1, D2, D3, etc., where D1 refers to the immediate and largest branches of the cranial or caudal artery, following subsequent branches from this artery will be labelled D2, and further branches will be labelled as D3, etc. [10], similar to what is seen in Figure 1.



**Figure A.1:** Division System Method: D1 refers to the immediate and largest branches of the caudal artery, subsequent branches of this artery are labelled D2, further branches labelled D3, etc. [10].

### **8.5.2 Procedure for Test Article Injection and Medical Imaging**

The TA will be delivered using sterile saline to monitor fluoroscopic visibility of the microspheres during injection. Fluoro-loops acquired during particle injection will be stored. Microspheres will be injected until effective stasis is reached (defined in Section 4.0) [9]. The total volume of TA delivered will be recorded for each animal, as well as total duration of the procedure for each animal, and the ease of use of the material. One shot films and cone beam CT (in the angio suite) acquisitions will be acquired to evaluate the distribution of the radiopaque microspheres in each pig. Post-embolization angiography will be performed to the degree of vessel occlusion and document embolization efficacy. All embolized arteries will be qualitatively evaluated for arterial perforation or rupture and embolization effectiveness. Semi-quantitative analysis of the procedure will be done by recording the level of occlusion of distal branches (both beginning and end of the bolus), as per Section 8.5.1 [modified from 10,11].

Lidocaine may be administered to treat arrhythmia. Nitroglycerin may be administered to treat arterial vasospasm. Atropine sulfate may be administered to treat bradycardia. Additional drugs may be administered as needed per the Operator's orders.

### **8.5.3 Complications**

Vessels that received an unsuccessful embolization (e.g., Operator's error) unrelated to either the Test or Control Articles may be replaced. Replacement may be achieved by embolization in an alternative location or in an additional animal. An animal that receives an unsuccessful embolization that may be life-threatening will be euthanized; no necropsy will be performed.

### **8.5.4 Closure**

All catheters and sheaths will be removed after embolization and completion of angiography. Manual pressure will be applied to percutaneous puncture access until hemostasis is achieved, followed by a purse string suture if deemed necessary by the technician (glue may also be used). If cutdown access is performed, the femoral artery will

be ligated and inguinal incision layers will be sutured. Antibiotic ointment will be applied to the wound.

## **8.6 Post-Interventional Procedures**

### **8.6.1 Animal Monitoring**

The anesthetic will be discontinued and the animals ventilated until the return of normal respiration [9].

### **8.6.2 Postoperative Analgesia and Antibiotic Therapy**

Buprenorphine (0.005mg/kg SC or IV) will be injected during recovery from anesthesia. Meloxicam (0.3 mg/kg OS) will be given as post-operative analgesia, and buprenorphine (0.005mg/kg SC) if pain persists regardless of the administration of meloxicam.

### **8.6.3 Veterinary Intervention and Care**

At the discretion of the facility veterinary team, the drugs listed in Table 2 will be available. If any of the following symptoms are observed, the animal will be euthanized as per Section 9.1:

During the procedure:

- Hemorrhage causing hypovolemia and risk of shock.
- Severe hypotension
- Unsuccessful embolization that may be life-threatening

During recovery & post-op:

- Respiratory distress non-responsive to supportive care
- Fever and prostration non-responsive to treatment
- Uncontrollable pain
- Uncontrollable bleeding

**Table A.2:** List of Drugs used in the Swine Renal Model

Drug	Drug type	Purpose	Administration	Manufacturer
Anesthesia				
Ketamine	Dissociative general anesthetic and NMDA receptor antagonist	Pre anesthesia	IM	Ketalean® Bimeda-MTC Animal Health Inc. /Santé animale INC. Cambridge , ON N3C 2W4
Xylazine	Alpha <sub>2</sub> -adrenergic agonist	Pre anesthesia	IM	Rompun®, Bayer Inc, Mississauga, On, Canada
Propofol	Anesthetic	Anesthesia induction	IV	Diprivan 1%, AstraZeneca, Mississauga, On, Canada
Isoflurane	General anesthetic, inhalant	Anesthesia	inhalation	Forane, Baxter, Mississauga, On, Canada)
Analgesia				
Meloxicam	Nonsteroidal anti-inflammatory drug	Pain prevention	SC or per os	Metacam, Boehringer Ingelheim, Ltd, Burlington, On, Canada
Bupivacaine	Local anesthetic	Pain prevention	Infusion surgical site	Marcaïne™ 0,50 % hydrochloride injection USP Hospira, Montreal, Qc, Canada).
Ketamine	Dissociative general anesthetic and NMDA receptor antagonist	Pain prevention	IV, bolus and constant rate infusion	Fentanyl citrate injection USP Sandoz Canada Inc.
Lidocaine	Antiarrhythmic/ Local anesthetic	Pain prevention Arrhythmia prevention	IV, bolus and constant rate infusion	Lidocaine hydrochloride 2 % (1.5 mg/kg/h, Hospira, Montreal, Qc, Canada).

<b>Drug</b>	<b>Drug type</b>	<b>Purpose</b>	<b>Administration</b>	<b>Manufacturer</b>
Fentanyl	Opioid	Pain prevention	IV, bolus and constant rate infusion	Fentanyl citrate injection USP Sandoz Canada Inc.
Antibiotherapy				
Cefazolin	1 <sup>st</sup> generation cephalosporin	Surgical prophylaxia	IV	Cefazolin for injection USP Hospira Health Care corporation St-Laurent , QC Distributed by Apotex, Inc Toronto Canada
Drugs that may be used during the procedure				
Atropine	Anticholinergic	Treatment of bradycardia	IV	Atropine Sulfate injection USP 0.5mg/ml, Rafter 8 Products, 87 Skyline Crescent N.E., Calgary, Alberta, T2K 5X2
Rocuronium	Non—depolarizing neuromuscular blocker	To control breathing during positive ventilation	IV	Bromide Injection, Sandoz Canada Inc, Québec, Canada, J4B 7K8
Phenylephrine	Alpha-adrenergic agonist	Treatment of hypotension	IV Bolus and infusion	Phenylephrine Hcl Sandoz 10mg/ml (to treat hypotension)
Heparin	Anticoagulant	Thromboprophylaxis	IV	Heparin sodium injection USP , 10 000 U/ml Sandoz , Canada Inc,
Buprenorphine	Opioid	Treatment of post-op pain	SC or IV	Vetergesic, Healthcare Ltd, Hull, UK, imported/distributed by GMD Distribution Inc., Oakville, ON, L6M 2W2 for: Champion Alstoe Animal Health Inc., Whitby, Ontario, L1N 4V1

\*\*Please note that the manufacturer may not be the same at the time of the study. The table will be amended accordingly.

#### **8.6.4 Additional Health Examinations**

All animals will be monitored postoperatively at 2, 4, 12, 24, and 36 h post-op by a trained employee (Testing Facility Veterinarian) and the following physical examinations will be conducted:

- i. Monitoring for signs of PES by taking temperature and inspecting for malaise and pain
- ii. Monitoring for signs of respiratory distress (O<sub>2</sub> sats, hemoptysis, respiration rate)
- iii. Neurological examination of the lower limbs by conducting motor and sensory exams
- iv. Monitoring for signs of stroke (gait)
- v. Monitoring for bleeding from the incision site

Clinical observations and findings during monitoring and examination will be included in the final report.

#### **8.6.5 Pre-Sacrifice Angiography for Assessment of Recanalization**

Immediately prior to the scheduled sacrifice time point, angiography will be performed in each animal using the methods outlined in Section 8.5.1 to assess the embolization status of the renal vasculature, and position of embolic agent (both beginning and end of the bolus). The following grade scale will be used for qualitative evaluation of recanalization: 0=no angiographic visible signs of arterial occlusion; 1=reduction of parenchymal staining of the dependent territory; 2=reduction of the parenchymal staining and occlusion of the supplying arcuate artery; 3=reduction of parenchymal staining, occlusion of the supplying arcuate artery and occlusion of the feeding artery downstream of the catheter tip [9]. On the baseline and follow-up cone beam CT the distribution of particles will be compared and distal migration will be evaluated by measurement the distance with the renal capsule [11].

## **9.0 Scheduled and Unscheduled Sacrifice**

### **9.1 Euthanasia**

After final angiography, animals (in deep anesthesia) will be euthanized by a lethal injection of sodium pentobarbital (euthanyl, rapid IV bolus, 108mg/kg). Death will be confirmed by observation of asystole or ventricular fibrillation on the ECG.

### **9.2 Necropsy and Tissue Harvest**

All treated animals will be subjected to necropsy, defined as gross examination of the embolized arteries and kidneys, whole body (external surface), all orifices, thoracic and abdominal cavities, and brain. Macroscopic pictures of all kidneys (ventral and dorsal views) and any lesions will be taken with a ruler adjacent to the tissue and properly labeled when possible (study number, animal number, organ). Kidneys will be evaluated macroscopically and measured (length, width and depth) before fixation. Three regions (cranial pole, middle region and caudal pole) will be evaluated individually on both surfaces (ventral and dorsal surfaces) for ischemic changes. An ischemic change score will be attributed to each region according to the following scale [8]:

- 0 = no macroscopic visible change;
- 1 = discoloration of renal surface;
- 2 = Surface scars and retractions (corresponding to score 1 and 2);
- 3 = volume shrinkage of the respective area (corresponding to score 1, 2 and 3).

Each kidney with the renal artery (entire length) for each animal will be harvested free of fat and cranial pole properly identified (with ink for example) in a consistent manner. To allow good fixation, the kidney will be cut longitudinally in two equal sections (but not completely to avoid damage of renal arteries before fixation) from the lateral aspect to the hilus. Both kidneys from an animal will be placed in neutral-buffered formalin (NBF) together and the right kidney will be identified with a suture on the hilus. Selected organs [adrenal glands, lungs (samples of right middle lobe and left caudal lobe)] will then be placed into an appropriately labeled container filled with NBF. Lesions will be documented and collected when feasible, immersion-fixed in NBF and processed for histology.



### **9.3 Unscheduled Sacrifice**

If an animal dies after recovery from embolization but prior to scheduled termination, the Study Director will be notified immediately. After the discovery of the death, the following procedures will be completed as soon as possible and same as per the Necropsy and Tissue Harvest section above (9.2)

The animal may be replaced at the discretion of the Study Director and documentation of the necropsy results may be included in the final report.

Moribund animals will be treated as described above (9.2), except that if possible a final angiogram and blood samples will be taken for clinical pathology

## **10.0 Sample Processing and Analyses**

### **10.1 Cone Beam CT**

After necropsy, all harvested organs was be fixed in a box containing formaldehyde. A cone-beam CT will be repeated on the explanted structures (Kidneys and accompanying renal vasculature, lungs and any structures showing signs of ischemia or necrosis on necropsy) to detect the best zones for samples.

### **10.2 Sample Preparation**

Following *ex vivo* imaging, the kidneys and renal vasculature will be sectioned, and specimens will be embedded in paraffin and placed in an individual cassette. Six blocks of one cm each will be taken in each kidney (four in infarcted areas upper pole and two controls in the lower pole = 48 blocs). This will also be completed for any tissues where possible infarction was located on necropsy or where microspheres were identified on cone beam CT.

### **10.3 Micro-CT and Sectioning**

The blocks will be analyzed by micro-CT in order to choice the three best samples in each kidney for histology analyses. The blocks will be sent to the histology platform for

processing and embedding. Ten sections will be cut 4-micrometer-thick tissue every mm and will be mounted on a glass microscope slide.

#### **10.4 Histological Staining and Tissue Processing**

Specimens will be stained with hematoxylin-eosin-saffron. Hematoxylin-eosin-saffron will allow observation of occluded vessels and the locations of identified microspheres, which will be labelled according to the different layer of renal vasculature as per Section 8.5.1 [10]

The number of microspheres in each layer will be recorded. The presence and extent of embolus surrounding each embolic will also be documented, as will the presence of inflammatory reaction and the types of inflammatory cells present (e.g. macrophages, multinucleated giant cells, lymphocytes, eosinophils). Identified microspheres (or microsphere fragments) will be measured (Section 10.4) and their shape will be qualitatively assessed (spherical vs. irregular). Vessel wall rupture, formation of new endothelium within the embolized vessel, and location of particles within the vessel walls should extravasation occur will be assessed and the degree of vascular injury will be rated as follows [12]:

- 0 = Internal elastic lamina (IEL) intact
- 1 = Disruption of the IEL without medial disruption.
- 2 = Disruption of the IEL with disruption of the media. The external elastic lamina is intact.
- 3 = Disruption of the IEL, media, and external elastic lamina.

Additional sections may be cut and stained with different stains at the discretion of the Study Pathologist with the approval of the Study Director.

**Table A.3: Summary of sample preparation, histological staining and tissue processing**

4 swines	0-01	024-01	48-01	48-02
8 kidneys	Test Article	Test Article	Test Article	Control Article
Six blocks of 1 cm each will be taken in each kidney (4 in infarcted areas upper pole and 2 control in the lower pole). $6 \times 8 = 48$				
The blocks will be processing and embedded in paraffin. A micro-CT will be made to choice the 3 relevant blocks.				
10 sections of about 4 $\mu\text{m}$ will be sliced on each block every mm and put on slides				
Specimens will be stained with hematoxylin-eosin-saffron. 4 blocs $\times 10 = 240$ slides				
The slides will be scanned at 40x				
1 cm block will be taken for all tissues where the infarction has been located during necropsy or when microspheres have been identified on imaging.				

### 10.5 Digital Imaging

All slides will be scanned for Software analysis. A low and a high-magnification image of each produced histology slide will be digitally captured and included in the Final Report. The magnification of each image will be obtained with a scale bar. Additional images will be captured and included in the Pathology Report to illustrate histopathology findings as per Study Pathologist, Study Director and/or Sponsor request following issuance of an Amendment.

### 10.6 Histological Measurements

Measurements of the scanned slides will be performed using a Software Program. All identified microspheres will be measured to approximate vessel diameter and indicate the extent of degradation. The number and size of all microspheres in the analyzed specimens will be documented, along with their qualitative distribution (aggregates vs. individual) and position (renal artery division).

## **11.0 Reporting**

A Draft Report will be provided to the Sponsor and any revisions to the study report mutually agreed upon by the Sponsor and Study Director and/or Pathologist will be incorporated in the Final Report. At the end of the revision process, the Report will be signed and considered final. The study Final Report will include a summary of the objectives and procedures of the study, description of the TA used, the methods used for histological processing, and a discussion of any circumstances that may have altered or affected the integrity of the data. Any corrections or additions to the Final Report will be in the form of a report amendment.

## 12.0 References

- [1] Food and Drug Administration. Class II Special Controls Guidance Document: Vascular and Neurovascular Embolization Devices. Dec 2004.
- [2] Food and Drug Administration, Department of Health and Human Services. 21 C.F.R. § 820.30 2012.
- [3] Targeting and Recanalization after Embolization with Calibrated Resorbable Microspheres versus Hand-cut Gelatin Sponge Particles in a Porcine Kidney Model. *Journal of vascular and interventional radiology*. 24(9), pp. 1391 -1398. 2013.
- [4] Giraud S., Favreau F., Chatauret N., Thuillier R., Maiga S., Hauet T. Contribution of Large Pig for Renal Ischemia-Reperfusion and Transplantation Studies: The Preclinical Model. *Journal of Biomedicine and Biotechnology*. 2011;2011:532127.
- [5] Stampfl, S. *et al.* Experimental Evaluation of Early and Long-Term Effects of Microparticle Embolization in Two Different Mini-Pig Models. Part I: Kidney. *CardioVascular and Interventional Radiology* . 30, pp. 257–267. 2007.
- [6] Pereira-Sampaio M., Favorito L.A., Henry R, Sampaio F.J. Proportional analysis of pig kidney arterial segments: differences from the human kidney. *J Endourol*. 21(7), pp. 784-788. 2007.
- [7] Owen, R.J., Nation, P.N., Polakowski, R., Biliske, J.A., Tiege, P.B., Griffith, I.J. A Preclinical Study of the Safety and Efficacy of Occlusion 500 Artificial Embolization Device in Sheep. *Cardiovascular Interventional Radiology*. 25, pp. 636-644. 2012.
- [8] Guide for the Care and Use of Laboratory Animals. National Research Council. *National Academy Press*. 1996.

- [9] Kehoe, S., Amensag, S., Looney, M., Abraham, R.J., Boyd, D. “Imageable” Zinc-Silicate Glass Microspheres for Transarterial Embolization: A Renal Artery Embolization Study. *Biomedical Glasses*. 1, pp. 70-79. 2015.
- [10] Zehtabi F., Ispas-Szabo P., Djerir D., Sivakumaran L., Annabi B., Soulez G., Mateescu M.A., Lerouge S. Chitosan-doxycycline hydrogel: An MMP inhibitor/sclerosing embolizing agent as a new approach to endoleak prevention and treatment after endovascular aneurysm repair. *Acta Biomaterialia*. 64, pp. 94–105. 2017.
- [11] Kilani M.S., Zehtabi F., Lerouge S., Soulez G., Bartoli J.M., Vidal V., Badran M.F. New Alcohol and Onyx Mixture for Embolization: Feasibility and Proof of Concept in Both In Vitro and In Vivo Models. *Cardiovasc Intervent Radiol*. 40, pp. 735–743. 2017.